Aus der Klinik für Augenheilkunde

der Medizinischen Fakultät Charité – Universitätsmedizin Berlin

DISSERTATION

Characterization of functional expression of cannabinoid receptor 1 and transient receptor potential vanilloid 1 channel in human corneal endothelial cells

Charakterisierung der funktionellen Expression des Cannabinoidrezeptors 1 und des Transient-Rezeptor-Potential-Vanilloid-1-Kanals in humanen Hornhautendothelzellen

zur Erlangung des akademischen Grades

Doctor medicinae (Dr. med.)

vorgelegt der Medizinischen Fakultät

Charité – Universitätsmedizin Berlin

von

Huan Luo

Aus Heilongjiang, Volksrepublik China

Datum der Promotion: 25.06.2023

TABLE OF CONTENTS

List of Figures and Tables

Abbreviations

HCE	Human corneal endothelium
HCEC(s)	Human corneal endothelial cell(s)
HCEC-12	Human corneal endothelial cell line 12
TRPV1-HCEC-12	TRPV1 transfected human corneal endothelial cell
RCEP	Rabbit corneal endothelial cells
Ca^{2+}	Calcium ions
K^{+}	Potassium ions
HCEP(s)	Human corneal epithelial cell(s)
ECD	Endothelial cell density
Na^{+}/K^{+}-ATPase	Sodium-potassium adenosine triphosphatase
SOCCs	Store-operated Ca^{2+} channels
VOCCs	Voltage-operated Ca^{2+} channels
LGICs	Ligand-gated ion channels
CED	Corneal endothelial disease
DLEK	Deep lamellar endothelial keratoplasty
DSEK/DSAEK	Descemet stripping (automated) endothelial keratoplasty
DMEK	Descemet membrane endothelial keratoplasty
TRPs	Transient receptor potential channels
Thermo-TRPs	Temperature-sensitive TRPs
TRP	Transient receptor potential
TRPV	Transient receptor potential channel vanilloid
TRPV1	Transient receptor potential vanilloid type 1 (capsaicin receptor)
TRPV1 – 6	Transient receptor potential channel vanilloid subtypes 1 to 6
VR1	Vanilloid receptor 1
GPCRs	G protein-coupled receptors
TRPM2	Transient receptor potential channel melastatin subtype 2

MAPK	Mitogen-activated protein kinase
TRPA	Transient receptor potential channel ankyrin subfamily
TRPM	Transient receptor potential channel melastatin subfamily
TRPML	Transient receptor potential channel mucolipin subfamily
TRPN	Transient receptor potential channel NO-mechano-potential subfamily
TRPP	Transient receptor potential channel polycystin subfamily
TRPM2	Transient receptor potential channel melastatin subtype 2
TRPM8	Transient receptor potential channel melastatin subtype 8 (menthol receptor)
CB1	Cannabinoid receptor subtype 1
CB2	Cannabinoid receptor subtype 2
PKA	protein kinase A
PKC	protein kinase C
GTP	Guanosine-5'-triphosphate
$[Ca^{2+}]_i$	Intracellular calcium concentration
CAP	Capsaicin (TRPV1 agonist)
NGF	Nerve growth factor
CPZ	Capsazepine (TRPV1 antagonist)
DRG	Dorsal root ganglia
VEGF	Vascular endothelial growth factor
IP3	Inositol trisphosphate
DMEM	Dulbecco’s modified eagle medium
HAM’s F12	Ham’s nutrient mixture F12
DMSO	Dimethyl sulfoxide
FBS	Fetal Bovine Serum
Fura-2/AM	Fura-2/acetoxymethyl ester
HEPES	4-(2-hydroxyethyl)-1-piperazineethanesulfonic acid

PBS	Phosphate buffered saline
SEM	Standard error mean
RB	Retinoblastoma
UM	Uveal melanoma
cAMP	Cyclic adenosine monophosphate
cDNA	Complementary DNA
G_i	G_i alpha subunit
G_q	G_q alpha subunit
TrkA	Tropomyosin receptor kinase A
HCF	Human corneal fibroblasts
HCK	Human corneal keratocytes
$HC_j EP$	Human conjunctival epithelial cells
IOP	lower intraocular pressure
ROI(s)	Region of interest(s)

ABSTRACT (Deutsch)

Korneale Endothelzellen sind maßgeblich an der Aufrechterhaltung der Transparenz der humanen Hornhaut involviert. Geringe Endothelzelldichte (ECD) kann zu kornealem Ödem, allmählichen Sehverlust und schlimmstenfalls zur Erblindung führen. Daran sind degenerative Prozesse und Apoptose mit Ca^{2+} beteiligt. Von daher sind die Eigenschaften dieser Zellen von Ca^{2+} abhängigen zellulären Mechanismen geprägt. In der Regulation der intrazellulären Ca^{2+} Konzentration ($[Ca^{2+}]_i$) sind „transient receptor potential“ (TRP) Kanäle substanziell beteiligt wobei der TRP Vanilloid 1 (TRPV1) bekannt als Capsaicinrezeptor Apoptose moduliert. Studien haben gezeigt, dass G-Protein gekoppelte Rezeptoren wie der Cannabinoid Rezeptor 1 (CB1) in humanen Hornhautepithelzellen (HCEPs) exprimiert werden. Studien zum Nervenwachstumsfaktor (NGF) ergaben, dass exogenes NGF die Proliferation von kornealen Endothel- und Epithelzellen von Kaninchen und Menschen stimuliert. In dieser Arbeit wurde die funktionelle Expression von TRPV1, CB1 und NGF in humanen kornealen Endothelzellen (HCEC) untersucht. $[Ca^{2+}]_i$ wurde mit Hilfe von Fluoreszenz Calcium Imaging und Ganzzellströme wurden mittels planarer Patch-Clamp Technik gemessen. Die HCEC-12 Zelllinie wurde als etabliertes *in vitro* Zellmodell sowie eine TRPV1-transduzierte HCEC-12 Zelllinie als heterologes Zellsystem verwendet. Extrazelluläre Applikation von 10 µM Capsaicin (CAP) führte sowohl zu Erhöhung des Fluoreszenzratios (f_{340}/f_{380}), das proportional zu $[Ca^{2+}]_i$ ist, also auch zu Erhöhung der Ganzzellströme. Beide Effekte konnten mit dem TRPV1 Kanalblocker Capsazepin (CPZ) (10 µM) unterdrückt werden. Der CB1 Agonist WIN 55,212-2 (10 µM) erhöhte $[Ca^{2+}]_i$ und Ganzzellströme, welche mit dem CB1 Antagonisten AM251 (10 µM) geblockt werden konnten. Der CAP-induzierte Ca^{2+} Anstieg konnten in Zellen, die mit 10 µM WIN 55,212-2 vorinkubiert wurden, bis unter die Ca^{2+} Basislinie unterdrückt werden, während 10 µM AM251 diesen Effekt eher geringfügig beeinflusste. Der CAP-induzierte Ca^{2+} Anstieg war in TRPV1-HCEC-12 erwartungsgemäß wesentlich stärker als in nicht-transduzierten HCEC-12 (Kontrollen). Das WIN 55,212-2-induzierte Ca^{2+} Antwortmuster änderte sich in Zellen, die mit CAP oder CPZ behandelt wurden (10 µM). Schließlich erhöhte auch NGF (50 ng/ml) $[Ca^{2+}]_i$, welche ebenfalls

durch CPZ unterdrückt werden konnte. Zusammenfassend konnte erstmalig die funktionale Expression von CB1 und TRPV1 in normalen HCEC-12 sowie TRPV1-transduzierten HCEC-12 gezeigt werden, wobei die Effekte in den transduzierten Zellen stärker waren und damit die erfolgreiche Transduktion von TRPV1 in HCEC-12 bestätigte. Darüber hinaus besteht ein Crosstalk zwischen TRPV1 und CB1 sowie NGF, welcher auf eine komplexe Ca^{2+} Regulation in HCEC-12 hindeutet. Die Ergebnisse tragen zu einem besseren Verständnis der Ca^{2+} Regulationsmechanismen bei und können für die Entwicklung neuartiger Strategien für die Verbesserung der Erhaltung von Hornhauttransplantaten für die Keratoplastik beitragen.

ABSTRACT (English)

Corneal endothelial cells are crucially involved in maintaining the transparency of the human cornea. Severe losses in corneal endothelial cell density (ECD) can lead to corneal edema, gradual loss of vision, and at worst blindness. Cell degeneration processes and apoptosis are implicated with Ca^{2+}. Thus, phenotypic characteristics of these cells are controlled by Ca^{2+}-dependent cellular mechanisms. Transient receptor potential channels (TRPs) are substantially involved in the regulation of intracellular calcium concentration ($[Ca^{2+}]_i$) whereby TRP vanilloid type 1 (TRPV1) (capsaicin receptor) modulates apoptosis. Studies have shown that G protein-coupled receptors (GPCRs) such as cannabinoid receptor type 1 (CB1) are expressed in human corneal epithelial cells (HCEPs). Further studies about nerve growth factor (NGF) revealed that exogenous NGF can stimulate the proliferation of HCEP. In this study, the functional expression of TRPV1, CB1, and NGF in human corneal endothelial cells (HCECs) was investigated. $[Ca^{2+}]_i$ was measured by fluorescence calcium imaging and whole-cell currents were measured by the planar patch-clamp technique. The human HCEC line (HCEC-12) was used as an established *in vitro* cell model and a TRPV1 transduced HCEC-12 (TRPV1-HCEC-12) was used as a heterologous cell expression system. Extracellular application of 10 µM capsaicin (CAP) led to an increase of the fluorescence ratio (f_{340}/f_{380}), which is proportional to $[Ca^{2+}]_i$, and an increase of whole-cell currents. Both effects were inhibited by the TRPV1 antagonist capsazepine (CPZ) (10 µM). The CB1 agonist WIN 55,212-2 (10 µM), increased $[Ca^{2+}]_i$ and whole-cell currents, which could be blocked with the CB1 antagonist AM251 (10 µM). The CAP (10 µM) induced Ca^{2+} rise was inhibited below the Ca^{2+} baseline if the HCEC-12 cells were preincubated with 10 µM WIN 55,212-2, whereas 10 µM AM251 only slightly influenced this effect. The CAP-induced Ca^{2+} increase was at considerably higher levels in TRPV1 transduced-HCEC-12 than in non-transduced HCEC-12 (controls). The WIN 55,212-2-induced Ca^{2+} response pattern was changed if the cells were preincubated with CAP or CPZ (both 10 µM). Finally, NGF (50 ng/ml) increased $[Ca^{2+}]_i$, which was suppressed by CPZ. Taken together, the functional expression of CB1 and TRPV1 was first shown in normal HCEC-12 as well as in TRPV1-HCEC-12, in which the effects were

at higher levels confirming the successful overexpression of TRPV1 in HCEC-12. Furthermore, there is a crosstalk between TRPV1 and CB1 as well as NGF indicating a complex Ca^{2+} regulation in HCEC-12. The results contribute to a better understanding of Ca^{2+} regulatory mechanisms and may be useful for the development of novel strategies to improve the preservation of corneal grafts for keratoplasty.

1. INTRODUCTION

1. 1. Anatomy of the human cornea

The human cornea is situated in front of the iris and pupil and is essential for supporting normal visual acuity. It is the densest neural tissue in the human body, which accounts for its exceptionally high pain sensitivity (1, 2). Most corneal nerves are sensory nerves that are ophthalmic branches of the trigeminal nerve. Therefore, many diseases that occur in the cornea can be remarkably painful (2, 3). In an adult, the average horizontal diameter of the cornea is about 11.5 mm, the maximum curvature of the vertical diameter cornea is 10.5 mm, and it maintains a reasonably uniform shape throughout its life cycle (4, 5). The cornea is avascular, and the branches of the anterior ciliary artery stop at the limbus, where they form an arcade to supply essential nutrients to the surrounding cornea. Therefore, the normal human cornea appears transparent, which is essential for preserving visual acuity.

The human cornea is a five-layered structure (6, 7) (Fig. 1). It includes the epithelial layer, Bowman's layer, the stroma layer, the Descemet membrane layer, and the endothelial layer (3). The epithelium has 5 – 6 layers and contains three different cell types: wing cells, basal cells, and surface cells. The superficial cells are composed of 2 – 3 layers of flat polygonal cells. In humans, the thickness of superficial cells is about 50 μm (7, 8). Bowman's layer is the acellular condensate behind the epithelial basement membrane (7). The stroma constitutes nearly 90% of the corneal thickness. This layer is a collagen-rich central layer in which there are embedded keratocytes that occupy 3 – 5% of the stromal volume (9). Descemet's membrane is a relatively transparent, thick, dense and acellular matrix, separating the posterior corneal stroma from the innermost corneal endothelium (7). Behind the Descemet's membrane is a single layer of corneal endothelial cells (10). The endothelial cells form a homogeneous hexagonal structure in humans, and they have no regeneration potential (11). Over time, endothelial cells continue to be flattened and they become stable at a specific thickness after reaching adulthood (9). The corneal endothelial cell density (ECD) at birth is about 3,500 – 4,000 cells/mm^2 in humans (12). For example, the mean ECD is 3,746 ± 370 cells/mm^2 in children

between 0.1 and 5 years old (13). In the Caucasian population, the cell density at ages less than 20 years old is 3,101 ± 268 cell/mm^2. A study has shown that there is a strong inverse correlation between age and ECD, which means that ECD decreases throughout its lifetime (Fig. 2). Other reports revealed that endothelial cells are lost over their lifetime at a rate of 10.92 cells/mm^2 per year (14).

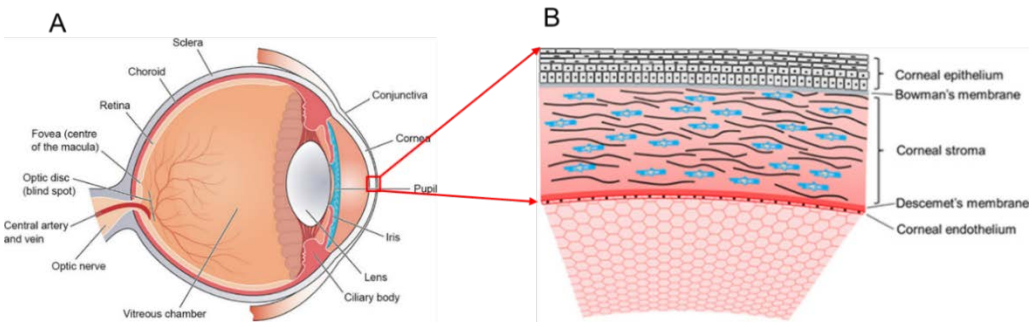

Fig. 1 | **Anatomical and histological illustration of ocular structures supporting normal vision. (A)** The transverse section of the eye shows that the cornea is the tissue in front of the eye, covering an area that accounts for about 1/6 of the outer wall of the eyeball (15). Reused with the kind permission from the American Physiological Society. **(B)** Details of the corneal histology show that human corneal endothelial cell (HCEC) constitute a monolayer of uniform hexagonal-shaped cells lining the innermost surface of the cornea (16). Reused with the kind permission of IOP Publishing.

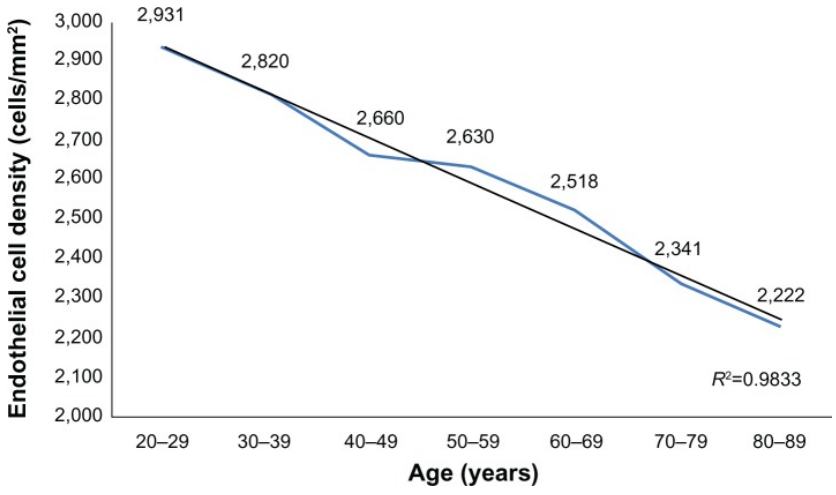

Fig. 2 | Age-dependent declines in endothelial cell density (ECD) (17). This diagram shows that corneal ECD gradually decreases with age. Reprinted with the kind permission of Dove Medical Press.

1.2. Function and physiology of the human cornea

The human cornea is like a window of the eye and its epithelial layer has a protective function to prevent harmful substances from entering the eye. The cornea, together with the lens for focusing impinging light on the retina, provides us with clear vision (3). Additionally, the cornea also acts as a filter to protect the retina from ultraviolet damage (18). At its surface, the corneal epithelium plays a vital role in vision and is the front line of the innate immune system, protecting the eyes from microbial invasion (19). Bowman's layer may play a role in protecting the subepithelial nerve plexus that passes through the anterior stroma (7). Many characteristics of the cornea, including its transparency, morphology and strength are attributed to its anatomical structure as well as stromal organization and composition (7, 20). The human corneal endothelium (HCE) layer plays a critical role in maintaining favorable vision and corneal transparency because it contains many sodium-potassium adenosine triphosphatase (Na^+/K^+-ATPase) pump sites and tight junctions, and it has minimal apoptotic properties (Fig. 3) (21). Notably, the most important tissue to maintain the transparency of the cornea is the corneal endothelium through its provision of barrier and an ion "pump" functions (22). The low transcellular electrical resistance facilitates nutrient uptake and the release of metabolites from the stroma into the anterior chamber. The primary role of the corneal endothelium is to regulate tissue hydration through controlling osmotically coupled fluid flow from the stroma into the aqueous humor. The activity of the Na^+/K^+-ATPase pumps expressed on the human corneal endothelial cell (HCEC) basolateral membranes maintains corneal transparency through mediating adequate fluid egress from the stroma, which offsets maladaptive increases in fluid imbibition by the stroma (9, 23-25). If the HCEC density declines, the remaining endothelial cells will increase their surface area, ensuring sufficient cell coverage to maintain corneal clarity. But to maintain the appropriate pump function, a critical number of HCEC is required. If HCEC can no longer maintain a proper fluid balance, the tissue thickness increases. As a result, there is stromal swelling due to excess fluid accumulation, which disrupts the collagenous stromal structure. Because of stromal thickening, the tissue loses its transparency, which is followed by visual impairment (26).

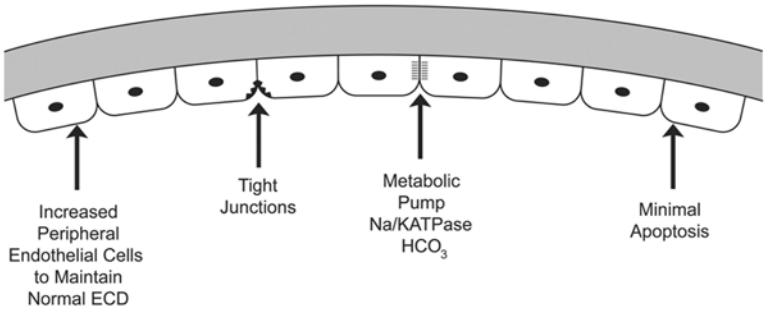

Fig. 3 | Diagrammatic representation of normal corneal endothelial functions maintaining corneal thinness and transparency (21). Reused with permission from the Vision and Ophthalmology Research Association.

Studies have pointed out that the corneal endothelial "pump" function and barrier function are responsible for regulating the hydration of the stromal matrix to maintain corneal transparency (7, 27). Numerous studies have indicated that the pump requires primary active transport (Na^+-K^+ ATPase), whose function is optimized with bicarbonate. These findings suggested that the pump mechanism is a bicarbonate secretory process (28). Electrophysiological evidence shows that the HCEC express multiple types of different ion channels, such as store-operated calcium channels (SOCCs) (e.g. TRPC4 in bovine endothelial cells), voltage-operated Ca^{2+} channels (VOCCs) (e.g. L-type channel), and potassium ions (K^+) channels (29-31). The corneal endothelium has a barrier function, and the maintenance of the barrier function depends on the calcium present in the extracellular environment (32). Therefore, regulation of the intracellular Ca^{2+} level is essential for preventing corneal swelling, which leads to losses in tissue transparency and disruption of normal vision (33).

1.3. Corneal endothelial cell loss and corneal transplantation (keratoplasty)

In humans, corneal endothelial cell density decreases with age, trauma, inflammation, and other diseases (34). The molecular mechanism leading to the loss of HCEC is still unclear. A report on ion channel and cell signaling indicated that exposure to oxidative stress induced apoptotic events as a consequence of declines in their activity (35). Another study showed that increased expression of inflammatory cytokines may cause this loss of function

(36, 37). The lack of corneal endothelium - or changes in corneal endothelial function due to various reasons - can lead to corneal edema, gradual loss of corneal transparency, and severe blindness (34, 38, 39). Since HCEC do not have a proliferative capacity in humans, the only feasible restorative method is to perform keratoplasty when the corneal endothelial cell sum is insufficient to sustain corneal transparency.

The leading causes of corneal endothelial disease (CED) include Fuchs' dystrophy, iris corneal endothelial syndrome, pseudophakic bullous keratopathy, and endothelial dysfunction after corneal transplantation and cataract surgery (22). Corneal edema is one of the most serious complications after intraocular surgery, mainly due to endothelial injury (40). Studies have shown that the loss of central endothelial cells ranges from 4% to 25% after phacoemulsification (41). At present, transplantation is the only feasible solution for treating CED. Studies have demonstrated two main types of corneal transplantation for treating CED, namely penetrating keratoplasty and endothelial keratoplasty. Penetrating keratoplasty involves replacing all of the corneal layers of a donor cornea. Endothelial keratoplasty means the selective replacement of the posterior segment of the cornea (42). In addition, due to the increasing shortage of donor corneas worldwide, there is an urgent need to implement effective therapies to increase the availability of viable eye bank donor corneas (22, 43).

Endothelial keratoplasty has been used worldwide as an alternative method for penetrating keratoplasty (PK) to treat corneal endothelial diseases. Figure 4 illustrates the different types of keratoplastic procedures used to surgically restore corneal function. Descemet stripping (automatic) endothelial keratoplasty (DSEK/DSAEK) may be regarded as the current standard, and Descemet membrane endothelial keratoplasty (DMEK) may lead to further improved clinical outcomes (44) (Fig. 4). Both deep lamellar endothelial keratoplasty (DLEK) and the use of Descemet membrane technology are advantageous because they could possibly reduce astigmatism and the incidence of allograft rejection (45). In addition, DMEK also has the potential to provide faster vision recovery. Although endothelial cell survival may improve using currently available implantation techniques, reducing iatrogenic cell loss may still continue to be a challenge in endothelial keratoplasty (46, 47).

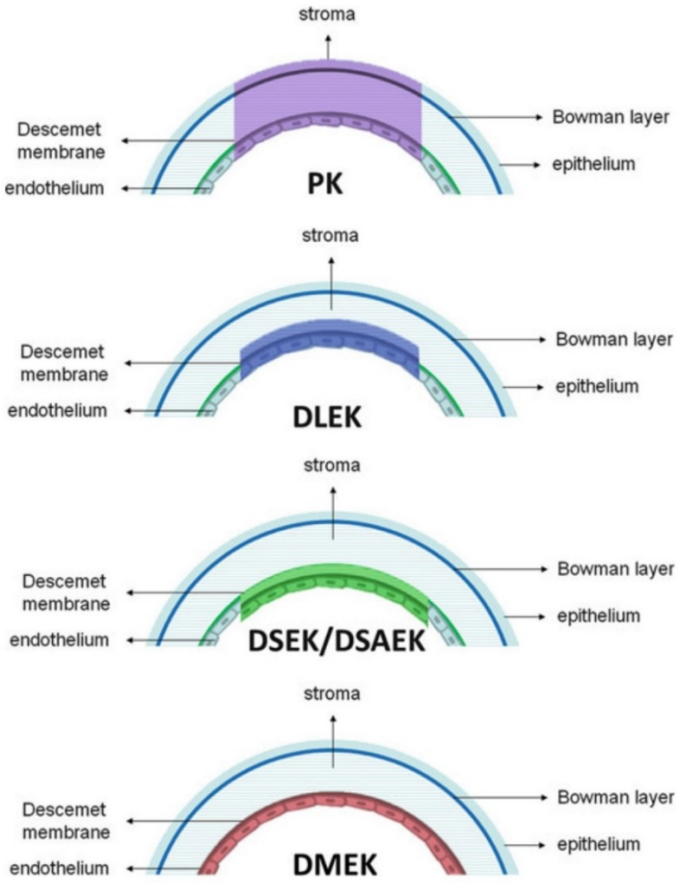

Fig. 4 | Schematic representation of penetrating keratoplasty and endothelial keratoplasty (48). PK = penetrating keratoplasty, DLEK = deep lamellar endothelial keratoplasty, DSEK/DSAEK = Descemet stripping (automated) endothelial keratoplasty, DMEK = Descemet membrane endothelial keratoplasty. Reprinted with kind permission from Springer Nature.

1.4. Calcium ion (Ca^{2+}) channels

Ion channels are cell membrane proteins whose functional modulation is critical for mediating signal transduction events underlying responses essential for normal tissue function (49). Among them, the Ca^{2+} channels include VOCCs, SOCCs, and receptor-operated Ca^{2+} channels (ROCCs) as well as ligand-gated cation channels (LGICs) and TRP channel subtypes (Fig. 5). Ca^{2+} transients induced by channel activation act as second messengers controlling numerous cellular processes, including cell proliferation, transmitter release, gene transcription, muscle contraction, cell migration and apoptosis (50). VOCCs are transmembrane ion channel proteins that selectively conduct Ca^{2+}

through the cell membrane in response to depolarization of the membrane potential (51).

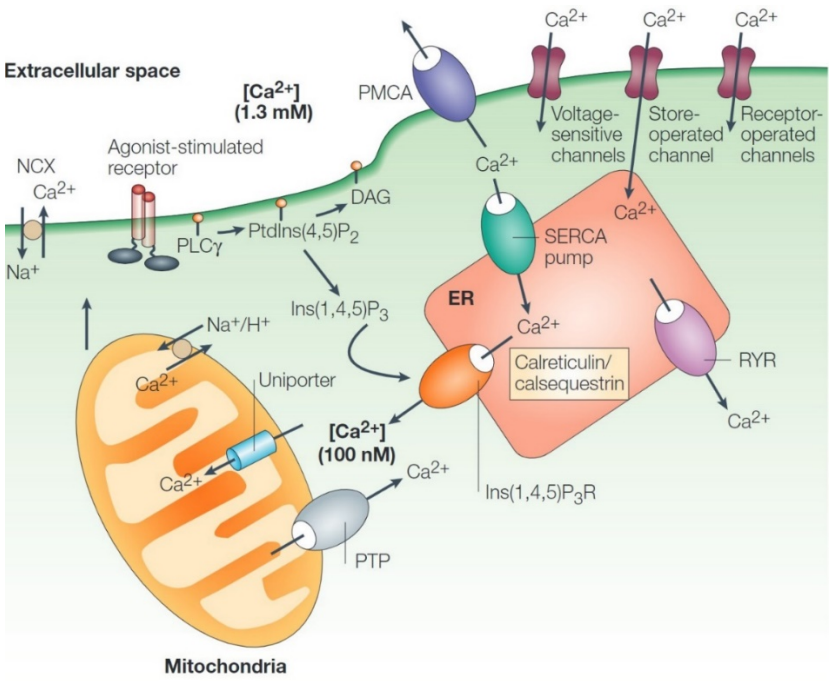

Fig. 5 | Diagrammatic representation of entities mediating responses to stimuli through the modulation of intracellular calcium ion (Ca^{2+}) levels (52). These pumps and channels, which are activated by a host of different stimuli, control intracellular Ca^{2+} concentration ($[Ca^{2+}]_i$). The influx of Ca^{2+} into cells through the plasma membrane occurs largely by activating voltage-sensitive-, store-operated-, and receptor-operated channels. Reprinted with kind permission from Springer Nature.

VOCCs are found in excitable cells like nerve and muscle but also in non-excitable cells such as HCEC. Specifically, Mergler et al. first detected the voltage-operated L-type channel in HCEC in 2003 (29, 53). On the other hand, SOCC seems to be very common, apparently present in all eukaryotes from yeast to humans. Therefore, it can be argued that SOCC represents the original Ca^{2+} entry pathway (54). LGIC is a complete membrane protein that contains a pore that regulates the passage of selected ions (55).

1.4.1. Transient receptor potential channels (TRPs) in the human cornea

TRPs form a superfamily of non-selective cation channels made up of at least 28 different subtypes. The first of these subtypes was discovered in 1969, when Cosens and Manning revealed the phenotype of a spontaneous Drosophila

mutant that are behaviorally impaired since they display only a transient rather than a sustained response to bright light (56). Subsequently, numerous studies in the last 20 years have uncovered the functional expression of an ever increasing number of different subtypes in many different tissues of the human body (57). TRPs play a crucial role in regulating sensations such as pain, inflammation, fibrosis, and neovascularization (58, 59). These 28 different TRP subtypes are divided into seven significant subfamilies (Fig. 6) (32, 60) in mammals. These seven TRP channel subfamily members are similar in structure, usually having six transmembrane helices, a hypothetical pore-forming loop, three to four ankyrin repeats, coiled-coil domains, C-terminals, calmodulin/inositol trisphosphate (IP3) binding regions, and TRP multifunctional sites (61, 62) (Fig. 7). Based on sequence homology, members of the transient receptor potential channel vanilloids (TRPV) subfamily were grouped accordingly: transient receptor potential channel vanilloids 1 – 6 (TRPV1 – 6) (63, 64).

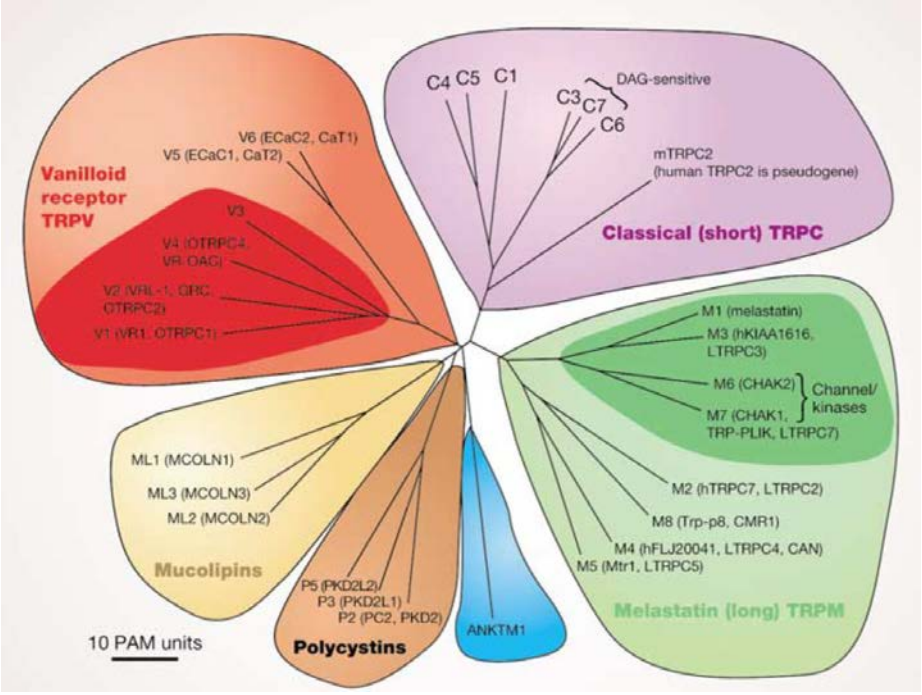

Fig. 6 | TRP ion channel family tree (65). The six subfamilies Transient receptor potential channel vanilloids (TRPV), TRP channel mucolipins (TRPML), TRP channel polycystins (TRPP), TRP channel ankyrin (TRPA), TRP channel melastatin (TRPM), and TRP channel canonical (TRPC) are divided by different color labelling, and they are identified in mammals. The subfamily TRP channel NO-mechano-potential (TRPN) has only been detected in the worm,

Drosophila, and zebrafish (60). Reused with permission from Springer Nature.

The activity of some TRPs is regulated by heat (e.g. thermo-TRPs like TRPV1 or TRPM8) and mechanical perturbations (e.g. TRPV4) or cellular signaling associated with G protein-coupled receptors (GPCRs) (33, 66, 67). Ca^{2+} signaling can be either initiated by TRPs themselves or by GPCRs, which leads to a feedback regulation (68). This interaction has been described in the literature as the so-called GPCR-TRP axis (reviewed in (66)). Therefore, TRPs are one of the most involved downstream targets of Ca^{2+} signaling (68). Furthermore, studies described some TRPs such as TRPV6 or TRPM3 as store-operated channels (SOCs), which could be activated after store depletion. However, the classification of these TRPs as SOCs are still not established according to Nilius et al. (60). Notable, retinal TRPs in the eye play a vital role in maintaining normal vision (69). In addition, some of their subtypes can convert environmental stress into cell signals, which can regulate different physiological responses of cells (70).

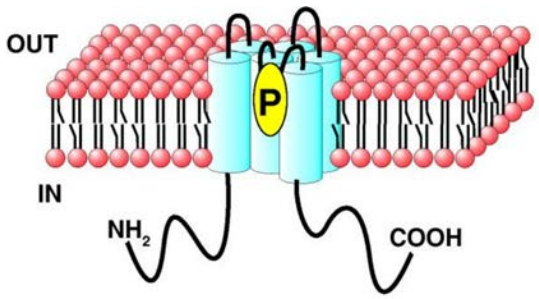

Fig. 7 | Diagrammatic representation of TRP channel delimited expression (71). TRP channels include six transmembrane segments and a putative pore region (P). The lengths of the amino and carboxyl ends are variable, and they consist of different sets of binding domains. Reused with kind permission from Springer Nature.

Previous studies have shown that there is a relationship between changes in the expression of functional TRPs and a variety of human corneal diseases. These subtypes of TRPs could become drug targets for reversing the decline in corneal endothelial function (70). Thermosensitive TRPV1 – 4 channel activities were identified in HCEC (Table 1) (26, 32, 64, 72). Mergler et al.

demonstrated that the regulation of TRPV activity by temperature is the basis of a vital homeostatic mechanism that can support corneal endothelial function under different environmental conditions (Table 1) (72). Studies have shown that corneal endothelial cells can adapt to thermal changes. They can also reduce oxidative stress by activating these TRP channel subtypes. In addition, the functional expression of TRPV1 – 3 in HCEC can also contribute to thermal sensing (Table 1) (64). Previous studies revealed that two of the TRP vanilloid subtypes are osmotic sensors. Unlike TRPV1, which can be activated by a hyperosmotic stress, TRPV4 channel activity is stimulated based on increases in both the TRP-like whole-cell currents and $[Ca^{2+}]_i$ rises when these cells are exposed to a hypotonic environment (32). In 2013, Mergler et al. described TRP melastatin subtype 8 (TRPM8) channel activity and its gene expression in HCEC-12 for the first time (Table 1) (26, 29). Another report showed that exposure to a hypertonic stress stimulated TRP vanilloid type 1 (TRPV1) channel activity and subsequently mitogen-activated protein kinase (MAPK) signaling that in turn upregulated the expression of proinflammatory cytokines in human corneal epithelial cells (HCEPs) (73, 74).

Table 1 . Summary of characteristics of TRP activators, inhibitors, functions, and tissue localization (72). Reprinted with permission from Karger Publishers.

	Selectivity, P_{Ca}:P_{Na}	Activation threshold temperature, °C	Pharmacology	Function	Cornea
TRPV1	4 – 10	>43	capsaicin (CAP), capsazepine (CPZ)	osmosensor[1] heat sensor	epithelium (33, 73), keratocytes (75, 76), fibroblasts (77), endothelium (64)
TRPV2	1 – 3	>52	2-APB	heat sensor	endothelium (64)
TRPV3	2.6	30 – 39	2-APB, camphor	moderate heat sensor	epithelium (78), endothelium (64)

TRPV4	6 – 10	24 – 27	4α-PDD, GSK1016790A	moderate heat sensor, osmosensor[2]	epithelium (79), endothelium (32)
TRPV5	>100	–	low $[Ca^{2+}]_i$	Ca^{2+} reabsorption in kidney	–
TRPV6	>100	–	low $[Ca^{2+}]_i$	–	–
TRPM8	3.3	<23 – 28	icilin, menthol, eucalyptol	moderate cold sensor	epithelium (80), nerve fibers (81), keratocytes (76) fibroblasts (76), endothelium (26, 29)
TRPA1	0.8	<17	icilin	cold sensor	endothelium (26, 29)

[1]Activation by hypertonic challenge (33, 64, 73, 77). [2] Activation by hypotonic challenge (32, 79). P = Permeability ratio; $[Ca^{2+}]_i$ = intracellular concentration Ca^{2+}; 2-APB = 2-aminoethoxydiphenyl borate.

1.4.1.1. Function of TRPV1

Pharmacologically, TRPV1 can be activated by capsaicin (CAP), which is responsible for the piquancy of hot-chili peppers (Fig. 8). This earliest described channel subtype was initially named as vanilloid receptor 1 (VR1) (82). TRPV1 are homo-tetramers whose 3D structure resembles that of VOCCs (83). TRPV1 belongs to the vanilloid-subfamily and is the prototype of other TRPs transducing various environmental stresses to cause adaptive responses (74, 84). TRPV1 is the most extensively investigated TRP channel. In 2010, TRPV1 gene-, protein-, and functional expression was firstly identified in HCEC (64). TRPV1 also can be activated by various activation mechanisms such as heating (> 43 °C), hypertonic challenge, lowering pH, endogenous cannabinoids, endogenous vanilloids, and pharmacologically via CAP present in red pepper extract (Table 1) (85-87). Studies have pointed out that activation of TRPV1 receptors induces the release of pro-inflammatory cytokines in sensory neurons (88). The results provided evidence that the TRPV1 channel is one of the most relevant target mechanisms for developing novel analgesics (89).

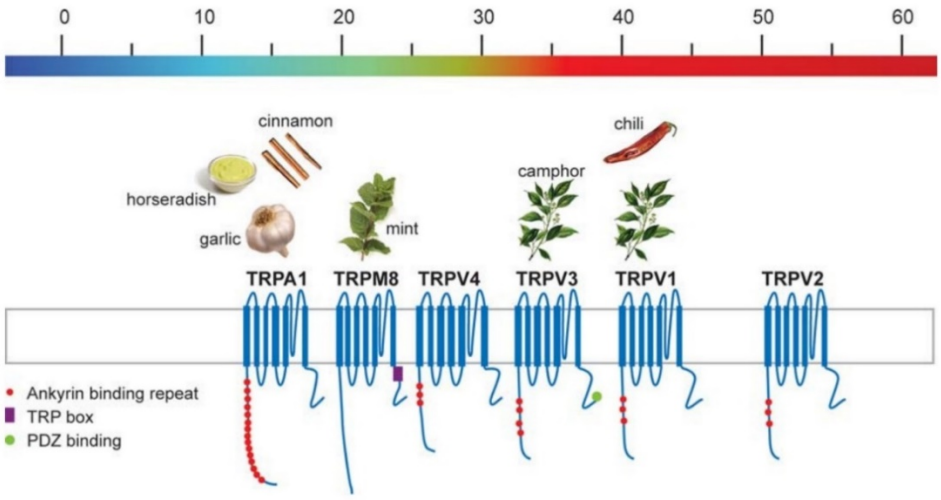

Fig. 8 | Activation of thermo-TRPs by naturally occurring compounds (90, 91). Physically, TRPV1 – 4 can be activated by heating, whereas TRPM8 and TRPA1 can be activated by cooling. Besides naturally occurring compounds, TRPV1 and TRPV4 can be activated by changing the osmolarity. In addition, TRPV1 can be also activated by pH lowering. Reused with permission from Annual Reviews.

1.5. Function of cannabinoid receptor subtype 1 (CB1)

Cannabinoid receptors are a type of GPCR, and they are composed of two subtypes, i.e., CB1 and cannabinoid receptor subtype 2 (CB2). Both are mainly present in the human brain. In addition, studies have detected CB2 in spleen macrophages and other immune cells. CB1 and CB2 also exist on nerves or non-neural tissues (92). The CB1 receptor regulates ion channels, thereby inducing, for example, the activation of inwardly rectifying K^+ channels and the inhibition of N-type as well as P/Q-type VOCCs (93). CB1 can be activated by specific agonists such as WIN 55,212-2 (94). CB1 also regulates many critical physiological processes in different tissues through guanosine-5'-triphosphate (GTP)-binding protein, including pain, analgesia, neurotransmitter release, control of immune cell function, and regulation of energy homeostasis (95, 96). Some studies showed that cannabinoid receptors are abundantly distributed on cutaneous nerve fibers and mast cells as cannabinoid receptor agonists can suppress inflammation, which provides hints for developing them for use in the treatment of injury (97, 98). Some studies also indicated that the cannabinoid system offers potential targets for treating diseases (99).

As early as 1999, the distribution of CB1 was characterized in human eyes. The

widespread distribution of CB1 in the anterior tissues of the human eyes and retinas indicated that cannabinoids in the human eye can perform different physiological functions. CB1 protein expression using immunohistochemistry staining was also detected in the ciliary epithelium, trabecular meshwork, corneal epithelium and endothelium, ciliary muscle, ciliary body blood vessels, Schlemm's canal, and human retina (Fig. 9) (100). Several studies identified co-expression of TRPV1 and CB1 in HCEP, prompting us to hypothesize that CB1 activation reduces TRPV1-induced inflammatory responses. If this prediction can be validated, it will be relevant to determine whether CB1 is a potential drug target for accelerating corneal epithelium wound healing by inhibiting inflammatory responses to injury (Fig. 9) (101-103). Finally, CB1 is also expressed in ocular tumors such as uveal melanoma (UM) and retinoblastoma (RB) which points to the possibility that they may serve as a target to treat these cancerous conditions (104, 105).

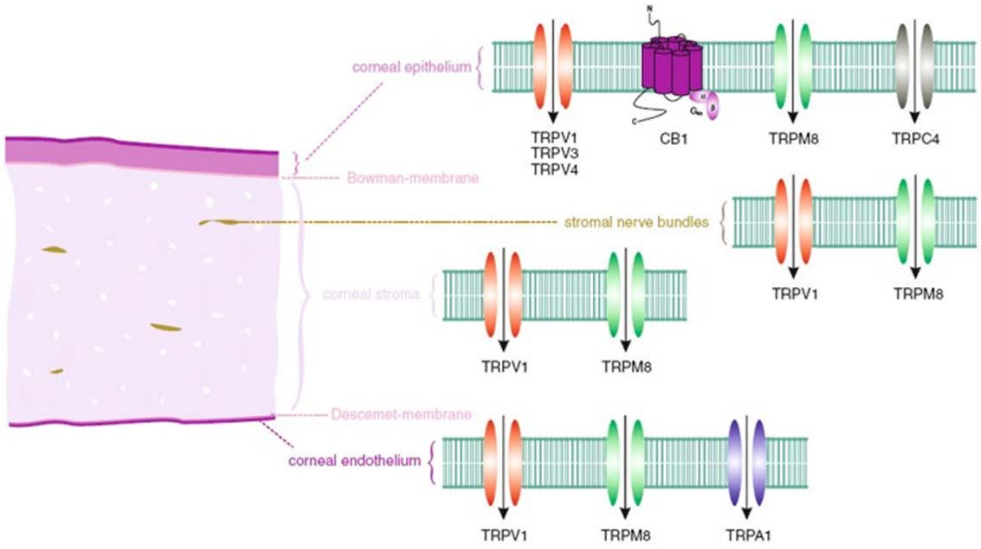

Fig. 9 | TRP and CB1 expression patterns in corneal tissues and cells (106). This simplified scheme describes the localization of TRP subtypes in different corneal tissues. Corneal epithelium expresses TRPV1/3/4 (33, 79, 107), TRPM8 (80), TRPC4 (108), and CB1 (101); corneal stroma expresses TRPM8 (76) and TRPV1 (77); corneal nerve fibers express TRPV1 (109), and TRPM8 (81); corneal endothelium expresses TRPV1 – 3 (64), TRPV4 (32), TRPA1 (26), and TRPM8 (110). Reused with permission from BMC Ophthalmology.

Even if CB1 expression is detected in isolated human corneas, the functional role of CB1 in HCE has so far only been described in HCEP (101, 111). Studies

have also pointed out that TRPV1 and CB1 are co-expressed and interact functionally in other non-ocular tissues (112, 113). Our previous studies showed that HCEC also express VOCC channel currents of the L-type (32, 58). Furthermore, the functional expression of thermosensitive TRPV1 channel and CB1 was confirmed because both CAP and WIN 55,212-2 can induce intracellular Ca^{2+} transients in HCEC (68). Human corneal endothelial cell line 12 (HCEC-12) is a member of the immortalized heterogenous HCEC population. The immortalized HCEC-12 is obtained by transfecting plasmids that encode SV40 t- and T- antigens (53, 114-116). Studies revealed that TRPV1 and CB1 are two potential drug targets for reducing corneal inflammation caused by injury. Strategies involving the inhibition of TRPV1 activation induced by CAP include reducing the Ca^{2+} influx signals that are associated with inhibiting inflammatory responses and in turn accelerating wound healing outcomes (117-120).

1.6. Nerve growth factor (NGF)

NGF is a neurotrophic factor which has been extensively studied for its role in promoting the growth and survival of sympathetic nerves and peripheral sensory cells in mammals (including humans) (121). Animal experiments have shown that tissues innervated by peripheral nerves release and express NGF. NGF is retrogradely transported by specific receptors, ultimately providing protection and functional neuronal integrity (122-124). In recent years, numerous studies have supplied evidence of the effect of NGF on a variety of non-neurocytes. NGF plays a vital role in many biological activities by regulating cell proliferation, and the maintenance of cell survival, migration, function and differentiation, as well as the plasticity of the anterior segment (including the posterior of the eye) (125). Studies have shown that several growth factors in the eye's anterior chamber play potentially important roles in supporting endothelial function and survival. Among these factors, NGF is the most characterized member of the neurotrophic factor family (126). External use of NGF can accelerate tear film production, improve corneal transparency, and enhance visual function in dry eye patients. In addition, studies have shown that topical NGF treatment can be used to reduce corneal surface damage by improving endothelial cell function (127, 128). Studies also showed that NGF is

present in the aqueous humor, its levels increase after eye damage, and it binds to cognate receptors expressed by the corneal endothelium (129).

Further studies have shown that topical administration of NGF eye drops can accelerate corneal wound healing and they have anti-inflammatory and immunomodulatory effects (130). NGF plays a vital role in ocular surface homeostasis and has been extensively studied (29). Among other clinical applications whose effectiveness have not yet been evaluated, NGF is a potential candidate for use as an ophthalmic therapeutic agent. Turner et al. provided the earliest evidence that NGF may play a role in the visual system in 1979 (131). Finally, further studies indicated that NGF can increase the expression of TRPV1 in a variety of neurological diseases through the action of tyrosine kinase A (TrkA) (132) (Fig. 10).

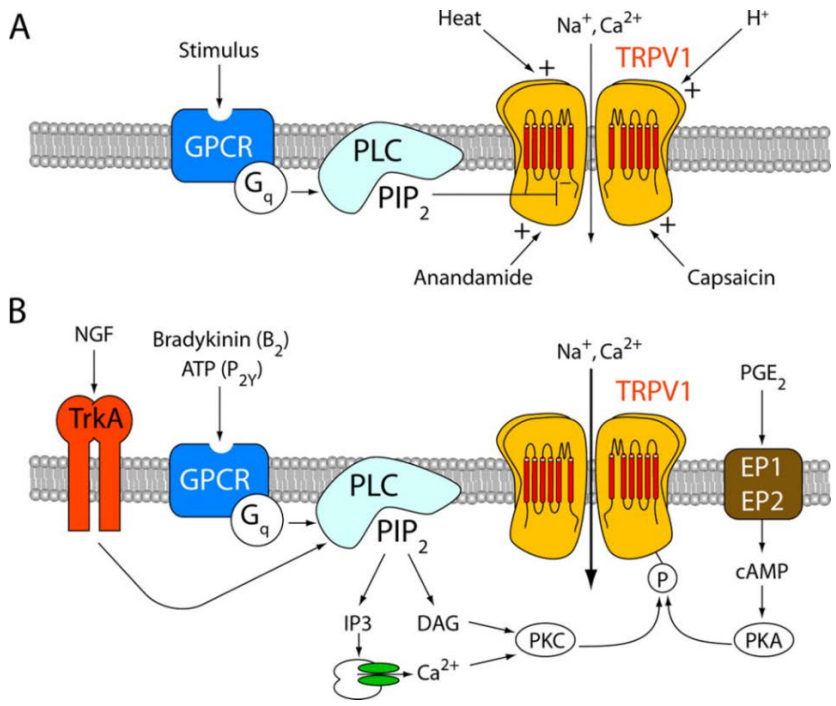

Fig. 10 | Interactions between TRPV1, NGF and bradykinin receptors in modulating the influx of sodium (Na^+) and calcium (Ca^{2+}) in nociceptive afferents (60, 132). (A) shows that TRPV1 is activated by acid (pH ≤ 5.9), noxious heat (≥ 43 °C), anandamide, and capsaicin (CAP). The ligands of guanine nucleotide-binding GPCRs that activate phospholipase C (PLC) induce hydrolysis of phosphatidyl 4,5, diphosphate (PIP_2), inhibiting the TRPV1 channels in neurologic disease. **(B)** indicates that sensing neuropathic pain depends on protein kinase A (PKA) or protein kinase C (PKC) activation inducing the sensitization of TRPV1, phosphorylation of nerve growth factor (NGF), increasing TRPV1 expression through the tyrosine kinase A (TrkA) receptor (132). Reused with kind permission from Wolters Kluwer Health, Inc.

1.7. Specific aims of the study

Based on the previous findings about the electrophysiological characteristics of HCEC-12 and primary cultivated HCEC, the following aims were undertaken:

1. To validate the functional expression of TRPV1 in human corneal endothelial cells (HCECs). Specifically, the CAP-induced activation of TRPV1 between TRPV1 transfected HCEC-12 (TRPV1-HCEC-12) and its normal HCEC-12 counterpart will be compared.
2. To characterize and compare the functional expression levels of CB1 in normal HCEC-12 and TRPV1-HCEC-12. This is done based on evaluating the WIN 55,212-2-induced activation of CB1 and the resulting Ca^{2+} influx with and without the CB1 blocker AM251.
3. To analyze a possible cross talk between TRPV1 and CB1 in HCEC-12. The effects will be evaluated of CB1 receptor activity modulation of CAP-induced increases in Ca^{2+} levels. Specifically, WIN 55,212-2 will be used as a specific CB1 agonist, and AM251 as a corresponding CB1 antagonist. The effects will be determined of TRPV1 channel activation with CAP, or its blockage with capsazepine (CPZ), on WIN 55,212-2-induced Ca^{2+} transients.
4. Although studies have shown that the corneal endothelium expresses NGF receptors (126), the mechanism underlying how NGF induces Ca^{2+} transients in endothelial cells has not yet been determined. Therefore, the NGF-induced Ca^{2+} increase will be investigated with and without the TRPV1 channel blocker CPZ to probe for a possible crosstalk between NGF and TRPV1 in HCEC-12.

2. MATERIALS AND METHODS

2.1. Materials

Table 2 . Laboratory reagents

Article	Company
Calcium chloride	Sigma-Aldrich, Darmstadt, Germany
Sodium chloride	Carl Roth GmbH + Co. KG, Germany
Potassium chloride	Merck KGaA, Germany
Distilled water	B.BRAUN Melsungrn AG, Deutschland
Fetal bovine serum (FBS)	Biochrom, Berlin, Germany
Ethanol	Avantor Performance Materials B.V., Netherlands
Fura-2/AM	PromoCell, Heidelberg, Germany
WIN 55,212-2	CAYMAN CHEMICAL COMPANY, Ann Arbor, Michigan, USA
CAP	Sigma-Aldrich, Darmstadt, Germany
CPZ	CAYMAN CHEMICAL COMPANY, Ann Arbor, Michigan, USA
AM251	CAYMAN CHEMICAL COMPANY, Ann Arbor, Michigan, USA
HEPES	Carl Roth GmbH + Co. KG, Germany
Dimethyl sulfoxide (DMSO)	Sigma-Aldrich, Darmstadt, Germany
Penicillin/streptomycin	Biochrom, Berlin, Germany
Accutase	EMD Millipore Corp., USA
PBS	Gibco, Life Technologies Limited, UK
Cesium chloride	Sigma-Aldrich, Darmstadt, Germany
Dulbecco's modified Eagle medium (DMEM)	Biochrom AG, Berlin, Germany
Basic fibroblast growth factor (bFGF)	Invitrogen, Life Technologies, Karlsruhe, Germany
Ham's nutrient mixture F12 (HAM's F12)	Lonza Bioscience, Belgium
Ascorbic acid	Sigma-Aldrich, Germany
Insulin	Sigma-Aldrich, Germany
Trypsin EDTA	Lonza, Basel, Switzerland

2.2. Methods

2.2.1. Cell culture and preparation of medium

TRPV1-transduced HCEC-12 (TRPV1-HCEC-12) are obtained by lentiviral gene transfection (133). HCEC-12 and TRPV1-HCEC-12 were kindly provided by Monika Valtink (Technische Universität Dresden). The cells were cultured in a humidified environment at 37°C in an incubator containing 5% CO_2. The HCEC-12 were grown in sterile-filtered Dulbecco's modified Eagle medium/Ham's nutrient mixture F12 (DMEM/HAM's F12) 1:1, supplemented with sterile-filtered 100 IU/ml penicillin/streptomycin antibiotics and sterile-filtered 10% fetal bovine serum (FBS) (26, 80, 134, 135). The TRPV1-HCEC-12 was grown in medium F99 (a 1:1 mixture of HAM's F12 and Medium 199

was sterile filtered), supplemented with 5% FBS (sterile filtered), 20 µg/ml ascorbic acid (sterile filtered), 20 µg/ml insulin (sterile filtered), 10 ng/ml human recombinant bFGF (sterile filtered), 10 µg/ml puromycin and 100 IU/ml penicillin/streptomycin antibiotics (sterile filtered) (136, 137). The cells were washed two times with PBS (calcium and magnesium-free). Then, the cells were dissociated using accutase, whose activity was stopped with growth medium supplemented with serum (32). The cells were centrifuged at 100x g and seeded onto 25 cm^2 cell culture flasks at a split ratio of 1:10. The cells were also plated onto a 12-well plate containing coverslips for fluorescence Ca^{2+} imaging. The medium was changed three times per week (26).

2.2.2. Cryopreservation and thawing

Freezing: following the end of an experiment, the cells were frozen. First, the HCEC-12 were detached using accutase. DMEM or F99 medium was added to terminate the enzymatic reaction, and the cells were suspended with a pipette. After that, the cells were centrifuged, and the supernatant was aspirated. Lastly, the cell pellet was resuspended in a cold low-temperature medium, i.e., 90% serum-free medium, 10% DMSO (v / v). This was frozen at -80 °C at -1 °C/min and transferred to liquid nitrogen; the cells were not left at -80 °C longer than overnight (138).

Thawing: the cells were quickly thawed until a small ice clump remained in the freezing vial. The contents were transferred from the freezing tube to a pre-warmed growth medium (in a 15 ml centrifuge tube; then, the medium was added to the cells until the tube was nearly filled). The cells were then centrifuged at 100x g for 5 minutes. The supernatant was aspirated. Then, the cells were resuspended in an appropriate amount of growth medium and seeded into a 25 cm^2 cell culture flask so that cells could attach to the surface. The medium was changed within 24 hours to remove any residual DMSO and cell debris (134).

2.2.3. Intracellular calcium fluorescence imaging

The calcium imaging experiment was started once the HCEC-12 and TRPV1-HCEC-12 density had become 80 – 90% confluent on the coverslips in the incubator (Fig. 15 A, B). 1 µM Fura-2/AM (Fig. 11) was used to load the cells at

37 °C for 20 – 40 minutes in a dark incubator. After incubation, the coverslip was rinsed in the bath chamber containing the pre-warmed Ringer-like (control) solution (pH 7.4) to terminate Fura-2/AM uptake. The cells adapted to the room temperature during this process. The Ringer-like solution contained 150 mM NaCl, 1.5 mM $CaCl_2$, 10 mM glucose, 6 mM CsCl, 1 mM $MgCl_2$ and 10 mM HEPES (osmolarity ≈ 300 mOsM). In the blocker experiment, the blocker was also added to the culture medium and preincubated for 20 minutes.

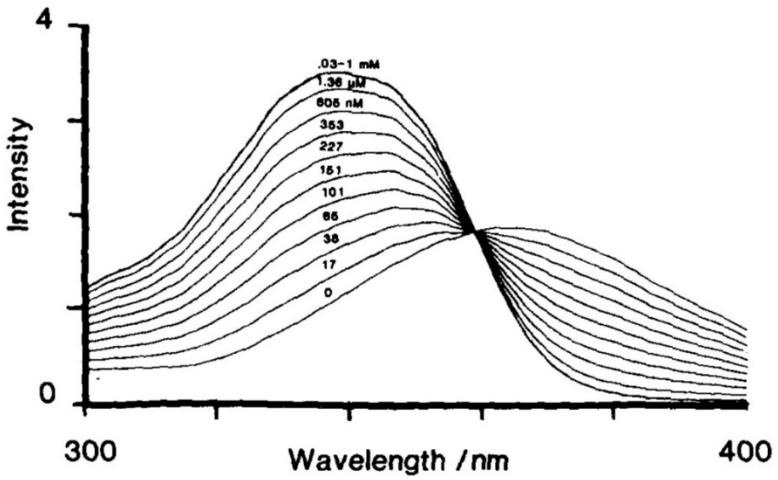

Fig. 11 | The excitation spectrum of 1 mM Fura-2/AM at 20 °C in the indicated Ca^{2+} containing buffers (139). The x-axis shows the range of the excitation wavelength, and the y-axis shows the fluorescence emission level. At 340 nm excitation, the increase in the fluorescence intensity at 510 nm is proportional to the intracellular Ca^{2+} concentration ($[Ca^{2+}]_i$). In contrast, the fluorescence level at 510 nm resulting from excitation at 380 nm increased, whereas it declined from excitation at 340 nm when the intracellular Ca^{2+} decreased at 360 nm, the fluorescence level does not change if the intracellular Ca^{2+} level changes (isosbestic point). Reused with permission from Elsevier.

Before the experiment, the cells were routinely tested to determine if the control baseline remained unchanged within 10 – 20 minutes. The cells were placed on the coverslip in the bath chamber containing the control solution. The microscope focus was adjusted, and the cellSens software was started (Olympus) (Figs. 12, 15). A few minutes after the experiment had started, usually after 4 minutes, an agonist was added into the stationary bath chamber with a pipette, using a pump to remove remaining control solution. The solution exchange was completed after pipetting three times 3 ml of the medium. This experiment was continued for 10 minutes. The same experiment was repeated

in the presence of different channel modulators. Previously, the cells had been preincubated with the drug for about 20 minutes. The experiments were carried out at a room temperature of approximately 18 – 22 °C in a dark room (140). Fura-2/AM fluorescence was excited alternately at 340 nm and 380 nm, and emission was measured at 510 nm. The exposure times of these two excitation wavelengths are not equal (3 sec for 340 nm and 1 sec for 380 nm). Single cells could be marked corresponding to the measurement area (region of interest). Measurements were repeated at least three times from groups of 5 – 20 single cells. Each measurement lasted for 10 minutes, or 15 minutes if applicable. Some agonists and antagonists were dissolved in DMSO at concentrations that did not exceed 0.1% to avoid any cytotoxic effects during fluorescence measurements (141, 142). The results were expressed as mean traces of fluorescence ratio (f_{340}/f_{380}) ± SEM and were evaluated using TIDA software (80, 139). All bar charts were generated using GraphPad Prism version 5 software. The graphs were plotted using SigmaPlot software version 12.5 (Systat Software, San Jose, CA, USA).

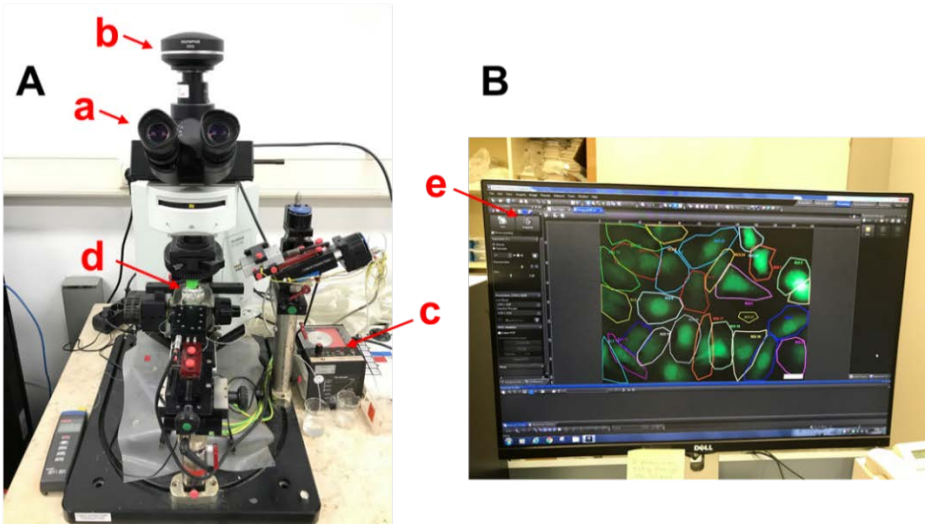

Fig. 12 | Fluorescence Ca^{2+} imaging experimental setup. (A) imaging experimental configuration including the photometry setup (a microscope (a), a camera (b)), a pump (c), a bath chamber (d), and a PC (e). **(B)** shows calcium imaging experimental output in progress (cellSens software by Olympus). Photos by Huan Luo.

2.2.4. Planar patch-clamp technique

The traditional patch-clamp technique process is relatively complicated and requires skilled experimenters since the setup is vibration sensitive. Consequently, the obtaining of meaningful results requires dedicated effort, which is less suitable for the high-throughput experimentation required for drug development. As an alternative, automated parallel patch-clamp measurements using microchip technology were applied in this study (143, 144).

More specifically, a Port-a-Patch setup (Nanion, Munich) was used to acquire and evaluate electrophysiological recordings (145). Before starting the experiment, a single cell suspension was prepared. At this point, the cell culture conditions play a crucial role. Second, intracellular and extracellular solutions were prepared, as well as the required agonists and blockers. The electrode was chloridized in advance to reduce drift of response signals. The intracellular solution (288 mOsmol) was used to measure whole-cell currents. This solution contained 10 mM NaCl, 50 mM CsCl, 20 mM EGTA, 10 mM HEPES, and 60 mM CsF. The pH adjustments to 7.2 were obtained with KOH (288 mOsmol). The extracellular solution contained 140 mM NaCl, 5 mM D-glucose monohydrate, 10 mM HEPES, 1 mM $MgCl_2$, 4 mM KCl and 2 mM $CaCl_2$, and the pH was adjusted to 7.4 with NaOH (298 mOsmol) (146, 147). A seal enhancing solution was used to improve cell sealing. This solution consisted of 80 mM NaCl, 35 mM $CaCl_2$, 3 mM KCl, 5 mM D-glucose monohydrate, 10 mM $MgCl_2$, and 10 mM HEPES (Na^+-salt), and the pH was controlled to 7.4 (298 mOsmol). All experiments were performed in an air-conditioned room at room temperature (22 °C).

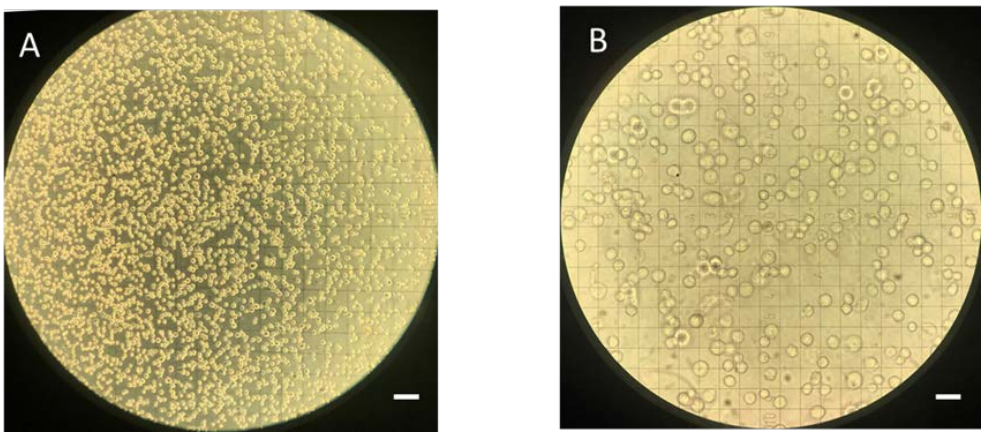

Fig. 13 | Light-microscopic image of a HCEC-12 cell suspension. (A) shows a drop of HCEC-12 cell suspension of single cells. A single-cell suspension is essential for the patch-clamp measurements (Scale bar ≈ 100 µm). **(B)** depicts the same image at a higher magnification. Single cells of different sizes are visible under the microscope (lattice spacing and scale bar ≈ 100 µm). Photos by Huan Luo.

Accutase was required to prepare cell suspensions. The cells were further separated into a single cell solution by rapid suspension with a pipette. The accutase reaction was stopped by adding medium containing serum. After centrifugation, the cells were slightly diluted with the extracellular solution. Before the measurements, a drop of the suspended cell solution was put under a microscope to ensure that single cells could be seen, and that the density was appropriate (Fig. 13). On a device equipped with the aforementioned intracellular and extracellular measuring solution (Nanion solution), 5 microliters of a single cell suspension were gently pipetted on top of a microchip with a small aperture (≈ 1 – 2 µm), having a resistance of a 2.0 – 3.5 MΩ, which is equivalent to the resistance of a normal patch pipette (143, 148) (Fig. 14). A negative suction is automatically applied by a software-controlled pump to draw individual cells onto an orifice on the surface of a microchip (143). Next, the negative pressure suction pulse was generated by the software to rupture the cell membrane (to break into whole-cell configuration). Additionally, the patch-clamp amplifier applied sufficient current to compensate for C-fast and C-slow capacitance transients and series resistances (144). The mean membrane capacitance C_m was 12 ± 1 pF (n = 6) (HCEC-12) and 13 ± 1 pF (n = 10) (TRPV1-HCEC-12) and the mean access resistance of the cells was 43 ± 14 MOhm (n = 6) (HCEC-12) and 31 ± 11 MOhm (n = 10) (TRPV1-HCEC-12),

which was calculated using the Patch-Master software. The liquid junction potential was always compensated for prior to the experiments (LJ = 4 mV) (149). The leak currents were also compensated for using the software. Leak currents larger than 100 pA were discarded from evaluation. The whole-cell currents were measured every 5 seconds using a voltage step between -60 and +130 mV. The holding potential was set to 0 mV to avoid activation of VOCCs. The current results were normalized to the cell membrane capacitance to evaluate the current density (pA/pF) (150). When using the drugs in stock solutions containing DMSO, the DMSO concentration was kept below 0.1% to avoid cytotoxic effects. All bar charts were created using GraphPad Prism software version 5. All other diagrams were plotted using SigmaPlot version 12.5 software (Systat Software, San Jose, CA, USA) in conjunction with an electrophysiological module (Systat, Bruxton).

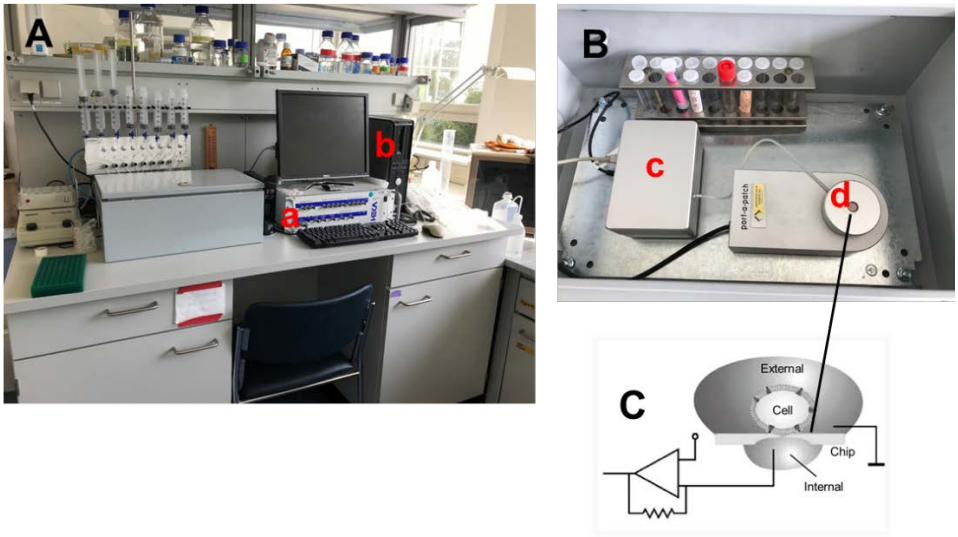

Fig. 14 | Planar patch-clamp configuration. (A) and **(B)** show the smallest planar patch-clamp setup in the world for patch-clamp recordings (photos by Huan Luo). The setup consists of an amplifier (a), a personal computer (b), a pump (c), and a microchip unit (d). The pre-amplifier (head stage) is built into the device. **(C)** shows a simplified scheme of the measuring principle with the microchip unit (143). The resistance of the chip was 2.5 – 3.5 MΩ, which was suitable for the corresponding cell size (143).

2.2.5. Statistical analysis

For paired data, a parametric Student's t-test was applied if the data passed a normality distribution test. Otherwise, the non-parametric Wilcoxon test was

applied. For unpaired data, the Student's t-test was applied if the data were in a normal distribution. If the unpaired data did not pass the normality distribution test, the non-parametric Mann-Whitney U test was applied. Data were collected and processed for statistical analysis using SigmaPlot software Version 12.5 for Windows (Systat Software, San Jose, California, USA). Statistical analyses were generated with GraphPad Prism software version 5.00 for Windows (La Jolla, California, USA). In the bar charts, all values appeared as means ± SEM (error bars in both directions). Among them, *p*-values < 0.05 were considered to be significant.

3. RESULTS

3.1. Cell morphology of normal HCEC-12 and TRPV1-HCEC-12

Firstly, for HCEC-12, a monolayer is shown of similarly arranged polygonal shaped cells of different densities (Fig. 15A). As shown in Figure 15B**,** normal HCEC-12 and TRPV1-HCEC-12 have similar cell sizes and shapes. Interestingly, HCEC-12 have differences in their shapes throughout their growth. Specifically, cells display variable polygonal (Fig. 16A) and spindle shapes (Fig. 16B) in different areas of the same medium prior to reaching confluence. Fig. 15C reveals Fura-2/AM HCEC-12-loaded cells viewed with imaging software. Cells were marked for measuring (ROI = region of interest) (Fig. 15).

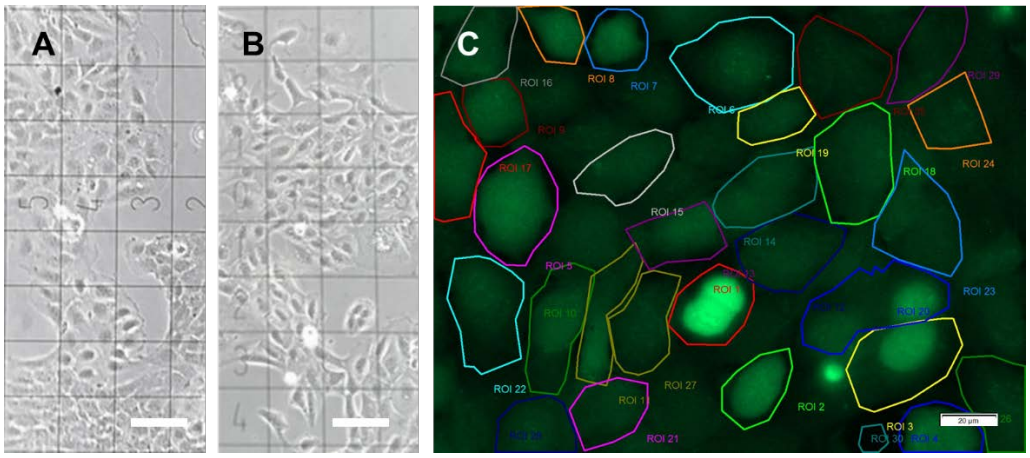

Fig. 15 | Normal HCEC-12 and TRPV1-HCEC-12 cell morphology. (A) Light microscopic image of normal HCEC-12. (Scale bar ≈ 100 µm, photo by Huan Luo). **(B)** Light microscopic image of TRPV1-HCEC-12. (Scale bar ≈ 100 µm, photo by Huan Luo). **(C)** Fluorescence microscopic image shows HCEC-12 on a coverslip after loading with Fura-2/AM (510 nm;

green-colored by imaging software). Some single cells were outlined by hand to mark regions of interest (ROIs) used for optical fluorescence measurements (Scale bar = 20 µm, photo by Stefan Mergler).

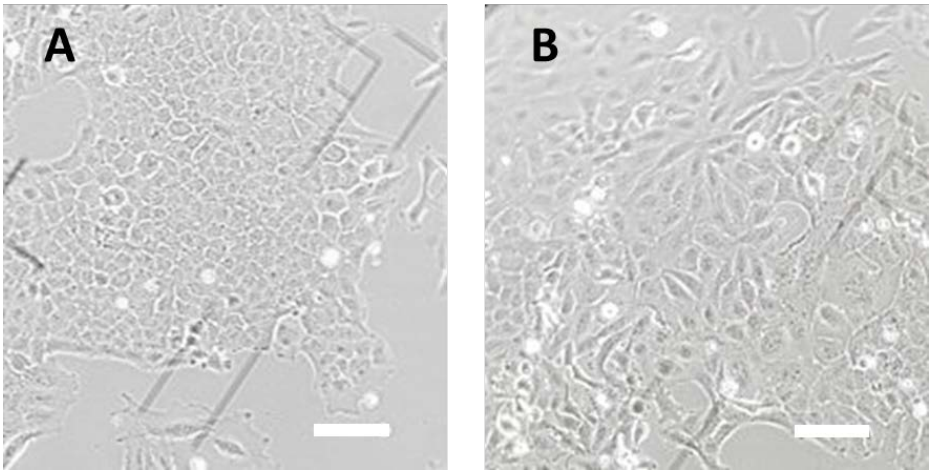

Fig. 16 | Light microscopic images of normal HCEC-12. (A) shows that HCEC-12 are dispersed in a regularly arranged monolayer possessing closely interconnected uniform polygonal shapes (Scale bar ≈ 100 µm, photo by Stefan Mergler). **(B)** shows that HCEC-12 can also have irregular shapes depending on cell density (Scale bar ≈ 100 µm, photo by Stefan Mergler).

3.2. TRPV1 channels in HCEC

3.2.1. Functional TRPV1 expression in HCEC-12 and in TRPV1-HCEC-12

Functional TRPV1 expression was confirmed by measuring Ca^{2+} response patterns after the application of the TRPV1 agonist CAP (10 µM) in HCEC-12 (59). Fig. 17 shows that CAP increased the fluorescence ratio f_{340}/f_{380} from 0.1012 ± 0.0001 at 100 s (control) to 0.1146 ± 0.003 at 600 s (n = 9 – 16, p < 0.005) (Fig. 17A). While the control baseline remained stable (Fig. 17A), these increases were all inhibited by the TRPV1 blocker CPZ (10 µM) (n = 9 – 14, *** p < 0.005) (Fig. 17B, C).

Similar responses of large magnitude could be observed in TRPV1- transfected HCEC-12 (TRPV1-HCEC-12) (Fig. 18). Specifically, CAP increased the fluorescence ratio f_{340}/f_{380} from 0.1029 ± 0.002 at 100 s (control) to 0.2207 ± 0.0298 at 400 s (n = 6, ** p < 0.01) (Fig. 18A). These responses were also blocked by CPZ (n = 6 – 9, *** p < 0.005) (Fig. 18B, C). Taken together, the results demonstrate the functional expression of TRPV1 in normal HCEC-12 as well as transduced TRPV1-HCEC-12. Obviously, the CAP-induced TRPV1

Ca^{2+} response in TRPV1-HCEC-12 was at considerably higher levels compared to normal HCEC-12, indicating the successful upregulation of the functional expression of TRPV1 in the transduced HCEC-12 cells (**Fig. 19**).

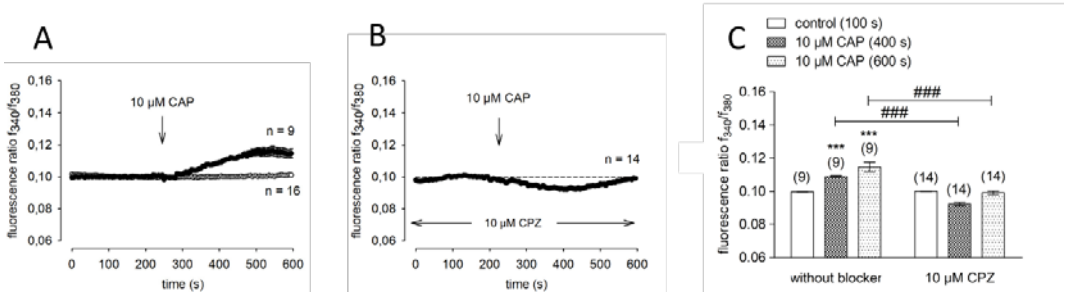

Fig. 17 | Functional expression of TRPV1 in normal HCEC-12. CPZ suppressed CAP induced Ca^{2+} increases in HCEC-12. Drug additions were conducted at the times indicated by arrows. **(A)** 10 µM CAP induced increases in the intracellular Ca^{2+} concentration ($[Ca^{2+}]_i$), shown as filled circles (n = 9), while the control group exhibited a constant Ca^{2+} ratio, shown as open circles (n = 16). **(B)** Except for the presence of 10 µM CPZ, the rest of the conditions are the same as those shown in (A). Notably, CPZ significantly inhibited the increase in Ca^{2+} induced by CAP in HCEC-12 (n = 14). **(C)** Statistical analyses of CAP and CPZ experiments (n = 9 – 14). The comparisons of 10 µM CAP (400 s) without blocker vs. control (100 s), 10 µM CAP (600 s) without blocker vs. control (100 s), 10 µM CAP (400 s) with 10 µM CPZ vs. control (100 s) with 10 µM CPZ, and 10 µM CAP (600 s) with 10 µM CPZ vs. control (100 s) with 10 µM CPZ were conducted by paired t-test or Wilcoxon test; *** $p < 0.005$. The comparisons of 10 µM CAP (400 s) with 10 µM CPZ vs. 10 µM CAP (400 s) without blocker and 10 µM CAP (600 s) with 10 µM CPZ vs. 10 µM CAP (600 s) without blocker were conducted with the unpaired t-test or Mann-Whitney U test; ###$p < 0.005$.

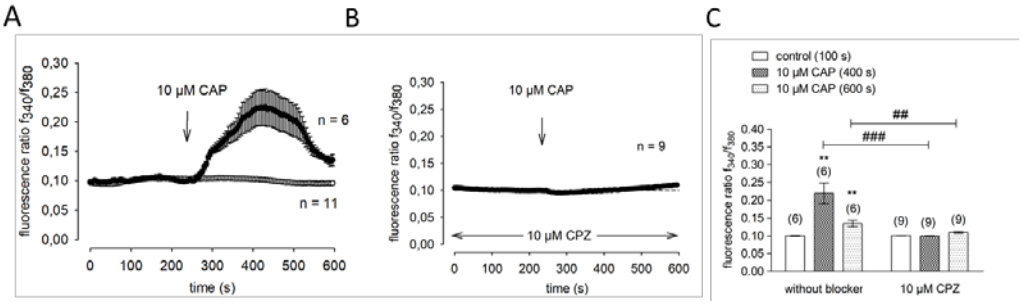

Fig. 18 | CAP induced increases of intracellular Ca^{2+} concentration ($[Ca^{2+}]_i$) in transduced TRPV1-HCEC-12 cells. The drug application is shown with an arrow. **(A)** 10 µM CAP induced larger increases in $[Ca^{2+}]_i$, shown as filled circles (n = 6), while the control group exhibited a constant Ca^{2+} ratio, shown as open circles (n = 11). **(B)** Except for the presence of 10 µM CPZ, the rest of the conditions are the same as those shown in (A). CPZ significantly inhibited the increase in Ca^{2+} induced by CAP in TRPV1-HCEC-12 (n = 9). **(C)** Overview of CAP and CPZ experiments (n = 6 – 9). Summary comparing the effects of 10 µM CAP (400 s) without blocker vs. control (100 s), 10 µM CAP (600 s) without blocker vs. control (100 s), 10 µM CAP (400 s) with 10 µM CPZ vs. control (100 s) with 10 µM CPZ, and 10 µM CAP (600 s) with 10 µM CPZ vs. control (100 s) with 10 µM CPZ were evaluated with the paired t-test or Wilcoxon test; ** $p < 0.01$; The comparisons of 10 µM CAP (400 s) with 10 µM CPZ vs. 10 µM CAP (400 s) without blocker and 10 µM CAP (600 s) with 10 µM CPZ vs. 10 µM CAP (600 s) without blocker were

evaluated with the unpaired t-test or Mann-Whitney U test; ## p < 0.01; ### p < 0.005.

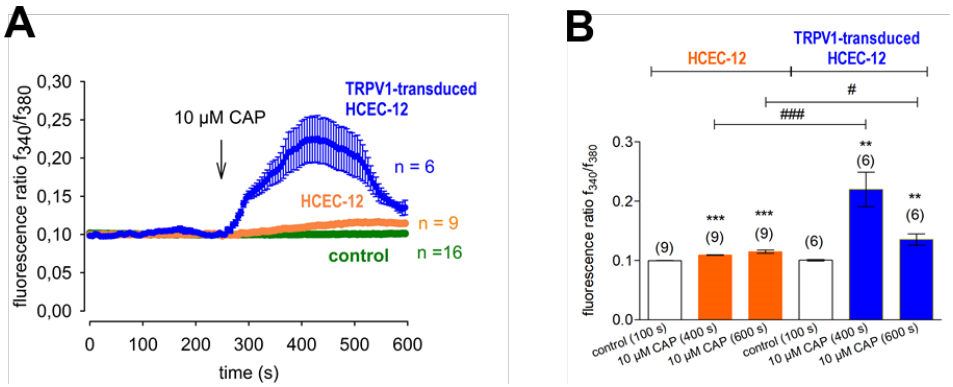

Fig. 19 | Larger CAP-induced Ca^{2+} influxes in TRPV1 transduced-HCEC-12 compared to normal HCEC-12. Summarized data from Fig. 17 and Fig. 18. Drug additions were conducted at the times indicated by the arrows. **(A)** 10 µM CAP induced rises in the intracellular Ca^{2+} concentration ($[Ca^{2+}]_i$) in TRPV1-HCEC-12 (blue filled circles) that were larger than in HCEC-12 (n = 6 – 9, orange filled circles). **(B)** Summary comparison of CAP effects (n = 6 – 9). 10 µM CAP (400 s) in HCEC-12 vs. control (100 s) in HCEC-12, 10 µM CAP (600 s) in HCEC-12 vs. control (100 s) in HCEC-12, 10 µM CAP (400 s) in TRPV1-HCEC-12 vs. control (100 s) in TRPV1-HCEC-12, and 10 µM CAP (600 s) in TRPV1-HCEC-12 vs. control (100 s) in TRPV1-HCEC-12 were evaluated with the paired t-test or Wilcoxon test; ** p < 0.01; *** p < 0.005. The comparisons of 10 µM CAP (400 s) in TRPV1-HCEC-12 vs. 10 µM CAP (400 s) in HCEC-12 and 10 µM CAP (600 s) in TRPV1-HCEC-12 vs. 10 µM CAP (600 s) in HCEC-12 were conducted with the unpaired t-test or Mann-Whitney U test; # p < 0.05; ### p < 0.005.

3.2.2. CAP increased the whole-cell currents in HCEC-12 and in TRPV1-HCEC-12

The planar patch-clamp technique was applied to determine the corresponding currents underlying TRPV1 activation by CAP. In the whole-cell configuration CAP (10 µM) increased the whole-cell currents in HCEC-12 (Fig. 20). Whole-cell current values are time dependent and vary depending on the imposed voltage difference across the seal (Fig. 20A, B). A run-down effect of currents was not clearly detected within the first 5 minutes. At the maximum positive and negative voltage pulse, 10 µM CAP activated typical TRPV1-like inwardly and outwardly rectifying currents in HCEC-12 (Fig. 20B). Specifically, CAP increased the inward current density from -21 ± 2 pA/pF (control) to -69 ± 4 pA/pF ($p < 0.05$; n = 4). This current was inhibited with CPZ (10 µM) to -26 ± 3 pA/pF ($p < 0.05$; n = 4) (Fig. 20C). The CAP outward current density rose from 243 ± 10 pA/pF (control) to 311 ± 19 pA/pF ($p < 0.05$; n = 4), while CPZ inhibited this rise to 209 ± 11 pA/pF ($p < 0.05$; n = 4) (Fig. 20C). Consistently, the CAP

maximum outward current amplitudes increased from the control 100 % to 126 ± 3% (p <0.05; n = 4), which CPZ suppressed to 86 ± 3% (p < 0.05; n = 4) of the baseline value. A similar effect was observed regarding the inward currents. The maximal CAP inward current amplitudes increased from the control 100 % to -148 ± 15 % (p < 0.01; n = 4), which CPZ suppressed to 78 ± 9 % of the baseline value (p < 0.05; n = 4) (Fig. 20D, E).

In TRPV1-HCEC-12, the CAP inward currents rose from -23 ± 2 pA/pF (control) to - 66 ± 8 pA/pF (p < 0.01; n = 11), which CPZ suppressed to -21 ± 2 pA/pF (p < 0.01; n = 11) (Fig. 21C). The maximal CAP outward currents increased from 341 ± 52 pA/pF (control) to 439 ± 57 pA/pF (p < 0.005; n = 11) (Fig. 21C). The maximal CAP inward current amplitudes increased from control 100 % to -112 ± 52 % (n = 11; p < 0.005), which CPZ suppressed to 95 ± 12 % (p < 0.05; n = 7). The maximal CAP outward current amplitudes rose from control 100 % to 142 ± 9 % (p < 0.005; n = 11), which CPZ suppressed to 81 ± 7 % (n = 7; p < 0.05) (Fig. 21D, E). Taken together, the functional expression of TRPV1 was confirmed in both the HCEC-12 and TRPV1-HCEC-12.

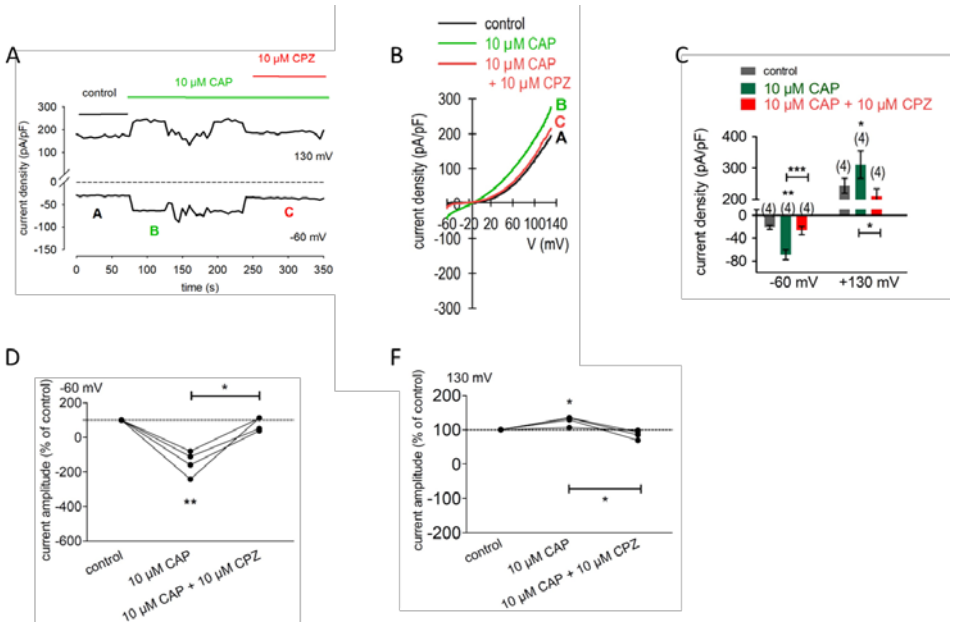

Fig. 20 | CAP-induced increases in the whole-cell currents in HCEC-12. CPZ inhibited CAP-induced increases of whole-cell currents. **(A)** Time dependent monitoring of 10 µM CAP-induced increases in the current density. There were minor fluctuations during the recordings. Exposure to 10 µM CPZ suppressed the CAP-induced current increases. **(B)** Voltage ramp current response plots. The current density is displayed before application (marked as A), during CAP (10 µM) application (marked as B), and for 10 µM CAP + 10 µM CPZ application

(marked as C). **(C)** Overview of CAP and CPZ patch-clamp experiments (n = 4). Significance was evaluated of 10 µM CAP vs. control and 10 µM CAP + 10 µM CPZ vs. 10 µM CAP, which were determined with the paired t-test or Wilcoxon test. **(D)** The maximum negative current amplitude caused by a voltage step (from 0 to -60 mV) is expressed as a percentage of the control value. In the presence of CPZ, the inward current induced by CAP is significantly suppressed (paired t-test). **(E)** The maximum positive current amplitude caused by a voltage step (from 0 to +130 mV) is displayed as a percentage of the control value. In the presence of CPZ, the outwardly rectifying currents induced by CAP are significantly suppressed (paired t-test). *p < 0.05; ** p < 0.01; *** p < 0.005.

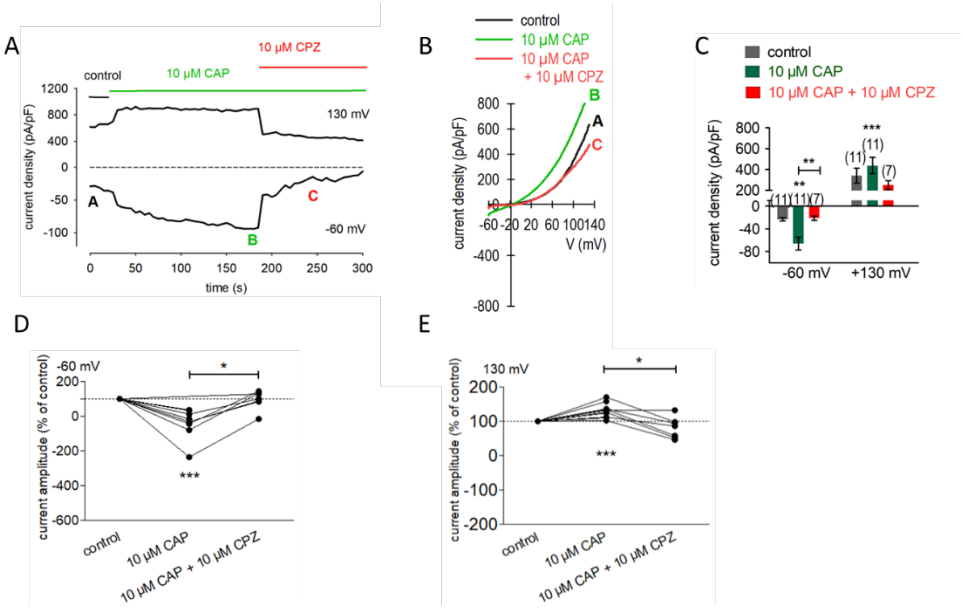

Fig. 21 | CAP-induced TRPV1 activation in TRPV1-HCEC-12. The CAP elicited whole-cell current increases are inhibited by CPZ, a TRPV1 blocker. **(A)** The time course record of 10 µM CAP-induced increase in the current and the 10 µM CPZ-induced decline. **(B)** A typical record contrasting the I-V plots under control conditions (marked as A) with those induced by CAP (10 µM) (marked as B) and 10 µM CAP + 10 µM CPZ application (marked as C). **(C)** Overview of CAP and CPZ patch-clamp experiments (n = 4). Comparisons are provided of 10 µM CAP vs. control and 10 µM CAP + 10 µM CPZ vs. 10 µM CAP based on the results of the paired t-test or Wilcoxon test. **(D)** The maximum negative current amplitude (from 0 to -60 mV) is displayed as a percentage of the control value. In the presence of CPZ, the inward current induced by CAP was significantly suppressed (paired t-test). **(E)** The maximum positive current amplitude (from 0 to +130 mV) is displayed as a percentage of the control value. In the presence of CPZ, the outwardly rectifying currents induced by CAP are significantly suppressed (paired t-test). * p < 0.05; ** p < 0.01; *** p < 0.005.

3.3. Functional CB1 expression in HCEC-12

3.3.1. CB1 activation induces Ca^{2+} transients in HCEC-12 and in TRPV1-HCEC-12

Functional CB1 expression was identified in HCEP and RB cells as well as in UM cells (101, 105, 111). To evaluate CB1 presence in HCEC-12 and in TRPV1-HCEC-12, the effects of the selective CB1 agonist and antagonist pair

WIN 55,212-2 (10 µM) and AM251 (10 µM), respectively, were determined on intracellular Ca^{2+} levels. WIN 55,212-2 increased the fluorescence ratio (f_{340}/f_{380}) from 0.1006 ± 0.0004 at 100 s (control) to 0.1267± 0.0002 at 350 s ($p < 0.005$; n = 41) (Fig. 22A, C), whereas preincubation with the CB1 blocker AM251 inhibited this increase (Fig. 22B, C).

As predicted, some of their effects were similar to one another in the HCEC-12 and in TRPV1-HCEC-12. However, WIN 55,212-2 induced a stable increase in Ca^{2+} response, as compared with a transient response in normal HCEC-12. Specifically, the fluorescence ratio (f_{340}/f_{380}) increased from 0.0990 ± 0.0003 at 100 s (control) to 0.1172 ± 0.0009 at 350 s ($p < 0.005$; n = 17), which remained at a high level (Fig. 23A, C). The CB1 blocker AM251 suppressed this response (Fig. 23B, C). Taken together, these responses are indicative of CB1 activation that are downstream, leading to changes in intracellular Ca^{2+} levels, even though the underlying mechanisms are unclear. The uncertainty that exists is whether CB1 modulates intracellular Ca^{2+} levels through a G_i alpha subunit (G_i) or a G_q alpha subunit (G_q) GPCR (151, 152) (Figs. 22A, 23A).

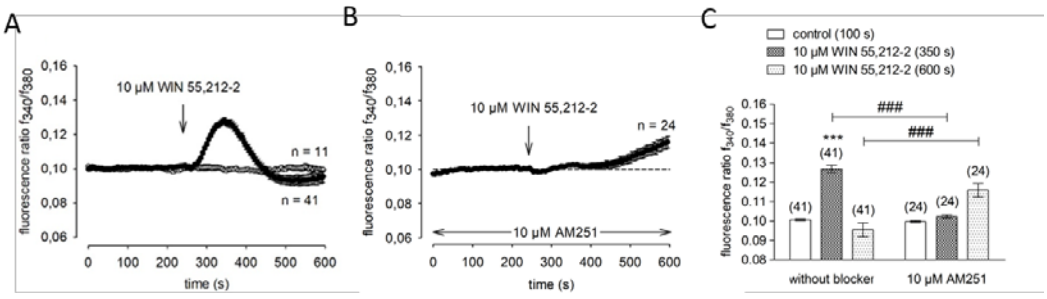

Fig. 22 | Suppression of WIN 55,212-2-induced Ca^{2+} transients by the CB1 blocker AM251 in HCEC-12. Drug applications were applied at the indicated time points. **(A)** WIN 55,212-2 (10 µM) induced increases in intracellular Ca^{2+} concentration ($[Ca^{2+}]_i$), shown as filled circles (n = 41), while the control group exhibited a constant Ca^{2+} baseline, shown as open circles (n = 11). **(B)** Except for the presence of 10 µM AM251, the conditions are the same as those shown in (A). AM251 significantly delayed a WIN 55,212-2-induced increase in Ca^{2+} in HCEC-12 (n = 24). **(C)** Summary of the effects of WIN 55,212-2 and AM251 (n = 24 – 41) in HCEC-12. Comparisons are provided of WIN 55,212-2 (350 s) without blocker vs. control (100 s), WIN 55,212-2 (600 s) without blocker vs. control (100 s), WIN 55,212-2 (350 s) with AM251 vs. control (100 s) with AM251, and WIN 55,212-2 (600 s) with AM251 vs. control (100 s) with AM251. The significance of changes was evaluated based on the results of the paired t-test or Wilcoxon test. The comparisons of WIN 55,212-2 (350 s) with AM251 vs. WIN 55,212-2 (350 s) without blocker and WIN 55,212-2 (600 s) with AM251 vs. WIN 55,212-2 (600 s) without blocker were conducted by unpaired t-test or Mann-Whitney U test. *** $p < 0.005$; ### $p < 0.005$.

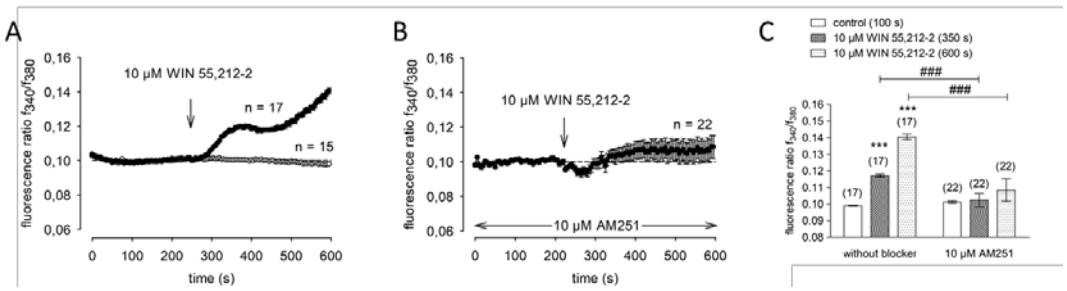

Fig. 23 | AM251 blocked WIN 55,212-2-induced Ca^{2+} transients in TRPV1-HCEC-12. **(A)** In TRPV1-HCEC-12, an irreversible Ca^{2+} increase was initially delayed (n = 17, filled circles). The control cells exhibited a constant Ca^{2+} baseline ratio, shown as open circles (n = 15). Drug applications were conducted at the indicated time points. The data are presented as mean ± SEM (n = 15 – 17). **(B)** Except for the presence of AM251 (10 µM), the conditions are the same as those in (A). AM251 again significantly inhibited the WIN 55,212-2-induced increase in Ca^{2+} (n = 22). **(C)** Summary of the effects of WIN 55,212-2 and AM251 (n = 17 – 22). The comparisons of WIN 55,212-2 (350 s) without blocker vs. control (100 s), WIN 55,212-2 (600 s) without blocker vs. control (100 s), WIN 55,212-2 (350 s) with AM251 vs. control (100 s) with AM251, and WIN 55,212-2 (600 s) with AM251 vs. control (100 s) with AM251 were conducted by paired t-test or Wilcoxon test. The comparisons of WIN 55,212-2 (350 s) with AM251 vs. WIN 55,212-2 (350 s) without blocker and WIN 55,212-2 (600 s) with AM251 vs. WIN 55,212-2 (600 s) without blocker were conducted by unpaired t-test or Mann-Whitney U test. *** $p < 0.005$; ### $p < 0.005$.

3.3.2. AM251 inhibits WIN 55,212-2-induced increases in whole-cell currents in HCEC-12 and in TRPV1-HCEC-12

As shown in Fig. 24, WIN 55,212-2 increased the inward currents from -11 ± 2 pA/pF (control) to -26 ± 4 pA/pF (n = 6; $p < 0.05$) (Fig. 24C), while AM251 inhibited this increase to -13 ± 2 pA/pF in HCEC-12 ($p < 0.01$; n = 6) (Fig. 24C). The maximal outward current amplitude rose from control 100 % to 164 ± 9 % ($p < 0.01$; n = 6). AM251 suppressed this current to 114 ± 6 % ($p < 0.01$; n = 6) (Fig. 24E). The maximal inward current amplitude rose from control 100 % to -97 ± 26 % ($p < 0.05$; n = 6), which AM251 suppressed to 70 ± 9 % ($p < 0.05$; n = 6) (Fig. 24D).

Similarly, in TRPV1-HCEC-12, WIN 55,212-2 increased the inward currents from -11 ± 1 pA/pF (control) to -26 ± 2 pA/pF (n = 11; $p < 0.005$) (Fig. 25C), whereas AM251 suppressed them to -15 ± 1 pA/pF (n = 7 – 11; $p < 0.01$) (Fig. 25C). The outward currents increased from 122 ± 12 pA/pF (control) to 174 ± 20 pA/pF (n = 11; $p < 0.005$) (Fig. 25C). The maximal outward current amplitude rose from control 100 % to 141 ± 5 % ($p < 0.005$; n = 11). AM251 suppressed these outward currents to 103 ± 4 % ($p < 0.01$; n = 11 – 7) (Fig. 25E). The

maximal inward current amplitude rose from its control of 100 % to -53 ± 12 % (n = 11; $p < 0.005$). AM251 suppressed these inward currents to 74 ± 8 % ($p < 0.005$; n = 11 – 7) (Fig. 25D). In summary, the correspondence between the aforementioned Ca^{2+} responses and the underlying changes in ionic currents confirm functional CB1 expression in both the HCEC-12 and TRPV1-HCEC-12.

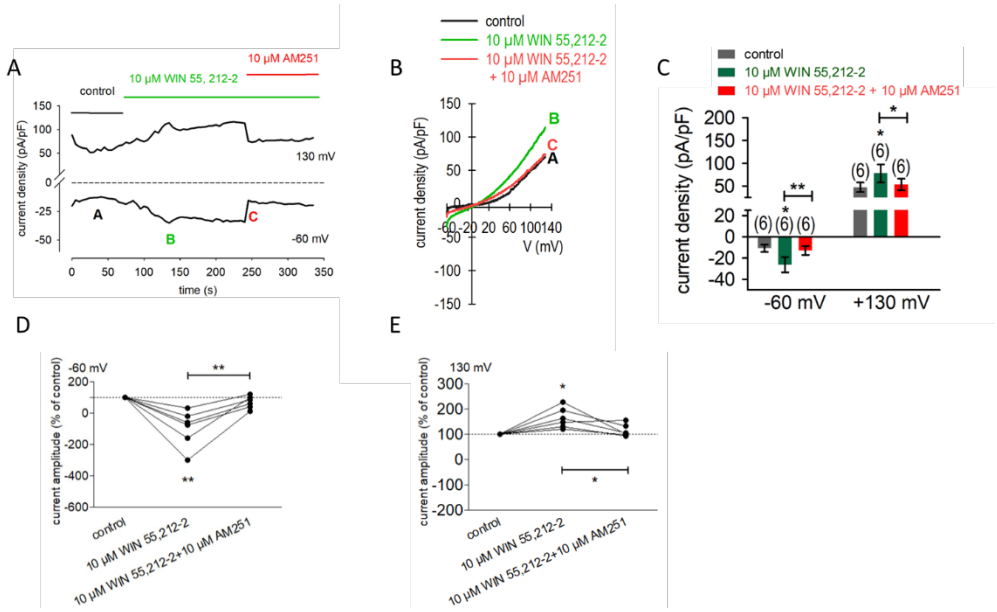

Fig. 24 | AM251 suppresses WIN 55,212-2-induced increases in whole-cell currents in HCEC-12. (A) WIN 55,212-2 (10 µM) induced time dependent increases in whole-cell currents and their reversal by applying 10 µM AM251. **(B)** Effects of 10 µM WIN 55,212-2 on changes in currents induced by the voltage ramp. The current density is displayed before application (marked as A), during WIN 55,212-2 (10 µM) application (marked as B), and for WIN 55,212-2 + AM251 (both 10 µM) application (marked as C). **(C)** Summary of WIN 55,212-2 and AM251 patch-clamp experiments (n = 6). Comparisons of the effect of 10 µM WIN 55,212-2 vs. control and 10 µM WIN 55,212-2 + 10 µM AM251 vs. 10 µM WIN 55,212-2 on currents were conducted by paired t-test or Wilcoxon test. **(D)** The maximum negative current amplitude caused by the voltage step (from 0 to -60 mV) is displayed as a percentage of the control value. In the presence of 10 µM AM251, the inward current induced by 10 µM WIN 55,212-2 was significantly suppressed (paired t-test). **(E)** The maximum positive current amplitude caused by the voltage step (from 0 to +130 mV) is displayed as a percentage of the control value. In the presence of 10 µM AM251, the outwardly rectifying currents induced by 10 µM WIN 55,212-2 were significantly suppressed (paired t-test). * $p < 0.05$; ** $p < 0.01$.

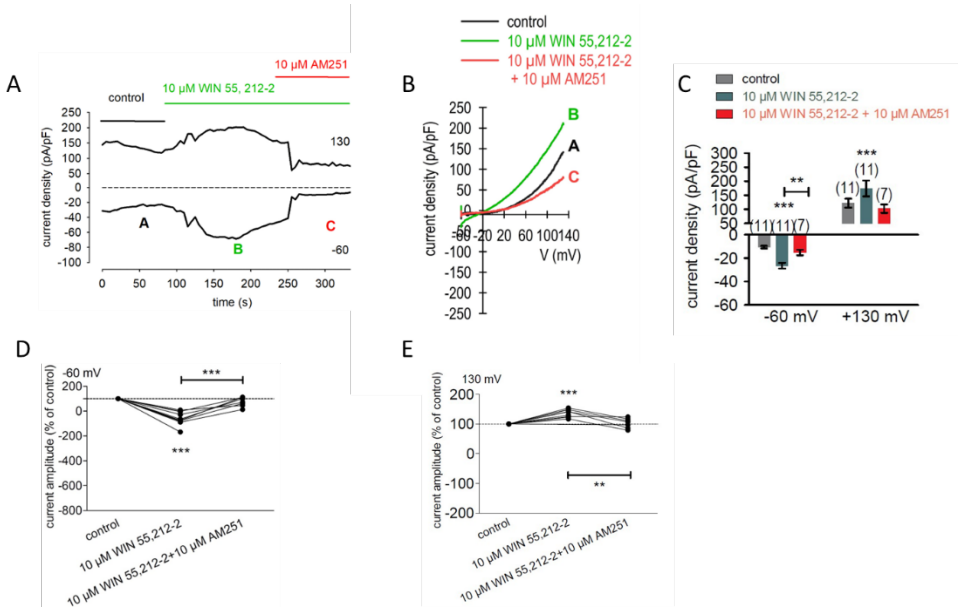

Fig. 25 | WIN 55,212-2 increased the whole-cell currents in TRPV1-HCEC-12. (A) Reversal by AM251 (10 μM) of the time dependent current increases induced by WIN 55,212-2 (10 μM). **(B)** Typical experimental record of the changes in currents induced by the voltage ramp in the presence and absence of 10 μM AM251. The current response behavior is displayed before application (marked as A), during WIN 55,212-2 (10 μM) application (marked as B), and after 10 μM AM251 addition (marked as C). **(C)** Summary of the effects of WIN 55,212-2 and AM251 on current patterns (n = 7 – 11). The comparisons of WIN 55,212-2 vs. control and WIN 55,212-2 + AM251 vs. WIN 55,212-2 were conducted by paired t-test or Wilcoxon test. **(D)** The maximum negative current amplitude caused by the voltage step (from 0 to -60 mV) is displayed as a percentage of the control value. In the presence of 10 μM AM251, the inward current induced by 10 μM WIN 55,212-2 was significantly suppressed (paired t-test). **(E)** The maximum positive current amplitude caused by the voltage step (from 0 to +130 mV) is displayed as a percentage of the control value. In the presence of 10 μM AM251, the outwardly rectifying currents induced by 10 μM WIN 55,212-2 were significantly suppressed (paired t-test). ** $p < 0.01$; *** $p < 0.005$.

3.4. Crosstalk between CB1 and TRPV1 in HCEC-12 and TRPV1-HCEC-12

3.4.1. CB1 activity suppresses CAP-induced TRPV1 activation

Based on indications of crosstalk between CB1 and TRPV1 in HCEP cells, in this set of experiments, it was determined whether CB1 also interacts with TRPV1 through crosstalk in HCEC-12. This assessment involved determining if the CB1 agonist WIN 55,212-2 alters the magnitude of Ca^{2+} transients induced by activation of TRPV1 with CAP in HCEC-12 cells and TRPV1 HCEC-12. As shown previously in HCEP, the results shown in Figure 26 indicate that WIN 55,212-2 suppressed the CAP-induced Ca^{2+} transients. This is evident since in the presence of WIN 55,212-2, CAP decreased the baseline fluorescence ratio f_{340}/f_{380} from 0.1089 ± 0.0006 (control) to 0.0868 ± 0.0017 at

400 s ($p < 0.005$; n = 9 – 16), and from 0.1146 ± 0.0028 (control) to the lower level of 0.0755 ± 0.0034 at 600 s ($p < 0.005$; n = 9 – 16) (Fig. 26A, B). Similarly, in TRPV1 HCEC-12 with WIN 55,212-2, CAP also caused the fluorescence ratio f_{340}/f_{380} to fall from 0.2196 ± 0.0290 to 0.1248 ± 0.0076 at 400 s ($p < 0.05$; n = 6) (Fig. 26C). Taken together, preincubation of the cells with WIN 55,212-2 abolished the CAP-induced Ca^{2+} increases by reducing them below their baseline levels.

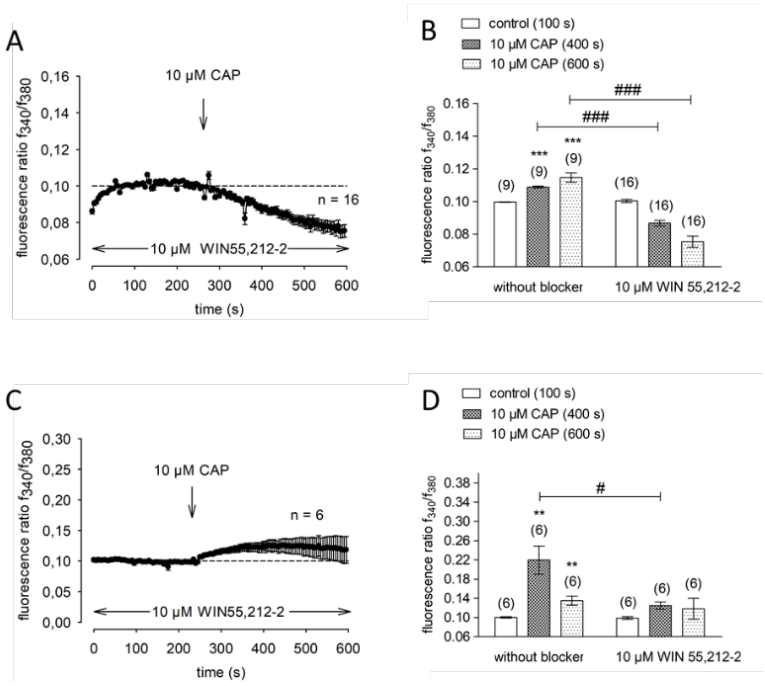

Fig. 26 | WIN 55,212-2 suppresses CAP-induced increases in Ca^{2+} influx in HCEC-12 (A and B) and in TRPV1-HCEC-12 (C and D). Drug applications were conducted at the indicated time points. **(A)** During exposure to WIN 55,212-2 (10 µM), CAP (10 µM) induced a decrease in the fluorescence ratio f_{340}/f_{380} than in the absence of this CB1 agonist in HCEC-12. **(B)** Summary of the effects of WIN 55,212-2 (10 µM) on CAP (10 µM) induced Ca^{2+} transients (n = 9 – 16) in HCEC-12. The paired t-test or Wilcoxon test evaluated the significance of changes induced by CAP (400 s) without WIN 55,212-2 vs. control (100 s), and CAP (600 s) without WIN 55,212-2 vs. control (100 s). **(C)** Repeat of the same experiment shown in (A), with TRPV1-HCEC-12 instead (n = 6). Similarly, WIN 55,212-2 inhibited the CAP-induced response. **(D)** Summary of the effects of 10 µM CAP on Ca^{2+} transients with or without 10 µM WIN 55,212-2 (n = 6) in TRPV1-HCEC-12. The paired t-test or Wilcoxon test were used to evaluate the significance of the effects of CAP (400 s) without WIN 55,212-2 vs. control (100 s), CAP (600 s) without WIN 55,212-2 vs. control (100 s). The paired t-test or Mann-Whitney U test were used to evaluate the significance of changes in CAP induced Ca^{2+} transients at 400 s with WIN 55,212-2 vs. CAP (400 s) without WIN 55,212-2 and CAP (600 s) with WIN 55,212-2 vs. CAP (600 s) without WIN 55,212-2. ** $p < 0.01$; *** $p < 0.005$; $^{\#}$ $p < 0.05$; $^{\#\#\#}$ $p < 0.005$.

3.4.2. TRPV1 modulation changes WIN 55,212-2-induced CB1 activation

The effects of changes in TRPV1 function on WIN 55,212-2-induced Ca^{2+} transients in normal HCEC-12 were characterized. In the presence of CAP, WIN 55,212-2 increased the fluorescence ratio f_{340}/f_{380} from 0.11351 ± 0.0023 at 100 s (control) to 0.12779 ± 0.0014 at 400 s ($p < 0.005$; n = 51 – 41), and from 0.09542 ± 0.0035 at 100 s (control) to 0.12479 ± 0.0016 at 600 s ($p < 0.005$; n = 51 – 41) (Figs. 22A; 27A, B). Interestingly, a transient decrease of the fluorescence ratio was observed at the beginning, followed by a steep increase when TRPV1 was blocked with CPZ (Fig. 27). More specifically, the fluorescence ratio f_{340}/f_{380} increased from 0.11351 ± 0.0022 at 100 s (control) to 0.12713 ± 0.0020 at 400 s ($p < 0.005$; n = 41 – 51), and from 0.09542 ± 0.0035 at 100 s (control) to 0.15462 ± 0.0027 at 600 s ($p < 0.005$; n = 41 – 57) (Figs. 22A; 27C, D). These larger Ca^{2+} responses induced by WIN 55,212-2 in the presence of CPZ than those induced in its absence (c.f., Figs. 22, 24; Fig. 27A, C) suggest that TRPV1 functions to suppress WIN 55,212-2-induced Ca^{2+} transients. In contrast, a reversal of the WIN 55,212-2 effect was only observed if TRPV1 was not modulated in HCEC-12 (Fig. 22A).

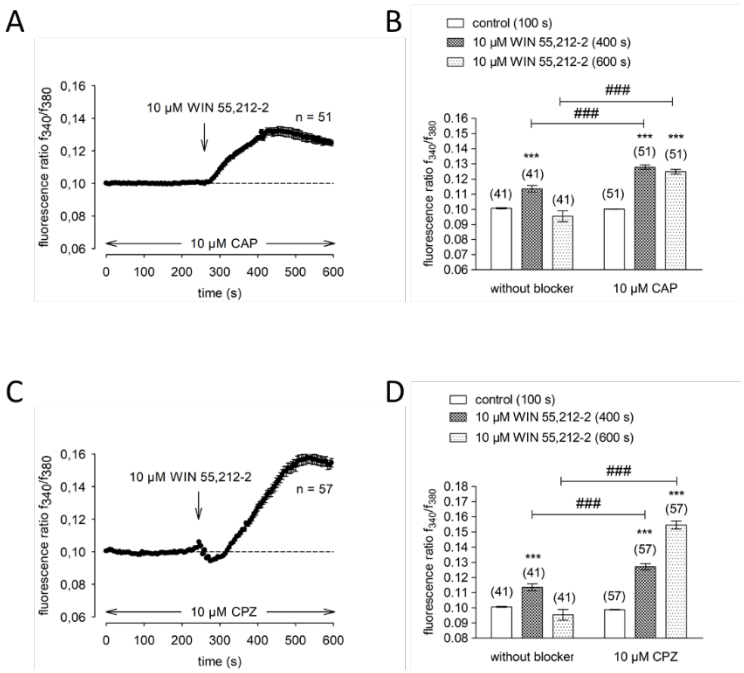

Fig. 27 | Activation or inhibition of TRPV1 activity alters WIN 55,212-2-induced Ca^{2+} transients in HCEC-12. (A) 10 µM WIN 55,212-2 augmented a 10 µM CAP-induced Ca^{2+} influx (n = 51). **(B)** Summary of WIN 55,212-2 (10 µM) induced Ca^{2+} transients with or without CAP

(10 µM) (n = 41 - 51) in HCEC-12. The comparisons of WIN 55,212-2 (400 s) without CAP vs. control (100 s) and WIN 55,212-2 (600 s) without CAP vs. control (100 s) were conducted by paired t-test or Wilcoxon test. The comparisons of WIN 55,212-2 (400 s) with CAP vs. WIN 55,212-2 (400 s) without CAP and WIN 55,212-2 (600 s) with CAP vs. WIN 55,212-2 (600 s) without CAP were conducted by unpaired t-test or Mann-Whitney U test. **(C)** Shows the same experiment as exhibited in (A), but with CPZ instead of CAP (n = 57). The WIN 55,212-2 response was time delayed, but ultimately markedly increased the intracellular Ca^{2+} level. **(D)** Summary of WIN 55,212-2 (10 µM) experiments with or without CPZ (10 µM) (n = 41 – 57) in HCEC-12. The comparisons of WIN 55,212-2 (400 s) without CPZ vs. control (100 s) and WIN 55,212-2 (600 s) without CPZ vs. control (100 s) were conducted by paired t-test or Wilcoxon test. The comparisons of WIN 55,212-2 (400 s) with CPZ vs. WIN 55,212-2 (400 s) without CPZ and WIN 55,212-2 (600 s) with CPZ vs. WIN 55,212-2 (600 s) without CPZ were conducted by unpaired t-test or Mann-Whitney U test. *** $p < 0.005$; ### $p < 0.005$.

3.5. CAP- and WIN 55,212-2-induced calcium regulation in an external Ca^{2+} free solution

The effects of WIN 55,212-2 on intracellular Ca^{2+} levels were determined in a Ca^{2+} free external solution with 1 mM EGTA Ca^{2+} -free external medium to ascertain whether the Ca^{2+} transients were due to delimited plasma membrane CB1 activation or to the release of Ca^{2+} from intracellular stores. Accordingly, Fig. 28A shows that the replacement of the Ca^{2+} containing medium with the aforementioned Ca^{2+} -free medium caused the signal to immediately fall below the baseline level. In a Ca^{2+} free solution, CAP did not change the fluorescence ratio f_{340}/f_{380}, indicating that the CAP-induced rise in Ca^{2+} influx is solely a result of an increase in plasma membrane influx (Figs. 17A, 28B). In contrast, CB1 activation by WIN 55,212-2 increased intracellular Ca^{2+} in the Ca^{2+} free condition, indicating that CB1 activation is more complex and dependent on the release of Ca^{2+} from intracellular stores (Figs. 22A, 28D, 28E).

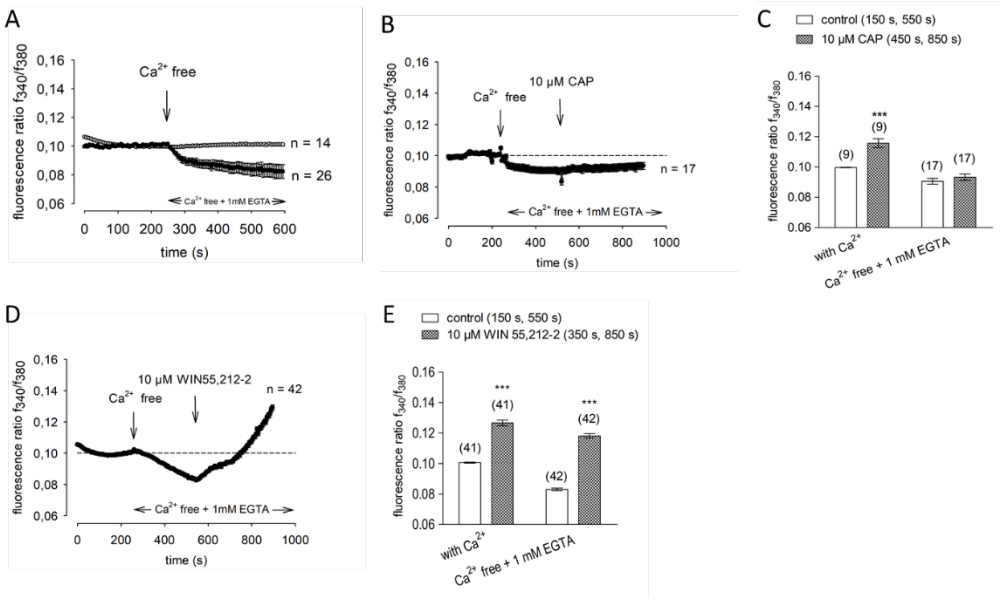

Fig. 28 | Different mechanisms of Ca^{2+} regulation induced by TRPV1 and CB1 activation in a Ca^{2+} free solution. Drug applications were conducted at the indicated times. The data are expressed as the mean ± SEM (n = 9 – 42). **(A)** Substitution of a Ca^{2+} free condition caused intracellular Ca^{2+} levels (shown as filled circles) to fall (n = 26), while the fluorescence ratio f_{340}/f_{380} ratio (shown as open circles) was invariant in the control group (n = 14). **(B)** The Ca^{2+} free condition downregulated the fluorescence ratio f_{340}/f_{380} ratio below the baseline, while 10 µM CAP supplementation did not change intracellular Ca^{2+} levels (n = 17). **(C)** Summary of the effects of 10 µM CAP on Ca^{2+} transient response experiments with or without external Ca^{2+} (n = 9 – 17). The comparisons of 10 µM CAP (450 s, 850 s) with Ca^{2+} vs. control (150 s, 550 s) with Ca^{2+} and 10 µM CAP (450 s, 850 s) with Ca^{2+} free vs. control (150 s, 550 s) with Ca^{2+} free were conducted by paired t-test or Wilcoxon test. **(D)** Shows the same experiment as shown in (B), but with WIN 55,212-2 instead of CAP (n = 42). WIN 55,212-2 upregulated the intracellular Ca^{2+} ratio. **(E)** Summary of the effects of WIN 55,212-2 (10 µM) on CB1-induced Ca^{2+} transients with or without external Ca^{2+} (n = 41 – 42). The comparisons of 10 µM WIN 55,212-2 (350 s, 850 s) with Ca^{2+} vs. control (150 s, 550 s) with Ca^{2+} and 10 µM WIN 55,212-2 (350 s, 850 s) with Ca^{2+} free vs. control (150 s, 550 s) with Ca^{2+} free were conducted by paired t-test or Wilcoxon test. *** $p < 0.005$.

3.6. CPZ suppresses NGF-induced Ca^{2+} influx in HCEC-12

We determined if NGF induces Ca^{2+} transients through interacting with TRPV1 channels in HCEC-12 cells, since such a dependence was described in some other tissues (153, 154). Fig. 29A shows that NGF (50 ng/ml) induced an increase of the fluorescence ratio f_{340}/f_{380} from a baseline level of 0.0997 ± 0.0001 at 100 s (control) to 0.1073 ± 0.0007 at 600 s. This increase in Ca^{2+} influx was inhibited by CPZ to a level even below the baseline at 400 s and 600 s ($p < 0.005$; n = 42 – 17) (Figs. 29B, C; 31B).

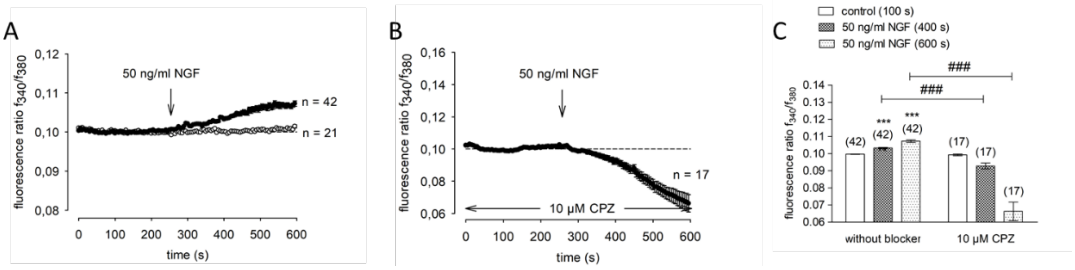

Fig. 29 | CPZ reverses NGF-induced Ca^{2+} transients in HCEC-12. Drugs were applied at the indicated times. The data are shown as mean ± SEM (n = 17 – 42). **(A)** NGF (50 ng/ml) upregulated the Ca^{2+} level in HCEC-12 at 400 s (n = 42, filled circles). The Ca^{2+} baseline ratio remained invariant in the control cells (shown as open circles) (n = 21). **(B)** Shows the same experiment as exhibited in (A), but with CPZ (10 µM) (n = 17). CPZ clearly inhibited the NGF-induced rise in Ca^{2+} influx (n = 17) and instead caused it to decline below the baseline in HCEC-12. **(C)** Summary of the effects of NGF on Ca^{2+} transient responses in the presence and absence of CPZ (n = 17 – 42) in HCEC-12. The comparisons of 50 ng/ml NGF (400 s) without blocker vs. control (100 s), 50 ng/ml NGF (600 s) without blocker vs. control (100s), 50 ng/ml NGF (400s) with 10 µM CPZ vs. control (100s) with 10 µM CPZ, and 50 ng/ml NGF (600 s) with 10 µM CPZ vs. control (100 s) with 10 µM CPZ were conducted by paired t-test or Wilcoxon test. The unpaired t-test or Mann-Whitney U test evaluated the significance of the effects of 50 ng/ml NGF (400 s) with 10 µM CPZ vs. 50 ng/ml NGF (400 s) without blocker and 50 ng/ml NGF (600 s) with 10 µM CPZ vs. 50 ng/ml NGF (600 s) without blocker on Ca^{2+}– transient responses. *** $p < 0.005$; ### $p < 0.005$.

4. DISCUSSION

This study is based on previous studies describing the functional roles of TRPs such as TRPV1 in HCEC-12. Its prime objective is to broaden our understanding of the biology of the corneal endothelium and the role of TRPs in non-excitable cells in general (64). In many studies involving the improvement of corneal organ culture or corneal endothelial cell transplantation, HCEC-12 is a widely accepted and relevant cell model that has been widely characterized (36). This relevance was confirmed by demonstrating that the properties of TRPM8 are similar to one another in both HCE-12 cells and fresh primary cultivated corneal endothelial cells (26). A further approach was to confirm the expression of similar responses induced by TRPV1 modulation, as shown in Figure 17 and described by Mergler et al. (64). Another study documenting the validity of the HCEC-12 model was based on showing that TRPV1 protein expression is present in both this cell line and in fresh HCEC (64). Therefore, studies employing this model are relevant for characterizing the roles of TRP channel activity in maintaining homeostatic control of corneal endothelial cell types, regardless of any obvious differences in their phenotypic expression and fate (64). Fluorescence calcium imaging and the planar patch-clamp technique assessed the functional involvement of the TRPV1 channel subtypes in mediating homeostatic control of intracellular Ca^{2+} changes. Both of these methods are commonly used for *in vitro* electrophysiological research (143, 155).

As expected, the CAP-induced activation of TRPV1 led to a larger Ca^{2+} influx in the TRPV1 transfected-HCEC-12 than was the case in normal HCEC-12 (Fig. 19A). Notably, functional CB1 expression in HCEC-12 was detected for the first time by using the specific CB1 agonist WIN 55,212-2. This was evident since the specific CB1 agonist WIN 55,212-2 induced Ca^{2+} transients and increases in ionic currents (Fig. 22A, B). Regarding a putative interaction between TRPV1 and CB1, WIN 55,212-2 suppressed CAP-induced transient increases in Ca^{2+} levels in HCEC-12 (Fig. 26A, B). The ability of CB1 activation by WIN 55,212-2 to blunt TRPV1 activation of Ca^{2+} transients induced by CAP was previously described in HCEP (101). The induction by WIN 55,212-2 of Ca^{2+} transients is

larger in the presence of CPZ than in its absence (Fig. 27C). This difference suggests that blockage of TRPV1 with CPZ suppresses TRPV1-induced inhibition of CB1 activation, allowing WIN 55,212-2 to induce a larger increase in the Ca^{2+} transient than in the absence of CPZ. Other results confirmed earlier descriptions of NGF-receptor expression in cultured immortalized HCEC (126, 156, 157). The results of this thesis provide reliable evidence documenting the functional expression of NGF, since this cytokine induced Ca^{2+} transients (Fig. 29A). Therefore, a possible interaction between corneal endothelial TRPV1 and NGF activity was evaluated. As anticipated based on previous results, CPZ inhibited the NGF-induced increase in Ca^{2+} influx (Fig. 29B). These results clearly demonstrate a role for NGF in modulating Ca^{2+} regulation in HCEC. It still needs to be investigated whether or not NGF has a protective effect on the corneal endothelium.

4.1. Cell morphology and the HCEC-12 model

The cell morphology of HCEC-12 and TRPV1-HCEC-12 was compared. In both cell lines, the morphology appeared to be similar and formed a regularly arranged monolayer structure (Fig. 15A, B). Interestingly, HCEC-12 had different cell morphologies during the growth process (Fig. 16A, B). For example, the cells at the edges were elongated and had irregular shapes (Figs. 15B, 16B). Subsequently, the corneal endothelial cells grew continually, and after reaching confluence they were arranged in tightly interconnected hexagonal arrays, as they are in the normal corneal endothelium (Fig. 16A). In TRPV1-HCEC-12, TRPV1 channels are overexpressed through lentiviral gene transfer. TRPV1-HCEC-12 exhibit normal morphology without any damage (Fig. 15A, B). To confirm that lentiviral gene transfer did not affect cell function, experiments were performed in parallel with the empty vector and virus transfected HCEC-12. It needs to be pointed out that the results in the empty vector HCEC-12 were the same as those in the normal HCEC-12. In agreement with previous studies, cultured HCEC-12 were morphologically similar to the *in vivo* corneal endothelial cells (Fig. 30) (158, 159). Moreover, the transplantation of immortalized HCEC-12 onto the recipient cornea resulted in establishing new endothelial layers, which have the same functional and morphological characteristics as the natural endothelial layers in the organ culture cornea

(160). Therefore, the HCEC-12 model is generally well established and has been successfully used in various studies including corneal organ culture or corneal endothelial cell transplantation (161-163).

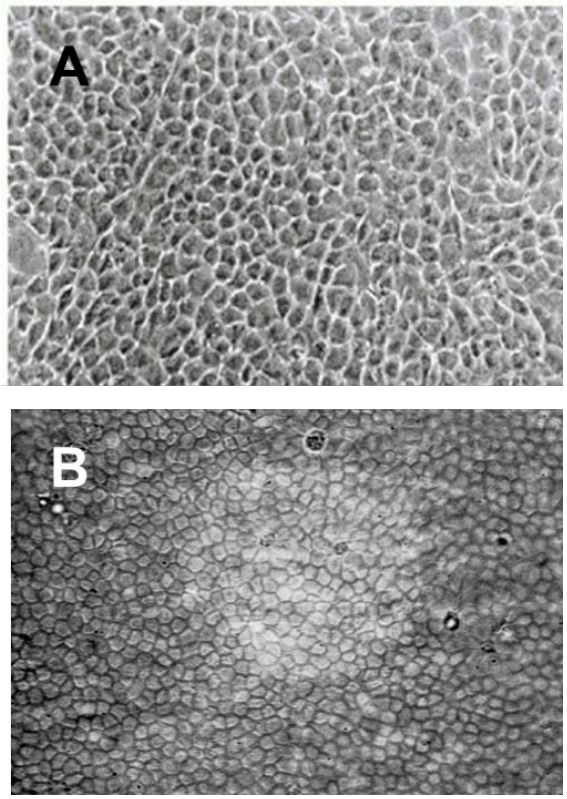

Fig. 30 | Retention of morphological features in in vitro HCEC cultures and in vivo. (A) The microscopic image shows that endothelial cells form a normal monolayer as well as homogeneous hexagonal and polygonal cell structures. Original magnification in primary untransformed HCEC = *110 (164). **(B)** Light micrograph of the corneal endothelium of a pig with similar cell morphological properties (58). Reused with kind permission from Elsevier.

4.2. Functional interactions between TRPV1 and CB1

4.2.1. Modulation by CB1 of TRPV1 activity

Documentation of functional TRPV1 expression in HCEC is dependent on evaluating the individual and combined influence of CAP and CPZ on intracellular Ca^{2+} levels and the whole-cell currents. According to the results obtained in this study (Fig. 17A), CPZ preincubation blocked CAP-induced increases in Ca^{2+} influx (Fig. 17B, C). This result validated functional TRPV1 expression in HCEC, as described previously (64). In addition, CAP induced increases in whole-cell currents (Fig. 20). Although the reversal potential was

around 0 mV, which is typical for non-selective cation channel currents, there was a large variation in the current response patterns of whole-cell currents in the presence of CAP (e.g., compare Fig. 20 with Fig. 21). It is possible that this variability is attributable to differences in viability as well as cell differences in their passage number. Irrespective of this variability, the CAP-induced Ca^{2+} increases in TRPV1 activation were completely abolished in a Ca^{2+} -free solution (Fig. 28B). This dependence on the presence of Ca^{2+} in the bathing solution for CAP to induce a Ca^{2+} transient is supportive of known delimited plasma membrane TRPV1 channel activity (165). The magnitude of the TRPV1 channel activation was considerably larger in the TRPV1-HCEC-12 than in the non-transfected HCEC-12 cells. This difference confirms a successful transduction of HCEC-12 with TRPV1. In addition, these whole-cell currents underlying TRPV1 increases in Ca^{2+} influx were inhibited by CPZ, which also validates functional TRPV1 expression (Figs. 17, 18). These results also verified that the TRPV1 channels are expressed at different cell passages in the HCEC-12, demonstrating a stable cell line.

In previous studies, Mergler et al. used the same cell type, but at a lower cell passage, which may explain slight differences in the calcium response patterns and whole-cell current patterns. The relatively slow increase (slope) with CAP could be explained as due to the slower delivery by manual pipetting of the drug into a stationary bathing solution. TRPV1 expression was also detected in both human corneal stromal keratocytes (HCK) and HCEP (33, 76). The current and calcium response patterns are comparable to one another. In human corneal fibroblasts (HCF), the expression of TRPV1 was also demonstrated, suggesting a physiological relevance (77). On the other hand, CPZ is a mixed blocker of TRPM8 and TRPV1 (118, 166), and the function of CPZ may be limited because functional expression of TRPM8 was also found in HCEC-12 (167). Nevertheless, TRPV1 channels were detected in TRPV1-transduced and normal HCEC-12, based on the similar responses obtained with the TRPV1 channel agonist CAP and antagonist CPZ that are customarily used to probe for such activity (63).

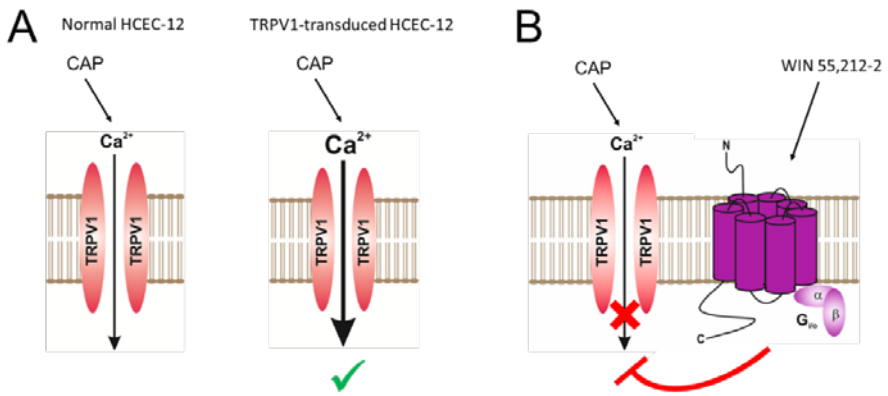

Fig. 31 | Signal transduction model accounting for how CB1 activation blunts CAP-induced TRPV1 activation. (A) CAP induces larger increases in Ca^{2+} influx in TRPV1-HCEC-12 than in normal HCEC-12 (Figs. 17 – 22). **(B)** WIN 55,212-2-induced CB1 activation suppresses CAP-induced increases in Ca^{2+} influx through TRPV1 channels (Fig. 26). Diagrams drawn by Huan Luo.

4.2.2. CB1 functional expression activity in HCEC

CB1 functional expression was validated based on showing that in the presence of WIN 55,212-2, a large increase in Ca^{2+} influx was detected in HCEC-12 cells. This response is similar to those described in several similar studies of corneal epithelial cells (111) and also ocular tumor cells (104, 105). The CB1-agonist-induced Ca^{2+} influx was clearly suppressed in the presence of AM251. This result confirms that CB1 acts as a GPCR modulator of Ca^{2+} influx through TRPs permeable pathways (66) (Figs. 22, 23). These findings are consistent with the planar patch-clamp recordings showing that WIN 55,212-2 increased whole-cell currents (Fig. 24, 25), which corresponds to a study on ocular tumor cells (105). CB1 is expressed in a variety of other ocular cell types including tumor cells (101, 105, 168). Specifically, CB1 expression was previously described in HCEP (101, 111) and HCK (unpublished observation by Mergler et al., 2020) as well as in the trabecular meshwork (169). The CB1 activator WIN 55,212-2 contributes to modulating intracellular Ca^{2+} regulation in HCEC-12 (152). Some studies have shown that direct targeting of CB1 with controlled inactivation ligands is a viable method for reducing intraocular pressure (IOP) in mouse models and is worthy of further study in other model systems (170). Cannabinoid receptors are also present in mouse and human conjunctival cells, and some functional responses have shown that CB1 and CB2 stimulation

mediate such changes by inhibiting cAMP levels and proliferation, and by modulating stress signaling pathways (171).

4.3. Tentative mechanism accounting for how NGF induces TRPV1 activation

NGF increased $[Ca^{2+}]_i$ levels in HCEC-12 (Fig. 29A), which validates a NGF receptor contribution to intracellular Ca^{2+} regulation in HCEC-12. NGF increased Ca^{2+} influx induced by TRPV1 activation, since CPZ suppressed the NGF-induced increase in Ca^{2+} influx. Previous studies have shown that NGF receptors rapidly increased membrane TRPV1 expression (172). In addition, a study suggested that exogenous NGF stimulates the proliferation of both rabbit corneal endothelial cells (RCEP) and HCEP (173). Another report described that NGF increases pain during wound healing and inhibits nerve remodeling and lymphatic degeneration (174). Therefore, these results provide evidence suggesting that NGF may also be an activator of TRPV1 in HCEC (Fig. 29A, B), as was described in HEK293 (172).

4.4. Interplay between NGF and CB1/TRPV1 receptor crosstalk

4.4.1. WIN 55,212-2 suppresses TRPV1 channel activity

In primary cultures of sensory neurones from the dorsal root ganglia of neonatal rats, exposure to high NGF alters cannabinoid-mediated modulation of TRPV1 receptor activation (175). Therefore, exposing these cells to high NGF concentrations modulates the CB1/TRPV1 receptor crosstalk. The hypothesis tested in this part of the thesis was that such an interaction also occurs in non-excitable cells such as HCEC. Since CB1 and TRPV1 are functionally expressed in HCEC, a possible interaction between GPCRs and TRPs was initially investigated to probe for the presence of a GPCR-TRP signaling axis in HCEC-12 (66). The results show that WIN 55,212-2, a selective CB1 agonist, suppressed CAP-induced transient increases in intracellular Ca^{2+} levels (Figs. 26, 31B). A similar result was obtained in HCEP (101, 111). This agreement suggests that a receptor crosstalk exists between CB1 and TRPV1. In other words, CB1 and TRPV1 interact with one another to suppress Ca^{2+} transient levels induced by either CB1 or TRPV1 activation. Interestingly, the increase caused by WIN 55,212-2 was larger than that induced by CAP (Figs. 22A, 17A),

which can also be observed in ocular tumor cells isolated from UM and RB (104, 105). A possible explanation for the larger response to WIN 55,212-2 than CAP is that the functional TRPV1 expression is larger in the transduced HCEC-12 cells than in their non-transduced counterpart. Alternatively, CB1 activation by WIN 55,212-2 may also induce upregulation of other Ca^{2+} permeant pathways. As shown in Fig. 28D, WIN 55,212-2 induced cytoplasmic Ca^{2+} upregulation in a Ca^{2+} free solution. A similar result was also obtained in the aforementioned RB cells (104). This agreement suggests that the effect of WIN 55,212-2 is more complex than previously understood, and probably connected with store depletion and the activation of intracellular Ca^{2+} releasing channels (ryanodine receptor) (176).

Notably, CB1 colocalization with TRPV1 was determined in the intact mouse corneal epithelium and in HCEC (72). Studies on UM cells isolated from patients as well as in many uveal cell lines have shown that TRPV1, CB1, and TRPM8 channels help control Ca^{2+} homeostasis (105). Furthermore, studies have shown that CB1 agonists (such as WIN 55,212-2) directly inhibit TRPV1 functional activity through the calcineurin pathway, which constitutes the mechanism of action of cannabinoids in peripheral tissues (177). Interestingly, previous studies showed a crosstalk between CB1 and TRPV1 in HCEP. Specifically, the CB1 agonist WIN 55,212-2 suppressed TRPV1-induced inflammatory responses to corneal injury in mouse corneal wound healing models (101). This result is consistent with the results of this study, which is focused on describing interactions between CB1 and TRPV1, based on showing how CB1 activation suppresses CAP-induced increases in Ca^{2+} influx induced by TRPV1 activity. Overall, the present study supports the notion that CB1-induced suppression of TRPV1 activity may serve as a novel target in a clinical context concerning corneal graft preservation, since CB1 activation may suppress TRPV1-induced Ca^{2+} overload. (Fig. 26A, B). A similar effect was observed again in ocular tumor cells. Specifically, the CAP effect was not only abolished by WIN 55,212-2 but also caused the Ca^{2+} trace to fall below the baseline (105). This phenomenon was also observed upon activating TRPM8 with menthol in the presence of BCTC (Fig. 7) (76). A possible explanation may be that activation of ATP dependent PMCA pumps led to a continuous calcium

outflow when some TRPs or GPCRs were blocked.

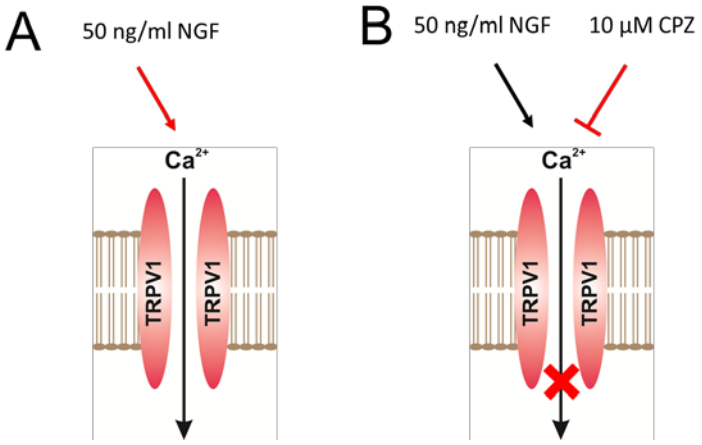

Fig. 32 | NGF promotes Ca^{2+} influx through activating TRPV1. (A) NGF-induced TRPV1 activation (Fig. 29A). **(B)** Confirmation of TRPV1 involvement in mediating NGF-induced increases in Ca^{2+} influx in HCEC-12 (Fig. 29B). Diagrams drawn by Huan Luo.

4.4.2. TRPV1 modulation alters CB1-induced Ca^{2+} transients

The mechanisms underlying TRPV1 and CB1-induced Ca^{2+} transients were delineated. We obtained evidence that they were different from one another, since WIN 55,212-2 induced Ca^{2+} transients irrespective of the presence or absence of CAP. As shown in Figure 22A, WIN 55,212-2 induced Ca^{2+} transients with recovery. The mechanism underlying this response appears to be different than the one underlying the Ca^{2+} transient induced by CAP since the WIN 55,212-2-induced transient was larger in the presence of CAP than in the absence of CAP (Fig. 27A). Another indication that these underlying mechanisms are different from one another is that preincubation with CPZ altered WIN 55,212-2-induced Ca^{2+} transients. At the outset, WIN 55-212-2 initially induced a slight decrease that was followed by an irreversible progressive steep Ca^{2+} increase (Fig. 27C). In summary, the Ca^{2+} transients induced by TRPV1 and CB1 activation are additive, suggesting different triggering mechanisms for their induction. Nevertheless, crosstalk between these two pathways is evident since the responses to WIN 55,212-2 are affected in different ways that are dependent on TRPV1 activated by CAP. It is possible that a portion of the WIN 55,212-2-induced Ca^{2+} transients may stem

from activation of TRPM8 by WIN 55,212-2. Taken together, the CB1/TRPV1 receptor crosstalk is complex and perhaps condition dependent. Each of these receptors mediates control of intracellular Ca^{2+} levels through unique pathways, since selective activation of each of these pathways has additive effects on the maximum increase in Ca^{2+} influx.

4.4.3. NGF induces increases in Ca^{2+} influx through crosstalk with TRPV1 Channels

NGF contributes to the maintenance of endothelial homeostasis through activation of its cognate receptor. Its involvement is based on results showing that NGF stimulated proliferation of endothelial cells as well as studies showing improved allograft survival (178, 179). Like CAP, NGF increased intracellular Ca^{2+}, demonstrating that NGF mediates downstream events by inducing Ca^{2+} transients (Figs. 29A, 32A). In contrast to the WIN 55,212-2 effect, the NGF-induced Ca^{2+} transients are smaller than those induced by WIN 55,212-2. Notably, CPZ suppressed the NGF-induced Ca^{2+} influx, indicating a link between NGF and TRPV1 (Figs. 29B, 32B), which was also described in sensory neurons (154). It remains unknown whether NGF induces TRPV1 activation directly or indirectly via an intermediate receptor in HCEC-12. Nevertheless, it is apparent that NGF-induced Ca^{2+} transients are dependent on TRPV1 activation, since they were eliminated in the presence of CPZ. On the other hand, activation of CB1 inhibits NGF-induced sensation in sensory neurons (153, 154). It still needs to be investigated whether or not this phenomenon also applies to non-excitable cells such as HCEC-12. Previous studies demonstrated that other growth factors such as EGF induce downstream Ca^{2+} signaling through TRPC4 transactivation in HCEP (180, 181). Mergler et al. confirmed that EGF suppresses hydrogen peroxide-induced Ca^{2+} influx by inhibiting L-type channel activity in cultured HCEC (58). Taken together, NGF may be able to modulate Ca^{2+} regulation via TRPV1 channels.

4.5. Clinical aspects

4.5.1. TRPV1 and apoptosis

Temperature- and pain-sensitive TRPs play an essential role in mediating corneal sensation. The cornea, with its complex neuroplexus within the

epithelium and stroma, has the highest sensory nerve density in any tissue of the human body (176). In contrast, different TRP channel subtypes are also expressed in non-excitable cells [reviewed in (72)]. The role of these channels is non-classical, since their activation cannot be triggered by imposition of an action potential. Nevertheless, TRPV1 activation releases pro-inflammatory cytokines via stimulation of MAPK protein kinases in non-excitable corneal epithelial cells (73). Therefore, suppression of TRPV1 serves as a potential target to improve therapeutic management of ocular pain reduction as well as those pain induced by proinflammatory cytokine upregulation (e.g. dry eye disease) (182, 183). Some studies have shown that exposure to oxidative stress can induce HCEC loss through apoptosis (184).

The regulation of TRPV1 activity by temperature is the basis of the fundamental homeostatic mechanism required to support corneal endothelial function under different environmental conditions (64). It is tenable that interactions between corneal cell types and nerve fibers are dependent on interactions between TRP channel subtypes and resident receptors on neighboring nerve cells. Apoptosis may be induced by the activation of linked signaling pathways (185). Mergler et al. reviewed studies characterizing changes in ion channel behavior under various conditions that may influence the behavior of apoptotic mechanisms mediating apoptotic cell losses (186). Such studies have so far indicated that prolonged activation of the TRPV1 channel may even lead to neuronal cell apoptosis (187). In summary, modulation of TRP activity makes an essential contribution to regulating intracellular Ca^{2+} at levels that are within physiological limits. For example, TRPV1 may serve as an effective drug target to block the Ca^{2+} rises from reaching levels that induce apoptotic events. If selective and effective TRPV1 blockers can be developed, they may prevent cell losses from occurring that are large enough to cause corneal opacification and possibly blindness.

4.5.2. Corneal endothelial cell density (ECD) and Ca^{2+}-dependent cell vitality

Age-dependent losses in corneal endothelial cell density (ECD) that occur throughout our lifetime do not compromise corneal transparency until their

density falls below a critical level (22). However, these losses can be accelerated after various impairments such as surgical trauma and following corneal transplantation (160, 163). Mergler et al. indicated that better characterization and improved knowledge of ion channel behavior might have an impact on improving protocols to suppress declines in ECD, which could increase the amount of viable corneal endothelial cells in donor tissue to be used for transplantation surgery (58). Achieving such a goal is relevant for improving the outcome of this surgical procedure, since measures to slow losses in HCE density affect the viability of corneal grafts for longer periods in storage (178). Preserving homeostasis of intracellular Ca^{2+} regulation by controlling Ca^{2+}-permeable channel activity plays a vital role in suppressing apoptosis (186). HCE cell vitality is likely to be improved by optimizing TRPV channel behavior through preserving them under favorable ambient conditions (e.g. temperature) (188). Extended periods of exposure to TRPV1 activators such as CAP or acidic pH desensitize TRPV1 in a Ca^{2+}-dependent manner. This process may be partially modulated by the opposing effects of inhibiting channel dephosphorylation with calcineurin and increasing PKA-induced channel phosphorylation status by increasing adenylyl cyclase activity. (189). It is known that TRPV1 is upregulated in sight compromising development of pterygium (190). The current study demonstrated that NGF increases intracellular Ca^{2+} influx through stimulating TRPV1 channel activity. Taken together, NGF combined with endogenous TRP channel modulators in the medium may help improve HCEC vitality during corneal storage.

4.5.3. Challenges in keratoplasty

Keratoplasty is used to treat patients with vision loss due to endothelial dysfunction (164). Although the clarity of the cornea is restored by keratoplasty, the problem of limited donor availability still exists (22). It is known that 20% of cornea donations must be discarded because of a too low HCE density and too many apoptotic cells (191). The density of HCE is a major determinant used to identify corneal tissues that are suitable for use in transplantation surgery (192), since ECD and survival determine the likelihood of a successful outcome (193). Mergler et al. showed that temperature changes could selectively affect intracellular calcium regulation by regulating specific temperature-sensitive

receptors that are members of the TRP family. Thus, temperature control during storage plays a vital role in maintaining the vitality of the stored human cornea (29, 194). On the other hand, there is a controversy regarding the optimal storage temperature of donor corneas (195-197). However, there are other studies suggesting instead that adjusting the environmental storage conditions of corneas deemed suitable for use in transplantation surgery possibly improves the likelihood of a favorable surgical outcome (58, 198). A recent report demonstrated that NGF gene therapy was successful at prolonging corneal graft survival in an experimental rat transplantation model (179). Therefore, it is conceivable that this therapy improves graft survival by inducing cytoprotective effects that reduce losses in corneal cell viability during culture (199).

4.6. Strengths and limitations of the study (biological and technical limitations)

Technically, the strength of this study is that the results using two different highly-sensitive functional assays agree with one another, which supports the conclusions of this study. In addition, the HCEC-12 cell line is an established cell model for HCEC (114), similarly to the HCK cell line, which is used as a model for human corneal keratocytes (200). This has been thoroughly discussed (26). The suitability of both transformed immortalized cell lines for functional studies is confirmed by a correspondence between their electrophysiological characteristics and those that were exhibited by primary cell cultures or tissue sections (26, 64, 76, 161).

On the other hand, it is necessary to consider the difference between *in vitro* experiments and the physiologically intact cornea of the human eye. Fluorescence calcium imaging and planar patch-clamp recordings play an essential role in studying ion channel expression. They have obvious advantages, but also some limitations, since the experiments are performed in unphysiological conditions. Calcium imaging interpretation needs to consider temperature differences between the *in vivo* condition and the measuring room temperature conditions. Technically, the bleaching effect from Fura-2/AM (Fig. 15C), as well as the interference caused by manual pipetting were sensitive

parameters in the experiments. It is experimentally less difficult to perform planar patch-clamp recordings rather than conventional patch-clamp recordings. However, both approaches require experience in assessing the current response patterns of the experimental results (e.g. leak current problems are the most relevant issue). In addition, experimental data errors or artefacts can be caused by insufficient sealing or hidden leak currents. Fig. 20A shows an example of temporary collapsing currents, which could nevertheless be evaluated because of the recovery during recording. It is worth noting that careful attention to technical details is essential in improving the preservation of functional responses.

4.7. Conclusions

This study demonstrated a functional interaction between CB1 and TRPV1 functional activity in HCEC-12 for the first time. The results are consistent with those reported in HCEP (101) and also in ocular tumor cells (104, 105), indicating that changes in CB1 activity modulate TRP channel behavior in these ocular cells. The most interesting finding is that the WIN 55,212-2-induced Ca^{2+} increases were at higher levels than of those using classical CAP-induced Ca^{2+} increases in HCEC-12. This difference suggests a strong triggering effect by GPCRs on CB1 and TRPs responses [reviewed in (66)]. Furthermore, NGF stimulates the activity of TRPV1, whereas CB1 inhibits TRPV1 activity, indicating a complex Ca^{2+} regulation in HCEC-12. Overall, the results of this study and the relevant GPCR-TRP channel axis may contribute to a better understanding of HCE Ca^{2+} regulatory mechanisms. The insights gained may be helpful in developing novel strategies for improving corneal graft preservation for keratoplasty.

5. REFERENCES

1. Marfurt CF, Cox J, Deek S, Dvorscak L. Anatomy of the human corneal innervation. Exp Eye Res. 2010;90(4):478-92.
2. Muller LJ, Marfurt CF, Kruse F, Tervo TM. Corneal nerves: structure, contents and function. Exp Eye Res. 2003;76(5):521-42.
3. Navaratnam J, Utheim TP, Rajasekhar VK, Shahdadfar A. Substrates for Expansion of Corneal Endothelial Cells towards Bioengineering of Human Corneal Endothelium. J Funct Biomater. 2015;6(3):917-45.
4. Rufer F, Schroder A, Erb C. White-to-white corneal diameter: normal values in healthy humans obtained with the Orbscan II topography system. Cornea. 2005;24(3):259-61.
5. Gharaee H, Abrishami M, Shafiee M, Ehsaei A. White-to-white corneal diameter: normal values in healthy Iranian population obtained with the Orbscan II. Int J Ophthalmol. 2014;7(2):309-12.
6. Shaheen BS, Bakir M, Jain S. Corneal nerves in health and disease. Surv Ophthalmol. 2014;59(3):263-85.
7. Eghrari AO, Riazuddin SA, Gottsch JD. Overview of the Cornea: Structure, Function, and Development. Prog Mol Biol Transl Sci. 2015;134:7-23.
8. Sridhar MS. Anatomy of cornea and ocular surface. Indian J Ophthalmol. 2018;66(2):190-4.
9. DelMonte DW, Kim T. Anatomy and physiology of the cornea. J Cataract Refract Surg. 2011;37(3):588-98.
10. Meek KM, Knupp C. Corneal structure and transparency. Prog Retin Eye Res. 2015;49:1-16.
11. Maugeri G, D'Amico AG, Castrogiovanni P, Saccone S, Federico C, Reibaldi M, Russo A, Bonfiglio V, Avitabile T, Longo A, D'Agata V. PACAP through EGFR transactivation preserves human corneal endothelial integrity. J Cell Biochem. 2019;120(6):10097-105.
12. Shaw EL, Rao GN, Arthur EJ, Aquavella JV. The functional reserve of corneal endothelium. Ophthalmology. 1978;85(6):640-9.
13. Elbaz U, Mireskandari K, Tehrani N, Shen C, Khan MS, Williams S, Ali A. Corneal Endothelial Cell Density in Children: Normative Data From Birth to

5 Years Old. Am J Ophthalmol. 2017;173:134-8.
14. Bourne WM, Nelson LR, Hodge DO. Central corneal endothelial cell changes over a ten-year period. Invest Ophthalmol Vis Sci. 1997;38(3):779-82.
15. Fitzgerald BW. Using Hawkeye from the Avengers to communicate on the eye. Adv Physiol Educ. 2018;42(1):90-8.
16. Chen Z, You J, Liu X, Cooper S, Hodge C, Sutton G, Crook JM, Wallace GG. Biomaterials for corneal bioengineering. Biomed Mater. 2018;13(3):032002.
17. Galgauskas S, Norvydaite D, Krasauskaite D, Stech S, Asoklis RS. Age-related changes in corneal thickness and endothelial characteristics. Clin Interv Aging. 2013;8:1445-50.
18. Marshall J. Radiation and the ageing eye. Ophthalmic Physiol Opt. 1985;5(3):241-63.
19. Zhu L, Titone R, Robertson DM. The impact of hyperglycemia on the corneal epithelium: Molecular mechanisms and insight. Ocul Surf. 2019;17(4):644-54.
20. Alio Del Barrio JL, Alio JL. Cellular therapy of the corneal stroma: a new type of corneal surgery for keratoconus and corneal dystrophies. Eye Vis (Lond). 2018;5:28.
21. Edelhauser HF. The balance between corneal transparency and edema the proctor lecture. Investigative ophthalmology & visual science. 2006;47(5):1755-67.
22. Joyce NC. Proliferative capacity of corneal endothelial cells. Exp Eye Res. 2012;95(1):16-23.
23. Torricelli AA, Singh V, Santhiago MR, Wilson SE. The corneal epithelial basement membrane: structure, function, and disease. Invest Ophthalmol Vis Sci. 2013;54(9):6390-400.
24. Maugeri G, D'Amico AG, Amenta A, Saccone S, Federico C, Reibaldi M, Russo A, Bonfiglio V, Avitabile T, Longo A, D'Agata V. Protective effect of PACAP against ultraviolet B radiation-induced human corneal endothelial cell injury. Neuropeptides. 2019:101978.
25. Bonanno JA. Molecular mechanisms underlying the corneal endothelial pump. Exp Eye Res. 2012;95(1):2-7.

26. Mergler S, Mertens C, Valtink M, Reinach PS, Szekely VC, Slavi N, Garreis F, Abdelmessih S, Turker E, Fels G, Pleyer U. Functional significance of thermosensitive transient receptor potential melastatin channel 8 (TRPM8) expression in immortalized human corneal endothelial cells. Exp Eye Res. 2013;116:337-49.
27. Lee JG, Jung E, Heur M. Fibroblast growth factor 2 induces proliferation and fibrosis via SNAI1-mediated activation of CDK2 and ZEB1 in corneal endothelium. J Biol Chem. 2018;293(10):3758-69.
28. Li S, Kim E, Ogando DG, Bonanno JA. Corneal Endothelial Pump Coupling to Lactic Acid Efflux in the Rabbit and Mouse. Invest Ophthalmol Vis Sci. 2020;61(2):7.
29. Mergler S, Pleyer U, Reinach P, Bednarz J, Dannowski H, Engelmann K, Hartmann C, Yousif T. EGF suppresses hydrogen peroxide induced Ca2+ influx by inhibiting L-type channel activity in cultured human corneal endothelial cells. Exp Eye Res. 2005;80(2):285-93.
30. Rae JL, Dewey J, Cooper K. Properties of single potassium-selective ionic channels from the apical membrane of rabbit corneal endothelium. Experimental eye research. 1989;49(4):591-609.
31. Xie Q, Zhang Y, Cai Sun X, Zhai C, Bonanno JA. Expression and functional evaluation of transient receptor potential channel 4 in bovine corneal endothelial cells. Exp Eye Res. 2005;81(1):5-14.
32. Mergler S, Valtink M, Taetz K, Sahlmuller M, Fels G, Reinach PS, Engelmann K, Pleyer U. Characterization of transient receptor potential vanilloid channel 4 (TRPV4) in human corneal endothelial cells. Exp Eye Res. 2011;93(5):710-9.
33. Mergler S, Garreis F, Sahlmuller M, Reinach PS, Paulsen F, Pleyer U. Thermosensitive transient receptor potential channels in human corneal epithelial cells. J Cell Physiol. 2011;226(7):1828-42.
34. Feizi S. Corneal endothelial cell dysfunction: etiologies and management. Ther Adv Ophthalmol. 2018;10:2515841418815802.
35. Lee A, Fakler B, Kaczmarek LK, Isom LL. More than a pore: ion channel signaling complexes. J Neurosci. 2014;34(46):15159-69.
36. Valtink M, Gruschwitz R, Funk RH, Engelmann K. Two clonal cell lines

of immortalized human corneal endothelial cells show either differentiated or precursor cell characteristics. Cells Tissues Organs. 2008;187(4):286-94.
37. Li QJ, Ashraf MF, Shen DF, Green WR, Stark WJ, Chan CC, O'Brien TP. The role of apoptosis in the pathogenesis of Fuchs endothelial dystrophy of the cornea. Arch Ophthalmol. 2001;119(11):1597-604.
38. Xia X, Atkins M, Dalal R, Kuzmenko O, Chang KC, Sun CB, Benatti CA, Rak DJ, Nahmou M, Kunzevitzky NJ, Goldberg JL. Magnetic Human Corneal Endothelial Cell Transplant: Delivery, Retention, and Short-Term Efficacy. Invest Ophthalmol Vis Sci. 2019;60(7):2438-48.
39. He Z, Campolmi N, Gain P, Ha Thi BM, Dumollard JM, Duband S, Peoc'h M, Piselli S, Garraud O, Thuret G. Revisited microanatomy of the corneal endothelial periphery: new evidence for continuous centripetal migration of endothelial cells in humans. Stem Cells. 2012;30(11):2523-34.
40. Price MO, Mehta JS, Jurkunas UV, Price FW, Jr. Corneal endothelial dysfunction: Evolving understanding and treatment options. Prog Retin Eye Res. 2021;82:100904.
41. Diaz-Valle D, Benitez del Castillo Sanchez JM, Castillo A, Sayagues O, Moriche M. Endothelial damage with cataract surgery techniques. J Cataract Refract Surg. 1998;24(7):951-5.
42. Melles GR, Ong TS, Ververs B, van der Wees J. Descemet membrane endothelial keratoplasty (DMEK). Cornea. 2006;25(8):987-90.
43. Shulman J, Kropinak M, Ritterband DC, Perry HD, Seedor JA, McCormick SA, Milman T. Failed descemet-stripping automated endothelial keratoplasty grafts: a clinicopathologic analysis. Am J Ophthalmol. 2009;148(5):752-9 e2.
44. Dapena I, Ham L, Melles GR. Endothelial keratoplasty: DSEK/DSAEK or DMEK--the thinner the better? Curr Opin Ophthalmol. 2009;20(4):299-307.
45. Aquavella JV. Challenges, opportunities and controversy in keratoplasty. Expert Review of Ophthalmology. 2007;2(1):1-4.
46. Bahar I, Kaiserman I, Sansanayudh W, Levinger E, Rootman DS. Busin Guide vs Forceps for the Insertion of the Donor Lenticule in Descemet Stripping Automated Endothelial Keratoplasty. Am J Ophthalmol. 2009;147(2):220-6 e1.
47. Melles GR. Posterior lamellar keratoplasty: DLEK to DSEK to DMEK.

Cornea. 2006;25(8):879-81.
48. Baydoun L, Dapena I, Melles G. Evolution of Posterior Lamellar Keratoplasty: PK–DLEK–DSEK/DSAEK–DMEK–DMET. Current Treatment Options for Fuchs Endothelial Dystrophy: Springer; 2017. p. 73-85.
49. Niemeyer BA, Mery L, Zawar C, Suckow A, Monje F, Pardo LA, Stuhmer W, Flockerzi V, Hoth M. Ion channels in health and disease. 83rd Boehringer Ingelheim Fonds International Titisee Conference. EMBO Rep. 2001;2(7):568-73.
50. Berridge MJ, Lipp P, Bootman MD. The versatility and universality of calcium signalling. Nat Rev Mol Cell Biol. 2000;1(1):11-21.
51. Cheli VT, Santiago Gonzalez DA, Smith J, Spreuer V, Murphy GG, Paez PM. L-type voltage-operated calcium channels contribute to astrocyte activation In vitro. Glia. 2016;64(8):1396-415.
52. Orrenius S, Zhivotovsky B, Nicotera P. Regulation of cell death: the calcium-apoptosis link. Nat Rev Mol Cell Biol. 2003;4(7):552-65.
53. Mergler S, Dannowski H, Bednarz J, Engelmann K, Hartmann C, Pleyer U. Calcium influx induced by activation of receptor tyrosine kinases in SV40-transfected human corneal endothelial cells. Exp Eye Res. 2003;77(4):485-95.
54. Prakriya M, Lewis RS. Store-Operated Calcium Channels. Physiol Rev. 2015;95(4):1383-436.
55. Alexander SP, Peters JA, Kelly E, Marrion NV, Faccenda E, Harding SD, Pawson AJ, Sharman JL, Southan C, Davies JA, Collaborators C. THE CONCISE GUIDE TO PHARMACOLOGY 2017/18: Ligand-gated ion channels. Br J Pharmacol. 2017;174 Suppl 1:S130-S59.
56. Cosens DJ, Manning A. Abnormal electroretinogram from a Drosophila mutant. Nature. 1969;224(5216):285-7.
57. Pan Z, Yang H, Reinach PS. Transient receptor potential (TRP) gene superfamily encoding cation channels. Hum Genomics. 2011;5(2):108-16.
58. Mergler S, Pleyer U. The human corneal endothelium: new insights into electrophysiology and ion channels. Prog Retin Eye Res. 2007;26(4):359-78.
59. Eguchi H, Hiura A, Nakagawa H, Kusaka S, Shimomura Y. Corneal Nerve Fiber Structure, Its Role in Corneal Function, and Its Changes in Corneal Diseases. Biomed Res Int. 2017;2017:3242649.

60. Nilius B, Owsianik G, Voets T, Peters JA. Transient receptor potential cation channels in disease. Physiol Rev. 2007;87(1):165-217.
61. Putney JW, Jr. The enigmatic TRPCs: multifunctional cation channels. Trends Cell Biol. 2004;14(6):282-6.
62. Vazquez G, Wedel BJ, Aziz O, Trebak M, Putney JW, Jr. The mammalian TRPC cation channels. Biochim Biophys Acta. 2004;1742(1-3):21-36.
63. Vriens J, Appendino G, Nilius B. Pharmacology of vanilloid transient receptor potential cation channels. Mol Pharmacol. 2009;75(6):1262-79.
64. Mergler S, Valtink M, Coulson-Thomas VJ, Lindemann D, Reinach PS, Engelmann K, Pleyer U. TRPV channels mediate temperature-sensing in human corneal endothelial cells. Exp Eye Res. 2010;90(6):758-70.
65. Clapham DE. TRP channels as cellular sensors. Nature. 2003;426(6966):517-24.
66. Veldhuis NA, Poole DP, Grace M, McIntyre P, Bunnett NW. The G protein-coupled receptor-transient receptor potential channel axis: molecular insights for targeting disorders of sensation and inflammation. Pharmacol Rev. 2015;67(1):36-73.
67. Tominaga M, Caterina MJ. Thermosensation and pain. J Neurobiol. 2004;61(1):3-12.
68. Hasan R, Zhang X. Ca(2+) Regulation of TRP Ion Channels. Int J Mol Sci. 2018;19(4).
69. Krizaj D, Cordeiro S, Strauss O. Retinal TRP channels: Cell-type-specific regulators of retinal homeostasis and multimodal integration. Prog Retin Eye Res. 2023;92:101114.
70. Reinach PS, Chen W, Mergler S. Polymodal roles of transient receptor potential channels in the control of ocular function. Eye Vis (Lond). 2015;2:5.
71. Nilius B, Owsianik G. The transient receptor potential family of ion channels. Genome Biol. 2011;12(3):218.
72. Mergler S, Valtink M, Takayoshi S, Okada Y, Miyajima M, Saika S, Reinach PS. Temperature-sensitive transient receptor potential channels in corneal tissue layers and cells. Ophthalmic Res. 2014;52(3):151-9.
73. Zhang F, Yang H, Wang Z, Mergler S, Liu H, Kawakita T, Tachado SD,

Pan Z, Capo-Aponte JE, Pleyer U, Koziel H, Kao WW, Reinach PS. Transient receptor potential vanilloid 1 activation induces inflammatory cytokine release in corneal epithelium through MAPK signaling. J Cell Physiol. 2007;213(3):730-9.

74. Alamri A, Bron R, Brock JA, Ivanusic JJ. Transient receptor potential cation channel subfamily V member 1 expressing corneal sensory neurons can be subdivided into at least three subpopulations. Front Neuroanat. 2015;9:71.

75. Turan E, Valtink M, Reinach PS, Skupin A, Luo H, Brockmann T, Ba Salem MHO, Pleyer U, Mergler S. L-carnitine suppresses transient receptor potential vanilloid type 1 activity and myofibroblast transdifferentiation in human corneal keratocytes. Lab Invest. 2021.

76. Turker E, Garreis F, Khajavi N, Reinach PS, Joshi P, Brockmann T, Lucius A, Ljubojevic N, Turan E, Cooper D, Schick F, Reinholz R, Pleyer U, Kohrle J, Mergler S. Vascular Endothelial Growth Factor (VEGF) Induced Downstream Responses to Transient Receptor Potential Vanilloid 1 (TRPV1) and 3-Iodothyronamine (3-T1AM) in Human Corneal Keratocytes. Front Endocrinol (Lausanne). 2018;9:670.

77. Yang Y, Yang H, Wang Z, Mergler S, Wolosin JM, Reinach PS. Functional TRPV1 expression in human corneal fibroblasts. Exp Eye Res. 2013;107:121-9.

78. Yamada T, Ueda T, Ugawa S, Ishida Y, Imayasu M, Koyama S, Shimada S. Functional expression of transient receptor potential vanilloid 3 (TRPV3) in corneal epithelial cells: involvement in thermosensation and wound healing. Exp Eye Res. 2010;90(1):121-9.

79. Pan Z, Yang H, Mergler S, Liu H, Tachado SD, Zhang F, Kao WW, Koziel H, Pleyer U, Reinach PS. Dependence of regulatory volume decrease on transient receptor potential vanilloid 4 (TRPV4) expression in human corneal epithelial cells. Cell Calcium. 2008;44(4):374-85.

80. Lucius A, Khajavi N, Reinach PS, Kohrle J, Dhandapani P, Huimann P, Ljubojevic N, Grotzinger C, Mergler S. 3-Iodothyronamine increases transient receptor potential melastatin channel 8 (TRPM8) activity in immortalized human corneal epithelial cells. Cell Signal. 2016;28(3):136-47.

81. Parra A, Madrid R, Echevarria D, del Olmo S, Morenilla-Palao C, Acosta

MC, Gallar J, Dhaka A, Viana F, Belmonte C. Ocular surface wetness is regulated by TRPM8-dependent cold thermoreceptors of the cornea. Nat Med. 2010;16(12):1396-9.

82. Caterina MJ, Schumacher MA, Tominaga M, Rosen TA, Levine JD, Julius D. The capsaicin receptor: a heat-activated ion channel in the pain pathway. Nature. 1997;389(6653):816-24.

83. Liao M, Cao E, Julius D, Cheng Y. Structure of the TRPV1 ion channel determined by electron cryo-microscopy. Nature. 2013;504(7478):107-12.

84. Por ED, Choi JH, Lund BJ. Low-Level Blast Exposure Increases Transient Receptor Potential Vanilloid 1 (TRPV1) Expression in the Rat Cornea. Curr Eye Res. 2016;41(10):1294-301.

85. Hatta A, Kurose M, Sullivan C, Okamoto K, Fujii N, Yamamura K, Meng ID. Dry eye sensitizes cool cells to capsaicin-induced changes in activity via TRPV1. J Neurophysiol. 2019;121(6):2191-201.

86. Krishnatreyya H, Hazarika H, Saha A, Chattopadhyay P. Capsaicin, the primary constituent of pepper sprays and its pharmacological effects on mammalian ocular tissues. Eur J Pharmacol. 2018;819:114-21.

87. Guzman M, Miglio MS, Zgajnar NR, Colado A, Almejun MB, Keitelman IA, Sabbione F, Fuentes F, Trevani AS, Giordano MN, Galletti JG. The mucosal surfaces of both eyes are immunologically linked by a neurogenic inflammatory reflex involving TRPV1 and substance P. Mucosal Immunol. 2018;11(5):1441-53.

88. Planells-Cases R, Garcia-Sanz N, Morenilla-Palao C, Ferrer-Montiel A. Functional aspects and mechanisms of TRPV1 involvement in neurogenic inflammation that leads to thermal hyperalgesia. Pflugers Arch. 2005;451(1):151-9.

89. Abbas MA. Modulation of TRPV1 channel function by natural products in the treatment of pain. Chem Biol Interact. 2020;330:109178.

90. Szallasi A, Cortright DN, Blum CA, Eid SR. The vanilloid receptor TRPV1: 10 years from channel cloning to antagonist proof-of-concept. Nat Rev Drug Discov. 2007;6(5):357-72.

91. Dhaka A, Viswanath V, Patapoutian A. Trp ion channels and temperature sensation. Annu Rev Neurosci. 2006;29:135-61.

92. Zou S, Kumar U. Cannabinoid Receptors and the Endocannabinoid System: Signaling and Function in the Central Nervous System. Int J Mol Sci. 2018;19(3).
93. Hazekamp A, Fischedick JT, Díez ML, Lubbe A, Ruhaak RL. Chemistry of cannabis. 2010.
94. Luca T, Di Benedetto G, Scuderi MR, Palumbo M, Clementi S, Bernardini R, Cantarella G. The CB1/CB2 receptor agonist WIN-55,212-2 reduces viability of human Kaposi's sarcoma cells in vitro. Eur J Pharmacol. 2009;616(1-3):16-21.
95. De Petrocellis L, Ligresti A, Moriello AS, Allara M, Bisogno T, Petrosino S, Stott CG, Di Marzo V. Effects of cannabinoids and cannabinoid-enriched Cannabis extracts on TRP channels and endocannabinoid metabolic enzymes. Br J Pharmacol. 2011;163(7):1479-94.
96. De Petrocellis L, Orlando P, Moriello AS, Aviello G, Stott C, Izzo AA, Di Marzo V. Cannabinoid actions at TRPV channels: effects on TRPV3 and TRPV4 and their potential relevance to gastrointestinal inflammation. Acta Physiol (Oxf). 2012;204(2):255-66.
97. Stander S, Schmelz M, Metze D, Luger T, Rukwied R. Distribution of cannabinoid receptor 1 (CB1) and 2 (CB2) on sensory nerve fibers and adnexal structures in human skin. J Dermatol Sci. 2005;38(3):177-88.
98. Iannotti FA, Hill CL, Leo A, Alhusaini A, Soubrane C, Mazzarella E, Russo E, Whalley BJ, Di Marzo V, Stephens GJ. Nonpsychotropic plant cannabinoids, cannabidivarin (CBDV) and cannabidiol (CBD), activate and desensitize transient receptor potential vanilloid 1 (TRPV1) channels in vitro: potential for the treatment of neuronal hyperexcitability. ACS Chem Neurosci. 2014;5(11):1131-41.
99. Ligresti A, Moriello AS, Starowicz K, Matias I, Pisanti S, De Petrocellis L, Laezza C, Portella G, Bifulco M, Di Marzo V. Antitumor activity of plant cannabinoids with emphasis on the effect of cannabidiol on human breast carcinoma. J Pharmacol Exp Ther. 2006;318(3):1375-87.
100. Straiker AJ, Maguire G, Mackie K, Lindsey J. Localization of cannabinoid CB1 receptors in the human anterior eye and retina. Invest Ophthalmol Vis Sci. 1999;40(10):2442-8.

101. Yang Y, Yang H, Wang Z, Varadaraj K, Kumari SS, Mergler S, Okada Y, Saika S, Kingsley PJ, Marnett LJ, Reinach PS. Cannabinoid receptor 1 suppresses transient receptor potential vanilloid 1-induced inflammatory responses to corneal injury. Cell Signal. 2013;25(2):501-11.
102. Nascimento Menezes PM, Valenca Pereira EC, Gomes da Cruz Silva ME, da Silva BAO, de Souza Duarte Filho LAM, de Lima Araujo TC, Bezerra Lima KS, Silva FS, Rolim LA. Cannabis and Cannabinoids on Treatment of Inflammation: A Patent Review. Recent Pat Biotechnol. 2019;13(4):256-67.
103. Diego LM, Viviana A. cannabinoid receptor cb1 activation in vivo leads to corneal wound healing after chemical iinjury via specific receptor vanilloid trpv1 desensitization. Ophthalmology Research and Reports. 2018.
104. Mergler S, Cheng Y, Skosyrski S, Garreis F, Pietrzak P, Kociok N, Dwarakanath A, Reinach PS, Kakkassery V. Altered calcium regulation by thermosensitive transient receptor potential channels in etoposide-resistant WERI-Rb1 retinoblastoma cells. Exp Eye Res. 2012;94(1):157-73.
105. Mergler S, Derckx R, Reinach PS, Garreis F, Bohm A, Schmelzer L, Skosyrski S, Ramesh N, Abdelmessih S, Polat OK, Khajavi N, Riechardt AI. Calcium regulation by temperature-sensitive transient receptor potential channels in human uveal melanoma cells. Cell Signal. 2014;26(1):56-69.
106. Reinach PS, Mergler S, Okada Y, Saika S. Ocular transient receptor potential channel function in health and disease. BMC ophthalmology. 2015;15(1):29-40.
107. Garreis F, Gottschalt M, Schlorf T, Glaser R, Harder J, Worlitzsch D, Paulsen FP. Expression and regulation of antimicrobial peptide psoriasin (S100A7) at the ocular surface and in the lacrimal apparatus. Invest Ophthalmol Vis Sci. 2011;52(7):4914-22.
108. Yang H, Mergler S, Sun X, Wang Z, Lu L, Bonanno JA, Pleyer U, Reinach PS. TRPC4 knockdown suppresses epidermal growth factor-induced store-operated channel activation and growth in human corneal epithelial cells. J Biol Chem. 2005;280(37):32230-7.
109. Murata Y, Masuko S. Peripheral and central distribution of TRPV1, substance P and CGRP of rat corneal neurons. Brain Res. 2006;1085(1):87-94.

110. Mergler S, Valtink M, Sahlmüller M, Reinach PS, Engelmann K, Pleyer U. Transient Receptor Potential Melastatin 8 (TRPM8) Channels Mediate Complex Calcium Responses in Human Corneal Endothelial Cells. Investigative Ophthalmology & Visual Science. 2012;53(14):6015-.
111. Yang H, Wang Z, Capo-Aponte JE, Zhang F, Pan Z, Reinach PS. Epidermal growth factor receptor transactivation by the cannabinoid receptor (CB1) and transient receptor potential vanilloid 1 (TRPV1) induces differential responses in corneal epithelial cells. Exp Eye Res. 2010;91(3):462-71.
112. Lowin T, Straub RH. Cannabinoid-based drugs targeting CB1 and TRPV1, the sympathetic nervous system, and arthritis. Arthritis Res Ther. 2015;17:226.
113. Caterina MJ. TRP channel cannabinoid receptors in skin sensation, homeostasis, and inflammation. ACS Chem Neurosci. 2014;5(11):1107-16.
114. Bednarz J, Teifel M, Friedl P, Engelmann K. Immortalization of human corneal endothelial cells using electroporation protocol optimized for human corneal endothelial and human retinal pigment epithelial cells. Acta Ophthalmol Scand. 2000;78(2):130-6.
115. Genova T, Grolez GP, Camillo C, Bernardini M, Bokhobza A, Richard E, Scianna M, Lemonnier L, Valdembri D, Munaron L, Philips MR, Mattot V, Serini G, Prevarskaya N, Gkika D, Pla AF. TRPM8 inhibits endothelial cell migration via a non-channel function by trapping the small GTPase Rap1. J Cell Biol. 2017;216(7):2107-30.
116. Kabosova A, Azar DT, Bannikov GA, Campbell KP, Durbeej M, Ghohestani RF, Jones JC, Kenney MC, Koch M, Ninomiya Y, Patton BL, Paulsson M, Sado Y, Sage EH, Sasaki T, Sorokin LM, Steiner-Champliaud MF, Sun TT, Sundarraj N, Timpl R, Virtanen I, Ljubimov AV. Compositional differences between infant and adult human corneal basement membranes. Invest Ophthalmol Vis Sci. 2007;48(11):4989-99.
117. Starowicz K, Przewlocka B. Modulation of neuropathic-pain-related behaviour by the spinal endocannabinoid/endovanilloid system. Philos Trans R Soc Lond B Biol Sci. 2012;367(1607):3286-99.
118. Ahluwalia J, Urban L, Bevan S, Nagy I. Anandamide regulates neuropeptide release from capsaicin-sensitive primary sensory neurons by

activating both the cannabinoid 1 receptor and the vanilloid receptor 1 in vitro. Eur J Neurosci. 2003;17(12):2611-8.

119. Anand U, Otto WR, Sanchez-Herrera D, Facer P, Yiangou Y, Korchev Y, Birch R, Benham C, Bountra C, Chessell IP, Anand P. Cannabinoid receptor CB2 localisation and agonist-mediated inhibition of capsaicin responses in human sensory neurons. Pain. 2008;138(3):667-80.

120. De Petrocellis L, Vellani V, Schiano-Moriello A, Marini P, Magherini PC, Orlando P, Di Marzo V. Plant-derived cannabinoids modulate the activity of transient receptor potential channels of ankyrin type-1 and melastatin type-8. J Pharmacol Exp Ther. 2008;325(3):1007-15.

121. Aloe L, Rocco ML, Balzamino BO, Micera A. Nerve Growth Factor: A Focus on Neuroscience and Therapy. Curr Neuropharmacol. 2015;13(3):294-303.

122. Levi-Montalcini R. The nerve growth factor 35 years later. Science. 1987;237(4819):1154-62.

123. Aloe L, Rocco ML, Bianchi P, Manni L. Nerve growth factor: from the early discoveries to the potential clinical use. J Transl Med. 2012;10:239.

124. Reichardt LF. Neurotrophin-regulated signalling pathways. Philos Trans R Soc Lond B Biol Sci. 2006;361(1473):1545-64.

125. Micera A, Lambiase A, Aloe L, Bonini S, Levi-Schaffer F, Bonini S. Nerve growth factor involvement in the visual system: implications in allergic and neurodegenerative diseases. Cytokine Growth Factor Rev. 2004;15(6):411-7.

126. Sornelli F, Lambiase A, Mantelli F, Aloe L. NGF and NGF-receptor expression of cultured immortalized human corneal endothelial cells. Mol Vis. 2010;16:1439-47.

127. Micera A, Puxeddu I, Lambiase A, Antonelli A, Bonini S, Bonini S, Aloe L, Pe'er J, Levi-Schaffer F. The pro-fibrogenic effect of nerve growth factor on conjunctival fibroblasts is mediated by transforming growth factor-beta. Clin Exp Allergy. 2005;35(5):650-6.

128. Micera A, Lambiase A, Puxeddu I, Aloe L, Stampachiacchiere B, Levi-Schaffer F, Bonini S, Bonini S. Nerve growth factor effect on human primary fibroblastic-keratocytes: possible mechanism during corneal healing. Exp Eye Res. 2006;83(4):747-57.

129. Bednarz J, Weich HA, Rodokanaki-von Schrenck A, Engelmann K. Expression of genes coding growth factors and growth factor receptors in differentiated and dedifferentiated human corneal endothelial cells. Cornea. 1995;14(4):372-81.
130. Cellini M, Bendo E, Bravetti GO, Campos EC. The use of nerve growth factor in surgical wound healing of the cornea. Ophthalmic Res. 2006;38(4):177-81.
131. Turner JE, Delaney RK. Retinal ganglion cell response to axotomy and nerve growth factor in the regenerating visual system of the newt (Notophthalmus viridescens): an ultrastructural morphometric analysis. Brain Res. 1979;171(2):197-212.
132. Benarroch EE. TRP channels: functions and involvement in neurologic disease. Neurology. 2008;70(8):648-52.
133. Valtink M, Knels L, Stanke N, Engelmann K, Funk RH, Lindemann D. Overexpression of human HMW FGF-2 but not LMW FGF-2 reduces the cytotoxic effect of lentiviral gene transfer in human corneal endothelial cells. Invest Ophthalmol Vis Sci. 2012;53(6):3207-14.
134. Valtink M, Stanke N, Knels L, Engelmann K, Funk RH, Lindemann D. Pseudotyping and culture conditions affect efficiency and cytotoxicity of retroviral gene transfer to human corneal endothelial cells. Invest Ophthalmol Vis Sci. 2011;52(9):6807-13.
135. Valtink M, Donath P, Engelmann K, Knels L. Effect of different culture media and deswelling agents on survival of human corneal endothelial and epithelial cells in vitro. Graefes Arch Clin Exp Ophthalmol. 2016;254(2):285-95.
136. Valtink M, Donath P, Engelmann K, Knels L. Erratum to: Effect of different culture media and deswelling agents on survival of human corneal endothelial and epithelial cells in vitro. Graefes Arch Clin Exp Ophthalmol. 2016;254(5):1029.
137. Brinks J, van Dijk EHC, Habeeb M, Nikolaou A, Tsonaka R, Peters HAB, Sips HCM, van de Merbel AF, de Jong EK, Notenboom RGE, Kielbasa SM, van der Maarel SM, Quax PHA, Meijer OC, Boon CJF. The Effect of Corticosteroids on Human Choroidal Endothelial Cells: A Model to Study Central Serous Chorioretinopathy. Invest Ophthalmol Vis Sci. 2018;59(13):5682-92.

138. Ebertz SL, McGann LE. Cryoinjury in endothelial cell monolayers. Cryobiology. 2004;49(1):37-44.
139. Grynkiewicz G, Poenie M, Tsien RY. A new generation of Ca2+ indicators with greatly improved fluorescence properties. J Biol Chem. 1985;260(6):3440-50.
140. Roedding AS, Li PP, Warsh JJ. Characterization of the transient receptor potential channels mediating lysophosphatidic acid-stimulated calcium mobilization in B lymphoblasts. Life Sci. 2006;80(2):89-97.
141. Khajavi N, Reinach PS, Slavi N, Skrzypski M, Lucius A, Strauss O, Kohrle J, Mergler S. Thyronamine induces TRPM8 channel activation in human conjunctival epithelial cells. Cell Signal. 2015;27(2):315-25.
142. Dinter J, Khajavi N, Muhlhaus J, Wienchol CL, Coster M, Hermsdorf T, Staubert C, Kohrle J, Schoneberg T, Kleinau G, Mergler S, Biebermann H. The Multitarget Ligand 3-Iodothyronamine Modulates beta-Adrenergic Receptor 2 Signaling. Eur Thyroid J. 2015;4(Suppl 1):21-9.
143. Bruggemann A, Stoelzle S, George M, Behrends JC, Fertig N. Microchip technology for automated and parallel patch-clamp recording. Small. 2006;2(7):840-6.
144. Milligan CJ, Li J, Sukumar P, Majeed Y, Dallas ML, English A, Emery P, Porter KE, Smith AM, McFadzean I, Beccano-Kelly D, Bahnasi Y, Cheong A, Naylor J, Zeng F, Liu X, Gamper N, Jiang LH, Pearson HA, Peers C, Robertson B, Beech DJ. Robotic multiwell planar patch-clamp for native and primary mammalian cells. Nat Protoc. 2009;4(2):244-55.
145. Bruggemann H, Cazalet C, Buchrieser C. Adaptation of Legionella pneumophila to the host environment: role of protein secretion, effectors and eukaryotic-like proteins. Curr Opin Microbiol. 2006;9(1):86-94.
146. Khajavi N, Reinach PS, Skrzypski M, Lude A, Mergler S. L-carnitine reduces in human conjunctival epithelial cells hypertonic-induced shrinkage through interacting with TRPV1 channels. Cell Physiol Biochem. 2014;34(3):790-803.
147. Bruggemann A, Farre C, Haarmann C, Haythornthwaite A, Kreir M, Stoelzle S, George M, Fertig N. Planar patch clamp: advances in electrophysiology. Methods Mol Biol. 2008;491:165-76.

148. Tammaro P, Shimomura K, Proks P. Xenopus oocytes as a heterologous expression system for studying ion channels with the patch-clamp technique. Methods Mol Biol. 2008;491:127-39.
149. Barry PH. JPCalc, a software package for calculating liquid junction potential corrections in patch-clamp, intracellular, epithelial and bilayer measurements and for correcting junction potential measurements. J Neurosci Methods. 1994;51(1):107-16.
150. Bosca A, Martina M, Py C. Planar patch clamp for neuronal networks--considerations and future perspectives. Methods Mol Biol. 2014;1183:93-113.
151. Coronado-Alvarez A, Romero-Cordero K, Macias-Triana L, Tatum-Kuri A, Vera-Barron A, Budde H, Machado S, Yamamoto T, Imperatori C, Murillo-Rodriguez E. The synthetic CB1 cannabinoid receptor selective agonists: Putative medical uses and their legalization. Prog Neuropsychopharmacol Biol Psychiatry. 2021;110:110301.
152. Lauckner JE, Hille B, Mackie K. The cannabinoid agonist WIN55,212-2 increases intracellular calcium via CB1 receptor coupling to Gq/11 G proteins. Proc Natl Acad Sci U S A. 2005;102(52):19144-9.
153. Wang ZY, McDowell T, Wang P, Alvarez R, Gomez T, Bjorling DE. Activation of CB1 inhibits NGF-induced sensitization of TRPV1 in adult mouse afferent neurons. Neuroscience. 2014;277:679-89.
154. McDowell TS, Wang ZY, Singh R, Bjorling D. CB1 cannabinoid receptor agonist prevents NGF-induced sensitization of TRPV1 in sensory neurons. Neurosci Lett. 2013;551:34-8.
155. Barreto-Chang OL, Dolmetsch RE. Calcium imaging of cortical neurons using Fura-2 AM. J Vis Exp. 2009(23).
156. Shao Y, Hu D, Chen J. [A study on effect of bFGF, EGF and NGF on growth of cultured human corneal endothelial cells]. Yan Ke Xue Bao. 2008;24(1):9-12.
157. Lambiase A, Bonini S, Micera A, Rama P, Bonini S, Aloe L. Expression of nerve growth factor receptors on the ocular surface in healthy subjects and during manifestation of inflammatory diseases. Invest Ophthalmol Vis Sci. 1998;39(7):1272-5.
158. Bartakova A, Kuzmenko O, Alvarez-Delfin K, Kunzevitzky NJ, Goldberg

JL. A cell culture approach to optimized human corneal endothelial cell function. Investigative ophthalmology & visual science. 2018;59(3):1617-29.
159. Bartakova A, Alvarez-Delfin K, Weisman AD, Salero E, Raffa GA, Merkhofer RM, Jr., Kunzevitzky NJ, Goldberg JL. Novel Identity and Functional Markers for Human Corneal Endothelial Cells. Invest Ophthalmol Vis Sci. 2016;57(6):2749-62.
160. ABOALCHAMAT B, ENGELMANN K, BÖHNKE M, EGGLI P, BEDNARZ J. Morphological and functional analysis of immortalized human corneal endothelial cells after transplantation. Experimental eye research. 1999;69(5):547-53.
161. Mergler S, Dannowski H, Bednarz J, Engelmann K, Hartmann C, Pleyer U. Calcium influx induced by activation of receptor tyrosine kinases in SV40-transfected human corneal endothelial cells. Experimental eye research. 2003;77(4):485-95.
162. Valtink M, Gruschwitz R, Funk RH, Engelmann K. Two clonal cell lines of immortalized human corneal endothelial cells show either differentiated or precursor cell characteristics. Cells Tissues Organs. 2008;187(4):286-94.
163. Engelmann K, Bednarz J, Valtink M. Prospects for endothelial transplantation. Exp Eye Res. 2004;78(3):573-8.
164. Joyce NC. Proliferative capacity of the corneal endothelium. Progress in retinal and eye research. 2003;22(3):359-89.
165. Srinivas SP, Yeh JC, Ong A, Bonanno JA. Ca2+ mobilization in bovine corneal endothelial cells by P2 purinergic receptors. Curr Eye Res. 1998;17(10):994-1004.
166. Mergler S, Strowski MZ, Kaiser S, Plath T, Giesecke Y, Neumann M, Hosokawa H, Kobayashi S, Langrehr J, Neuhaus P, Plockinger U, Wiedenmann B, Grotzinger C. Transient receptor potential channel TRPM8 agonists stimulate calcium influx and neurotensin secretion in neuroendocrine tumor cells. Neuroendocrinology. 2007;85(2):81-92.
167. Mergler S, Mertens C, Valtink M, Reinach PS, Székely VC, Slavi N, Garreis F, Abdelmessih S, Türker E, Fels G. Functional significance of thermosensitive transient receptor potential melastatin channel 8 (TRPM8) expression in immortalized human corneal endothelial cells. Experimental eye

research. 2013;116:337-49.
168. Assimakopoulou M, Pagoulatos D, Nterma P, Pharmakakis N. Immunolocalization of cannabinoid receptor type 1 and CB2 cannabinoid receptors, and transient receptor potential vanilloid channels in pterygium. Mol Med Rep. 2017;16(4):5285-93.
169. Stumpff F, Boxberger M, Krauss A, Rosenthal R, Meissner S, Choritz L, Wiederholt M, Thieme H. Stimulation of cannabinoid (CB1) and prostanoid (EP2) receptors opens BKCa channels and relaxes ocular trabecular meshwork. Exp Eye Res. 2005;80(5):697-708.
170. Miller S, Kulkarni S, Ciesielski A, Nikas SP, Mackie K, Makriyannis A, Straiker A. Controlled-Deactivation CB1 Receptor Ligands as a Novel Strategy to Lower Intraocular Pressure. Pharmaceuticals (Basel). 2018;11(2).
171. Iribarne M, Torbidoni V, Julian K, Prestifilippo JP, Sinha D, Rettori V, Berra A, Suburo AM. Cannabinoid receptors in conjunctival epithelium: identification and functional properties. Invest Ophthalmol Vis Sci. 2008;49(10):4535-44.
172. Zhang X, Huang J, McNaughton PA. NGF rapidly increases membrane expression of TRPV1 heat-gated ion channels. EMBO J. 2005;24(24):4211-23.
173. Li X, Li Z, Qiu L, Zhao C, Hu Z. Nerve growth factor modulate proliferation of cultured rabbit corneal endothelial cells and epithelial cells. J Huazhong Univ Sci Technolog Med Sci. 2005;25(5):575-7.
174. Fink DM, Connor AL, Kelley PM, Steele MM, Hollingsworth MA, Tempero RM. Nerve growth factor regulates neurolymphatic remodeling during corneal inflammation and resolution. PLoS One. 2014;9(11):e112737.
175. Evans RM, Scott RH, Ross RA. Chronic exposure of sensory neurones to increased levels of nerve growth factor modulates CB1/TRPV1 receptor crosstalk. Br J Pharmacol. 2007;152(3):404-13.
176. Olah T, Bodnar D, Toth A, Vincze J, Fodor J, Reischl B, Kovacs A, Ruzsnavszky O, Dienes B, Szentesi P, Friedrich O, Csernoch L. Cannabinoid signalling inhibits sarcoplasmic Ca(2+) release and regulates excitation-contraction coupling in mammalian skeletal muscle. J Physiol. 2016;594(24):7381-98.
177. Patwardhan AM, Jeske NA, Price TJ, Gamper N, Akopian AN,

Hargreaves KM. The cannabinoid WIN 55,212-2 inhibits transient receptor potential vanilloid 1 (TRPV1) and evokes peripheral antihyperalgesia via calcineurin. Proc Natl Acad Sci U S A. 2006;103(30):11393-8.
178. Joyce NC, Zhu CC. Human corneal endothelial cell proliferation: potential for use in regenerative medicine. Cornea. 2004;23(8 Suppl):S8-S19.
179. Gong N, Pleyer U, Vogt K, Anegon I, Flugel A, Volk HD, Ritter T. Local overexpression of nerve growth factor in rat corneal transplants improves allograft survival. Invest Ophthalmol Vis Sci. 2007;48(3):1043-52.
180. Yang H, Sun X, Wang Z, Ning G, Zhang F, Kong J, Lu L, Reinach P. EGF stimulates growth by enhancing capacitative calcium entry in corneal epithelial cells. The Journal of membrane biology. 2003;194(1):47-58.
181. Yang H, Mergler S, Sun X, Wang Z, Lu L, Bonanno JA, Pleyer U, Reinach PS. TRPC4 knockdown suppresses epidermal growth factor-induced store-operated channel activation and growth in human corneal epithelial cells. Journal of Biological Chemistry. 2005;280(37):32230-7.
182. Fakih D, Guerrero-Moreno A, Baudouin C, Réaux-Le Goazigo A, Parsadaniantz SM. Capsazepine decreases corneal pain syndrome in severe dry eye disease. Journal of Neuroinflammation. 2021;18(1):1-21.
183. Benitez-Del-Castillo JM, Moreno-Montanes J, Jimenez-Alfaro I, Munoz-Negrete FJ, Turman K, Palumaa K, Sadaba B, Gonzalez MV, Ruz V, Vargas B, Paneda C, Martinez T, Bleau AM, Jimenez AI. Safety and Efficacy Clinical Trials for SYL1001, a Novel Short Interfering RNA for the Treatment of Dry Eye Disease. Invest Ophthalmol Vis Sci. 2016;57(14):6447-54.
184. Cho KS, Lee EH, Choi JS, Joo CK. Reactive oxygen species-induced apoptosis and necrosis in bovine corneal endothelial cells. Invest Ophthalmol Vis Sci. 1999;40(5):911-9.
185. Fink SL, Cookson BT. Apoptosis, pyroptosis, and necrosis: mechanistic description of dead and dying eukaryotic cells. Infect Immun. 2005;73(4):1907-16.
186. Mergler S, Pleyer U. The human corneal endothelium: new insights into electrophysiology and ion channels. Progress in retinal and eye research. 2007;26(4):359-78.
187. Song J, Lee JH, Lee SH, Park KA, Lee WT, Lee JE. TRPV1 Activation

in Primary Cortical Neurons Induces Calcium-Dependent Programmed Cell Death. Exp Neurobiol. 2013;22(1):51-7.

188. Mergler S, Valtink M, Coulson-Thomas VJ, Lindemann D, Reinach PS, Engelmann K, Pleyer U. TRPV channels mediate temperature-sensing in human corneal endothelial cells. Experimental eye research. 2010;90(6):758-70.

189. Mohapatra DP, Nau C. Regulation of Ca2+-dependent desensitization in the vanilloid receptor TRPV1 by calcineurin and cAMP-dependent protein kinase. J Biol Chem. 2005;280(14):13424-32.

190. Garreis F, Schröder A, Reinach PS, Zoll S, Khajavi N, Dhandapani P, Lucius A, Pleyer U, Paulsen F, Mergler S. Upregulation of transient receptor potential vanilloid type-1 channel activity and Ca2+ influx dysfunction in human pterygial cells. Investigative Ophthalmology & Visual Science. 2016;57(6):2564-77.

191. Joyce NC. Cell cycle status in human corneal endothelium. Exp Eye Res. 2005;81(6):629-38.

192. Zhu C, Joyce NC. Proliferative response of corneal endothelial cells from young and older donors. Invest Ophthalmol Vis Sci. 2004;45(6):1743-51.

193. Price MO, Lass JH, Price FW. Clinical Factors for Early and Late Endothelial Cell Loss After Corneal Transplantation. Current Ophthalmology Reports. 2018;6(3):191-9.

194. Mergler S, Pleyer U, Reinach P, Bednarz J, Dannowski H, Engelmann K, Hartmann C, Yousif T. EGF suppresses hydrogen peroxide induced Ca2+ influx by inhibiting L-type channel activity in cultured human corneal endothelial cells. Experimental eye research. 2005;80(2):285-93.

195. Moller-Pedersen T, Hartmann U, Moller HJ, Ehlers N, Engelmann K. Evaluation of potential organ culture media for eye banking using human donor corneas. Br J Ophthalmol. 2001;85(9):1075-9.

196. Yap C, Wong AM, Naor J, Rootman DS. Corneal temperature reversal after storage in Chen medium compared with Optisol GS. Cornea. 2001;20(5):501-4.

197. Mergler S. Functional expression of temperature-sensitive transient receptor potential channels (TRPs) in cultured human corneal and conjunctival

cells: Relevance in the pathophysiology of ocular surface diseases. 2015.
198. Di Zazzo A, Tahvildari M, Subbarayal B, Yin J, Dohlman TH, Inomata T, Mashaghi A, Chauhan SK, Dana R. Proangiogenic Function of T Cells in Corneal Transplantation. Transplantation. 2017;101(4):778-85.
199. Gong N, Ecke I, Mergler S, Yang J, Metzner S, Schu S, Volk HD, Pleyer U, Ritter T. Gene transfer of cyto-protective molecules in corneal endothelial cells and cultured corneas: analysis of protective effects in vitro and in vivo. Biochem Biophys Res Commun. 2007;357(1):302-7.
200. Zorn-Kruppa M, Tykhonova S, Belge G, Bednarz J, Diehl HA, Engelke M. A human corneal equivalent constructed from SV40-immortalised corneal cell lines. Altern Lab Anim. 2005;33(1):37-45.

Eidesstattliche Versicherung

„Ich, Huan Luo, versichere an Eides statt durch meine eigenhändige Unterschrift, dass ich die vorgelegte Dissertation mit dem Thema: „ Charakterisierung der funktionellen Expression des Cannabinoidrezeptors 1 und des Transient-Rezeptor-Potential-Vanilloid-1-Kanals in humanen Hornhautendothelzellen; Characterization of functional expression of cannabinoid receptor 1 and transient receptor potential vanilloid 1 channel in human corneal endothelial cells" selbstständig und ohne nicht offengelegte Hilfe Dritter verfasst und keine anderen als die angegebenen Quellen und Hilfsmittel genutzt habe.

Alle Stellen, die wörtlich oder dem Sinne nach auf Publikationen oder Vorträgen anderer Autoren/innen beruhen, sind als solche in korrekter Zitierung kenntlich gemacht. Die Abschnitte zu Methodik (insbesondere praktische Arbeiten, Laborbestimmungen, statistische Aufarbeitung) und Resultaten (insbesondere Abbildungen, Graphiken und Tabellen) werden von mir verantwortet.

[Für den Fall, dass Sie die Forschung für Ihre Promotion ganz oder teilweise in Gruppenarbeit durchgeführt haben:] Ich versichere ferner, dass ich die in Zusammenarbeit mit anderen Personen generierten Daten, Datenauswertungen und Schlussfolgerungen korrekt gekennzeichnet und meinen eigenen Beitrag sowie die Beiträge anderer Personen korrekt kenntlich gemacht habe (siehe Anteilserklärung). Texte oder Textteile, die gemeinsam mit anderen erstellt oder verwendet wurden, habe ich korrekt kenntlich gemacht.

Meine Anteile an etwaigen Publikationen zu dieser Dissertation entsprechen denen, die in der untenstehenden gemeinsamen Erklärung mit dem/der Erstbetreuer/in, angegeben sind. Für sämtliche im Rahmen der Dissertation entstandenen Publikationen wurden die Richtlinien des ICMJE (International Committee of Medical Journal Editors; www.icmje.og) zur Autorenschaft eingehalten. Ich erkläre ferner, dass ich mich zur Einhaltung der Satzung der

Charité – Universitätsmedizin Berlin zur Sicherung Guter Wissenschaftlicher Praxis verpflichte.

Weiterhin versichere ich, dass ich diese Dissertation weder in gleicher noch in ähnlicher Form bereits an einer anderen Fakultät eingereicht habe.

Die Bedeutung dieser eidesstattlichen Versicherung und die strafrechtlichen Folgen einer unwahren eidesstattlichen Versicherung (§§156, 161 des Strafgesetzbuches) sind mir bekannt und bewusst.“

Datum Unterschrift

"My curriculum vitae does not appear in the electronic version of my paper for reasons of data protection."

List of publications

1. Oronowicz J, Reinhard J, Reinach PS, Ludwiczak S, **Luo H**, Salem MH, Kraemer MM, Biebermann H, Kakkassery V, Mergler S. Ascorbate-induced oxidative stress mediates TRP channel activation and cytotoxicity in human etoposide-sensitive and-resistant retinoblastoma cells. Laboratory Investigation. 2020 Sep 18:1-9.

2. Turan E, Valtink M, Reinach PS, Skupin A, **Luo H**, Brockmann T, Salem MH, Pleyer U, Mergler S. L-carnitine suppresses transient receptor potential vanilloid type 1 activity and myofibroblast transdifferentiation in human corneal keratocytes. Laboratory Investigation. 2021 Feb 26:1-0.

3. Donau J, **Luo H**, Virta I, Skupin A, Pushina M, Loeffler J, Haertel FV, Das A, Kurth T, Gerlach M, Lindemann D, Reinach PS, Mergler S, Valtink M. TRPV4 Stimulation Level Regulates Ca^{2+}-Dependent Control of Human Corneal Endothelial Cell Viability and Survival. Membranes. 2022; 12(3):281.

Acknowledgments

First of all, I would like to express sincere thanks to my supervisor, PD Dr. Stefan Mergler, for providing me an excellent opportunity to study in Berlin. He gave me numerous encouragement and support during the entire period of study. I am deeply grateful to him. He taught me the basic theory of experiment, helped me improve my presentation, and took me to essential conferences. Thank him for reviewing my thesis and giving me many valuable comments. Words cannot express my gratitude. I think I am very fortunate to be his student.

I also want to extend my thanks to my second supervisor Prof. Dr. Uwe Pleyer, whose efforts for my study smoothly in the Department of Ophthalmology of Charité.

Throughout my entire research phase in Germany, I appreciate the selfless assistance from Prof. Dr. Olaf Strauß, PD Dr. Susanne Wolf, and Dr. Norbert Kociok.

I appreciate Dr. Peter S. Reinach and PD Dr. Monika Valtink for providing their expertise in experimental cell physiology and TRP channel research. I also want to thank Dr. Peter S. Reinach for reviewing my thesis.

I am grateful for the doctoral students Julia Maria Caliman, Iiris Virta, and Marah Hussain provided help for the research.

I especially thank my husband and my son for being with me during the most challenging period.

Finally, I genuinely thank my family and friends for encouraging and supporting me in completing my studies.

Confirmation by a statistician

CHARITÉ

CharitéCentrum für Human- und Gesundheitswissenschaften

Charité | Campus Charité Mitte 10117 Berlin

Institut für Biometrie und Klinische Epidemiologie (iBikE)

Direktor: Prof. Dr. Geraldine Rauch

Postantschrift:
Charitéplatz 1 | 10117 Berlin
Besucheranschrift:
Reinhardtstr. 58 | 10117 Berlin

Tel. +49 (0)30 450 562171
geraldine.rauch@charite.de
https://biometrie.charite.de/

Surame, Name: Luo, Huan

Email: huan.luo@charite.de

Immatriculation Number: 226105

Thesis Advisor: PD Dr. phil. nat. Stefan Mergler

Institution / Clinic: Klinik für Augenheilkunde - Experimentelle Ophthalmologie

Certification

I hereby certify that Ms. Huan Luo has received a statistical consultation on a PhD project with me, within the Service Unit Biometry of the Institute of Biometry and Clinical Epidemiology (iBikE). The following consultation dates were attended:

- Appointment 1: 8.6.2021
- Appointment 2: 11.6.2021

The following key advice regarding meaningful analysis and interpretation of data was given during the consultation:

- *Focus should be on good descriptive data analysis and graphical display, separately for intervention and control group, especially for longitudinal trajectories.*
- *For the comparison of two independent groups one can use the t-test or the Mann-Whitney U-test, for the comparison of two dependent groups the paired t-test or the Wilcoxon test - depending on whether the parameters are sufficiently normally distributed. The use of tests for normal distribution is discouraged.*
- *For multiple comparisons, p-values should be adjusted for multiple testing (e.g., using the Bonferroni method) or their purely exploratory nature should be adequately and critically discussed.*

This certificate does not guarantee the correct implementation of the suggestions made in the consultation, the correct performance of the recommended statistical procedures, nor the correct presentation and interpretation of the results. The responsibility for this rests solely with the doctoral student. The Institute of Biometry and Clinical Epidemiology assumes no liability for this.

Date: 21.6.2021 Annette Aigner

Digital unterschrieben von Annette Aigner
Datum: 2021.06.21 08:51:33 +02'00'

Name of consultant: Annette Aigner, PhD

Signature consultant, institute stamp

CHARITÉ
UNIVERSITÄTSMEDIZIN BERLIN
Institut für Biometrie und Klinische Epidemiologie
Campus Charité Mitte
Charitéplatz 1 | D-10117 Berlin
Sitz: Reinhardtstr. 58